To the Graduate Council:

I am submitting herewith a dissertation written by John Alan Bounds entitled "Nuclear Structure of Light Thallium Isotopes as Deduced from Laser Spectroscopy on a Fast Atom Beam." I have examined the final copy of this dissertation for form and content and recommend that it be accepted in partial fulfillment of the requirements for the degree of Doctor of Philosophy, with a major in Physics.

Carrol R. Bingham
Carrol R. Bingham, Major Professor

We have read this dissertation
and recommend its acceptance:

G W Hoffman

David Hegg

M W Guidry

W. K. Carter

Eugene H. Spejewski

Accepted for the Council:

Lawrence Winkel
Vice Provost
and Dean of The Graduate School

NUCLEAR STRUCTURE OF LIGHT THALLIUM ISOTOPES AS DEDUCED FROM LASER SPECTROSCOPY ON A FAST ATOM BEAM

A Dissertation

Presented for the

Doctor of Philosophy

Degree

The University of Tennessee, Knoxville

John Alan Bounds

August 1985

This dissertation is dedicated to

Alison McNutt

and all of the many other fine teachers of

Holston High School in the years

1972 - 1976.

ACKNOWLEDGMENTS

This dissertation research could not have been a success without the contributions of many people. Foremost among these was Ken Carter, mentor of the laser project. Ron Mlekodaj and Gene Spejewski were instrumental in target selection, ion source development and separator control. Carrol Bingham provided valuable guidance and suggestions. Georg Leander provided much of the theoretical interpretation of the data. Bill Fairbank, Jr., first developed the optical pumping model and supplied valuable advice. Also contributing to the laser project were Michel Gaillard, Dave Pegg, Patrick Juncar, Dave Thomson, and Jeff Griffin. Curt Bemis, Jr., and Paul Griffin provided valuable advice and support. Ken Toth, John Wood, Ed Zganjar and Bob Braga have all contributed to UNISOR research on the light thallium isotopes and have encouraged those on the laser project. Charles Thomas, Charles Reed and Jerry Cole helped with technical support.

The author was supported during his research by the U.S. Department of Energy Laboratory Graduate Participation Program administered by Oak Ridge Associated Universities. UNISOR is supported by the Office of Energy Research of the U.S. Department of Energy under contract number DE-AS05-76OR00033 with Oak Ridge Associated Universities. The University of Tennessee physics research is partially supported by the U.S. Department of Energy under contract number DE-AS05-76ER04936 and by the National Science Foundation.

ABSTRACT

After optimizing the system by experiments on ^{201,203,205}Tl, the neutron-deficient isotopes $^{189-193}$Tl have been studied using the collinear fast atom beam laser spectroscopy system at UNISOR on-line to the Holifield Heavy Ion Research Facility. A sensitive system for the measurements was developed since the light isotopes were available in mass-separated beams of only 7 x 10^4 to 4 x 10^5 atoms per second. By laser excitation of the 535 nm atomic transitions of atoms in the beam, the $6s^2 7s\ ^2S_{1/2}$ and $6s^2 6s\ ^2P_{3/2}$ hyperfine structures were measured, as were the isotope shifts of the 535 nm transitions. From these, the magnetic dipole moments, spectroscopic quadrupole moments and isotopic changes in mean-square charge radius were deduced. The magnetic dipole moments are consistent with previous data. The ^{190,192}Tl isotopes show a considerable difference in quadrupole deformations as well as an anomalous isotope shift with respect to ^{194}Tl. A large isomer shift in ^{193}Tl is observed implying a larger deformation in the $9/2^-$ isomer than in the $1/2^+$ ground state. The ^{189,191,193}Tl isomers show increasing deformation away from stability. A deformed shell model calculation indicates that this increase in deformation can account for the dropping of the $9/2^-$ band in these isotopes while an increase in neutron pairing correlations, having opposite and compensating effects on the rotational moment of inertia, maintains the $9/2^-$ strong-coupled band structure.

TABLE OF CONTENTS

SECTION		PAGE
I.	INTRODUCTION	1
II.	EXPERIMENTAL SETUP AND METHOD	8
III.	PROBLEMS ALONG THE WAY	24
IV.	DATA ACQUISITION	32
V.	DATA ANALYSIS A. Theoretical Background B. Experimental Analysis: Extraction of hfs and IS from Data	40
VI.	INTERPRETATION OF RESULTS	67
LIST OF REFERENCES		83
APPENDIX		89
VITA		104

LIST OF TABLES

TABLE		PAGE
I.	Summed Spectra Information for Fig. 13	37
II.	Tl Hyperfine Constants Measured at UNISOR (in MHz)	62
III.	Tl Magnetic Moments and 535 nm Isotope Shifts	64
IV.	Tl Quadrupole Moments and Deformations	77

LIST OF FIGURES

FIGURE		PAGE
1.	Nuclear Shell Model Levels of Interest for Tl	2
2.	Light Odd-A Thallium Isotope Nuclear Levels	4
3.	Simplified Schematic of the Holifield Heavy Ion Research Facility	9
4.	The UNISOR Laser Facility	11
5.	Typical Data Set: ^{203}Tl	15
6.	Neutralization of Fast Ion Beams	17
7.	Thallium Atomic Levels	19
8.	The Fiber Optic Light Collector	20
9.	^{201,203,205}Tl Hyperfine Structure	23
10.	First On-Line Data: ^{192}Tl	34
11.	Second Set of On-Line Data (2 Oct 84)	35
12.	Data Set for ^{193}Tl	36
13.	Normalized Data for $^{189-193}$Tl	38
14.	Thallium hfs Splitting for Various Nuclear Spins	41
15.	Relative Line Strengths for Tl	48
16.	Effect of Nuclear Moments on Tl Atomic Levels for I = 9/2	58
17.	Effect of Nuclear Moments on Tl Atomic Levels for I = 7	60
18.	Tl Magnetic Dipole Moments	65
19.	Tl 535 nm Isotope Shifts	66
20.	Relative Isotope Shifts of Hg, Tl and Pb	70
21.	Tl 535 nm Field Shifts and Droplet Model Deformations	75
22.	Comparison of Theory and Experiment in Tl	80
A1.	Output Generated by OPTPUM	91

FIGURE PAGE

A2. The OPTPUM program 93

A3. Transitions and Their Notation for the Optical Pumping Model . 95

A4. Optical Pumping of the 535 nm Transitions in Tl for I = 7 . . . 102

A5. Relative Intensities of the hfs Components in Tl for I = 7 . . 103

I. INTRODUCTION

Thallium is one of the 92 naturally occurring elements on earth. However, it was not until 1861 that it was discovered (Weast, 1972). In that year, Crookes observed a previously unidentified, beautiful green spectral line and attributed it to a "new" element, thallium, named from the Greek word thallos, meaning a green shoot or twig. Thallium is found in several ores including pyrites, zinc and lead ores. Its appearance resembles that of lead, the next higher element in the periodic table. Thallium belongs to the third group of elements in the table, which it occupies with the chemically similar boron, aluminum, gallium and indium. Various thallium compounds are used commercially in photocells, infrared detectors, low melting glasses, high index of refraction glasses, rodentcides and ant killers. In all, more than 25 isotopes of thallium are known, most of them lacking the neutrons needed for the stability of ^{203}Tl and ^{205}Tl.

The feature that makes thallium the most interesting from a nuclear physics standpoint is that it has 81 protons, just one less than a magic number (Fig. 1). The stable isotopes of Tl are known to have a ground state nuclear spin of $1/2^+$, attributed to a single unpaired proton in the $3s_{1/2}$ level. This ground state spin has been detected or inferred both in the higher mass ^{207,209}Tl and in the lighter odd-mass Tl's down to ^{185}Tl (Tuli, 1985). In all of these, the neutrons remain paired as their number changes and so do not influence the ground state spin. Higher energy states of $3/2^+$ and $5/2^+$ have been observed in most of these isotopes (Newton et al., 1970; Schmidt, 1977; Kahler, 1978). Particularly intriguing, however, is that a $9/2^-$ isomeric level and its

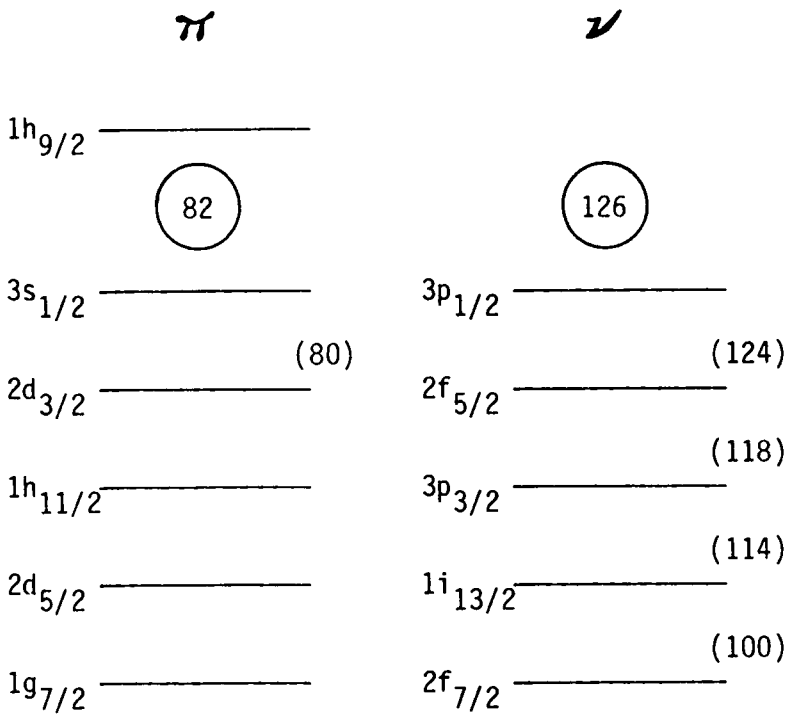


FIG. 1. Nuclear shell model levels of interest for Tl. Shell gaps occur at the magic numbers 82 and 126. Numbers in parentheses are total occupation numbers upon filling of an orbital.

higher collective band states have been observed to coexist in these lighter isotopes (Fig. 2), with the $9/2^-$ band dropping in energy with respect to the $1/2^+$ ground state as the neutron number N decreases until mass 189, then increasing in relative energy at mass 187 and lower. Throughout this region, the states built on the $9/2^-$ state maintain nearly constant energy level spacings. This $9/2^-$ band structure is ascribed to a $1h_{9/2}$ intruder state from across the Z = 82 shell gap (Fig. 1). The systematics of intruder states in the Z = 82 region are described in more detail in the review article by Heyde et al. (1983). It is noteworthy that similar intruder states are known in Au, Hg, Pb and Bi. There have been several attempts to explain this dropping of the $9/2^-$ band (Diamond and Stephens, 1963; Newton et al., 1970; Goodman, 1977). One simple explanation is that deformation produces the lowering, but the constancy of the level spacing of the states built on the $9/2^-$ isomer implies that the moment of inertia is not changing as one might expect it would for changing deformation. It is clear that these odd-mass isotopes represent worthy candidates for further study of their nuclear properties.

The even-mass Tl isotopes by their very nature present a more complicated picture in that they derive their properties from coupling of at least a single proton and a single neutron. In these, a ground state spin 2^- and isomeric 7^+ are the rule, with the 7^+ dropping relative to the 2^- much as its analog, the $9/2^-$ state in the odd-mass Tl's. For the even masses the intrigue arises from the magnetic dipole moments as well, for although the 2^- moments have been measured to change in a fairly consistent manner with mass number, the 7^+ isomer moments have

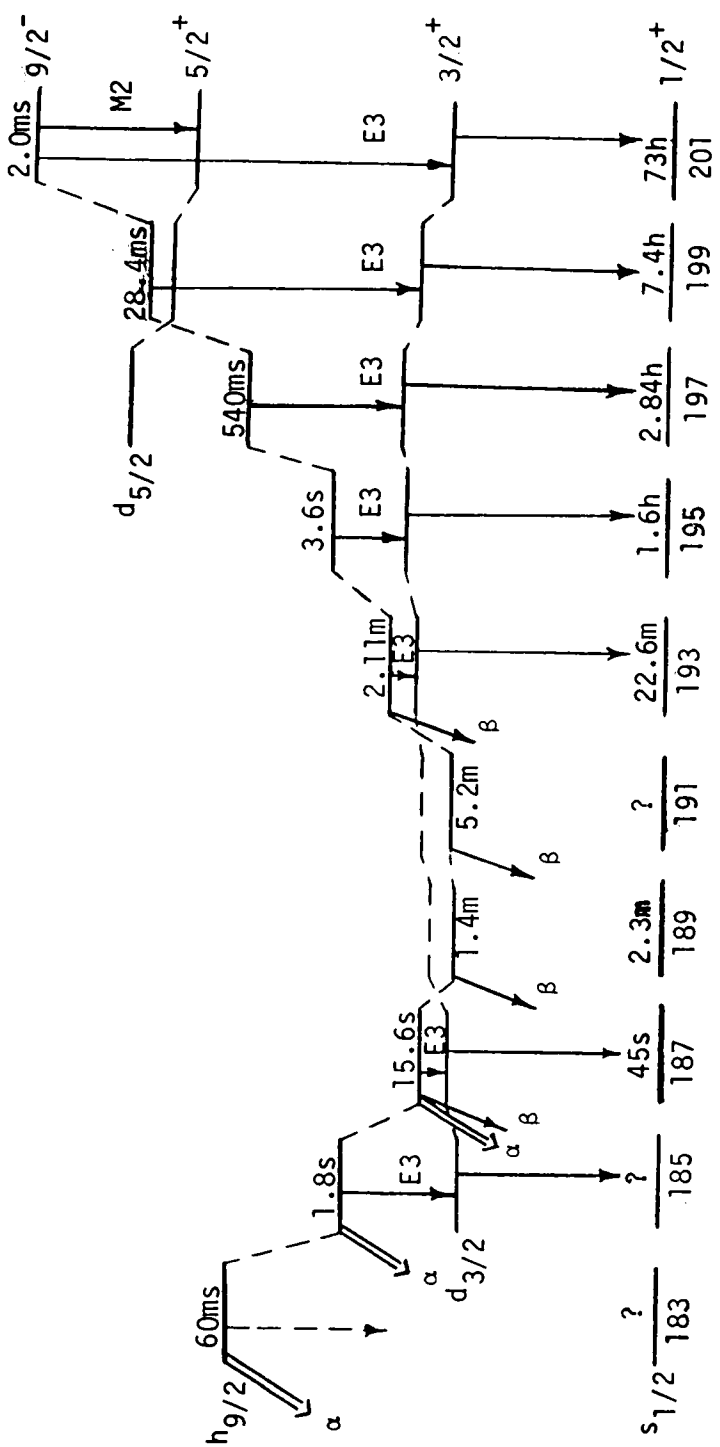


FIG. 2. Light odd-A thallium isotope nuclear levels. Information depicted comes from Goodman (1977), Heyde et al. (1983) and Coenen et al. (1984).

been observed to have quite a non-linear behavior as a function of neutron number N (Ekstrom, Wannberg and Shishodia, 1976). The ground state dipole moments have been attributed to mixtures of the configurations $\pi s_{1/2}\nu f_{5/2}$, $\pi s_{1/2}\nu p_{3/2}$ and $\pi d_{3/2}\nu p_{1/2}$, whereas the isomeric 7^+ dipole moments are the result of a $\pi s_{1/2}\nu i_{13/2}$ configuration having admixtures of $\pi h_{11/2}\nu p_{3/2}$, $\pi h_{9/2}\nu f_{5/2}$ and $\pi h_{11/2}\nu f_{5/2}$.

Since the nucleus of an atom interacts with the atom's electrons, one way to study nuclei is to carefully measure the atoms' electronic structures. An energy level diagram for the electrons of a given atom and charge state typically shows the terms of the atoms' fine structure due, for Russell-Saunders or L-S coupling, to different electron total angular momenta J. These terms are in fact split into hyperfine structure (hfs) levels having different values of another quantum number, F, caused by the coupling of J with the nuclear spin I.

The hfs of thallium has been the object of many investigations. Among these in this century, McLennan, McLay and Crawford studied the spark spectrum of singly ionized Tl II (1929) and interpreted the observed hfs (1931). Around 1930, a series of German articles appeared describing the hfs and effects of a magnetic field on the Tl optical spectra (Back and Wulff, 1930; Schuler and Keyston, 1931; Racah, 1931). Schuler and Keyston were the first to report the isotope shift (IS), or change in centers of gravity of levels, between ^{203}Tl and ^{205}Tl (1931). Racah (1932) and Rosenthal and Breit (1932) in their classic articles used Tl as an example for IS. Goudsmit (1933) derived Tl's nuclear magnetic moments from its hfs separations but was off by 10%. Crawford

and Schawlow (1949) compared theoretical predictions with experimental data on Tl to test several nuclear models.

Brink et al. (1957) performed atomic beam magnetic resonance (ABMR) experiments to measure the spins of ^{197,198,199,204}Tl and the ^{204}Tl hfs splitting. In a 1960 article, Odinstov reported measurements of the IS and hfs of six different lines of the stable ^{203,205}Tl obtaining an accuracy of better than 15 MHz using an atomic beam and a Fabry-Perot etalon. In 1961, Hull and Stroke reported the first IS measurements on the radioactive nuclei ^{199,200,201,202,204}Tl produced by Au(α,xn)Tl and Hg(d,xn)Tl reactions whose products were placed in a lamp. They observed lines at 377 nm and 535 nm but were unable to resolve all of the hfs splittings due to a Doppler broadening of about 900 MHz. Their estimated uncertainties in hfs splitting determinations were ± 120 MHz (± one standard deviation). Schuler et al. (1962) remeasured ^{203,205}Tl using atomic beam absorption and a Fabry-Perot etalon crossed with a 10-inch diffraction grating to determine the $7^2S_{1/2}$ to $6^2P_{3/2}$ IS. Davis, Kleiman and Aung (1964) extended measurements to ^{197,198}Tl and Goorvitch, Kleiman and Davis (1966 and 1967) to ^{194,195,196}Tl. These experiments used lamps and also had measurement uncertainties of 120 MHz. The latest article summarizing the optical hfs and IS measurements of Tl was by Goorvitch, Kleiman and Davis in 1969. Since that time, more ABMR experiments have been performed, these by Ekstrom, Wannberg and Shishodia (1976) who measured Tl's $6^2P_{1/2}$ atomic ground state. Their measurements produced more accurate hfs splitting values, moments and also spin determinations in $^{194-202}$Tl, but could by their ABMR origin supply no IS information. Two-photon

absorption was used by Flusberg, Mossberg and Hartman (1976) to measure the hfs and IS of the 7^2P states in natural Tl. As recently as 1984, Neugart reported results with Stroke of the optical measurements of ^{207}Tl, while Baig and Connerade (1985) returned to ^{nat}Tl using synchrotron radiation to measure high lying states and to obtain a precise value for the ionization potential of Tl.

No electromagnetic moments have been previously measured below mass 194 in Tl. Isotope shifts of spectral lines, from which can be extracted information on the changes of size of nuclei, also extend only as low as ^{194}Tl. This dissertation reports on the laser spectroscopy measurements of the stable isotopes of Tl and some light Tl isotopes with $A < 194$. Results from these measurements are presented herein and comparisons and contrasts are made to data on the other isotopes. Possible explanations of some features are also presented. The present tense of verbs is used frequently in the discussion of the equipment since the laser facility described has only begun with this data its study of nuclei far from stability. Future experiments on other Tl nuclei and even other elements will be made using nearly the same equipment.

II. EXPERIMENTAL SETUP AND METHOD

The University Isotope Separator at Oak Ridge (UNISOR) is one of the many target stations of the Holifield Heavy Ion Research Facility (HHIRF). The facility is shown in a simplified form in Fig. 3. Originally based around the Oak Ridge Isochronous Cyclotron (ORIC), HHIRF now operates primarily with its National Electrostatics Corporation 25 MV tandem accelerator; occasionally in coupled operation the tandem serves as the injector to the cyclotron. A large variety of elements can be injected into the tandem from its negative ion source, which essentially attaches an extra electron to neutral atoms. The negative ions are then accelerated toward the tandem terminal whose potential is typically 16 to 22 MV. At arrival the negative ions have several electrons removed by either a foil or gas stripper. Now with a large positive charge, the ions are deflected and then accelerated away from the terminal. At the base of the tandem, the now fully accelerated heavy ions are directed along the appropriate beam line where, with the use of ion optics, they are delivered to the required target station.

UNISOR, representing a consortium of several academic institutions, was created in the early 1970's primarily to study neutron-deficient nuclei far from β-stability (Spejewski, Mlekodaj and Carter, 1981). The HHIRF heavy ion beams are used as projectiles whose target is often part of the UNISOR ion source. Exotic nuclei created by these heavy ion collisions are electrically extracted from the ion source and accelerated, usually by a 50 kV potential, to the isotope separating magnet. As many as three masses can be studied at once by utilizing all three end beam lines. Many successful studies on the mass-separated

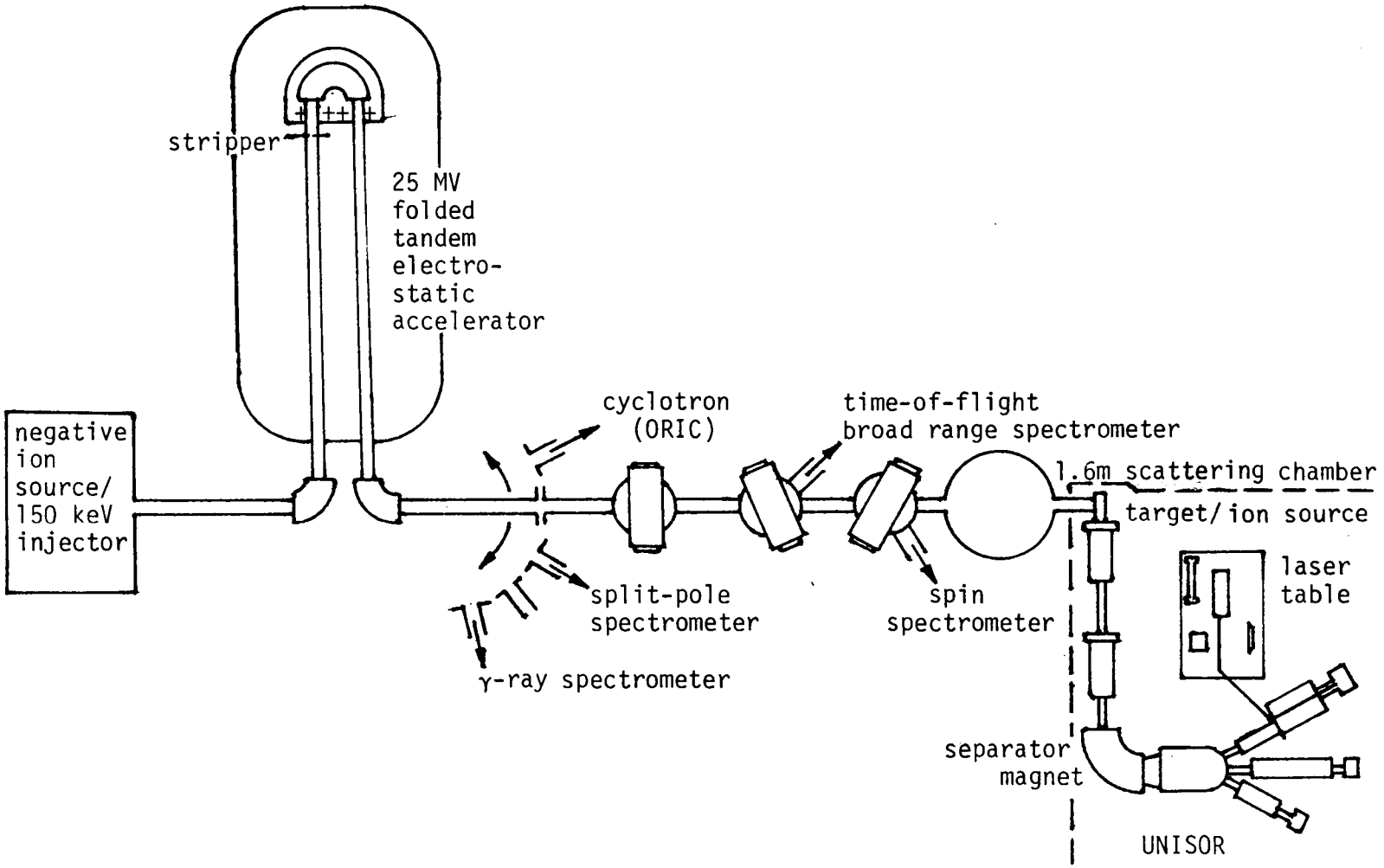


FIG. 3. Simplified schematic of the Holifield Heavy Ion Research Facility.

isotopes have been made using γ-ray, α and e^- detectors. After several years of operating, it was decided to add a laser to increase the amount of nuclear information extracted from these isotopes. In particular and as will be detailed later in this work, the hyperfine structure of atoms can be measured with a laser to reveal the nuclear spin I, the magnetic dipole moment μ, the spectroscopic quadrupole moment Q_S, and the change in radial moments of the charge distribution. This dissertation research is the first successful application of the UNISOR laser facility to study neutron-deficient nuclei. As with UNISOR as a whole, the laser project's success is due to the efforts of many individuals contributing as part of a team. Many but by no means all of these people were mentioned in the acknowledgments.

A more detailed schematic of the laser facility at UNISOR is given in Fig. 4. The method chosen to measure atomic hfs is collinear fast atom beam laser spectroscopy. In this method, the ion beam from the separator is electrostatically deflected to be collinear with a laser beam. The laser light is used to excite atomic transitions in either the ions in the beam or in neutralized atoms that can be created by letting the ion beam pass through a vapor cell in which it can undergo charge exchange. The effects of excitation, normally fluorescence (the induced reemission of light), is detected and recorded as a function of laser frequency. Variations of this, such as two-photon excitation for resonance ionization spectroscopy, saturated absorption spectroscopy, or tuning the accelerating voltage rather than the laser frequency are possible. Collinear laser spectroscopy is not a Doppler-free technique, but Kaufmann (1976) showed that it results in a reduced

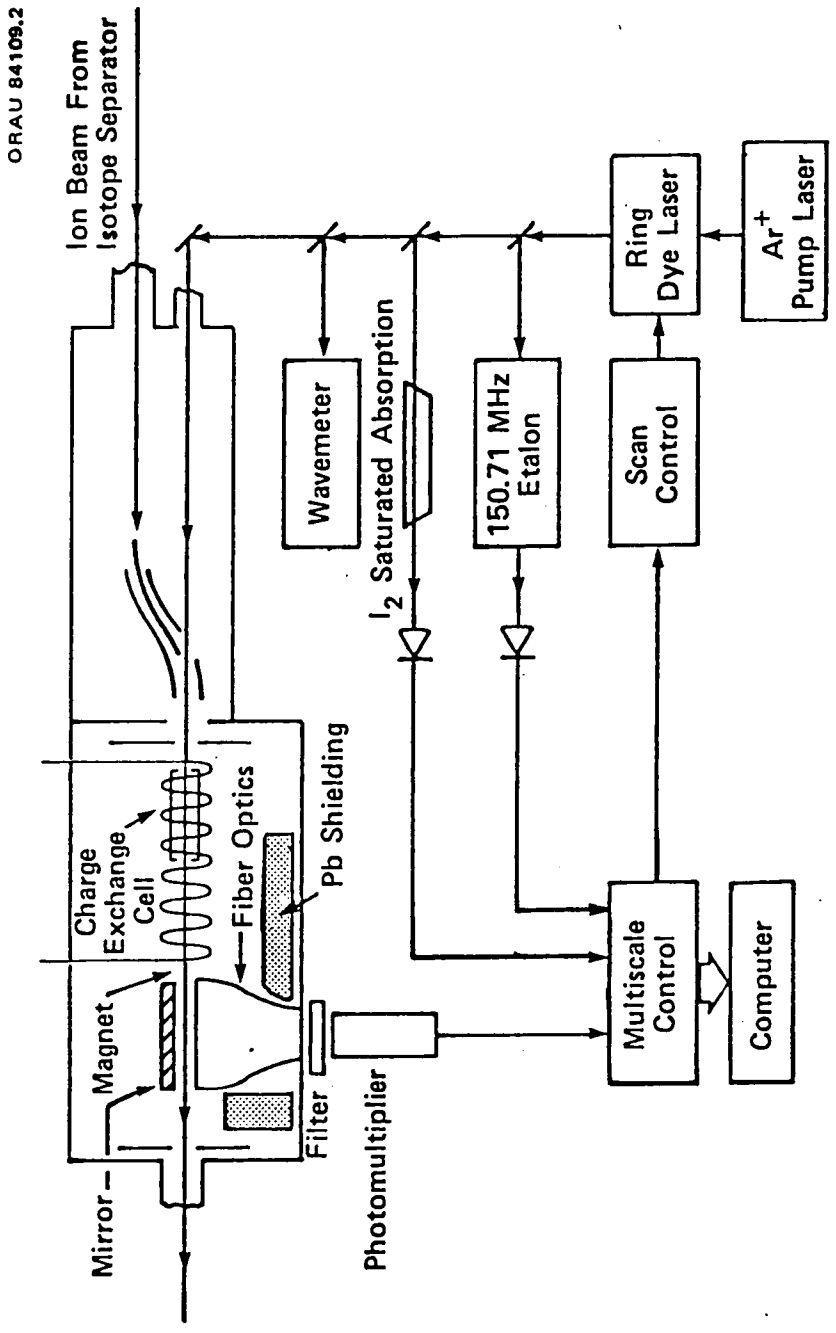


FIG. 4. The UNISOR laser facility.

Doppler width as compared to spectroscopy on atoms confined to a cell due to velocity bunching of the ions. Accelerated ions have essentially the same energy distribution as in a cell, but the distribution is centered about a much higher energy, qV_{acc}. Since the velocity goes as the square root of the energy, the relative velocity spread is reduced and the Doppler width, which depends on this spread, is decreased.

The lasers used at the UNISOR laser facility are an Ar^+ ion laser, a Coherent 699-21 ring dye laser, and a small HeNe laser. The Ar^+ laser, running at about six watts output power, serves as the pumping laser for the dye. The excited dye fluoresces and lases at a somewhat independent longer wavelength determined by the dye and optics in the ring. This wavelength is electronically tunable in the 699-21 laser over a range of up to 30 GHz. For green light at 500 nm the absolute frequency is 6×10^{14} Hz, hence the maximum scan range is in fact a change in frequency of only one part in twenty thousand. Whereas this seems to be a small amount, it is quite sufficient when one considers that the laser linewidth is less than 1 MHz, many atomic linewidths are of the order of tens of MHz, and many hyperfine structures (hfs) and isotope shifts (IS) are on the order of a few GHz.

To correctly tune the dye laser for an experiment, its lasing wavelength must be known precisely. To this end, a "homemade" wavemeter (Carter et al., 1982) was used initially. A travelling Michelson interferometer, the wavemeter worked by counting beats between the dye laser beam and the beam from a stabilized HeNe laser. A microprocessor interpreted these beats to display the dye laser beam's wave number to 0.001 cm^{-1}. (Here it is useful to note that throughout this work the

most common nomenclatures will be used. In the case of atomic spectroscopy it is the norm to speak of frequencies in hertz, optical wavelengths in nanometers (or sometimes in angstroms), and wave numbers in inverse centimeters. Although any one of the three could be used to replace the other two, it is not normal to do so.) The original wavemeter has since been replaced by a commercial version which is not quite as accurate but is easier to use.

The wavemeter accuracy is excellent for tuning the dye laser to the correct wavelength but is too coarse for measurements of the sort desired in this work. For measurements of hyperfine splittings, the frequency markers from a passively stabilized 150 MHz etalon are used: laser light passing through an etalon reaches peak transmission intensities which are spaced apart in frequency by the free spectral range (FSR) of the etalon, thus forming distinct markers. The etalon rests in its own vacuum housing, designed by the author, to reduce peak drifts due to pressure fluctuations and, to a lesser extent, temperature variations. As the laser is electronically scanned in frequency, the etalon creates with its markers a frequency ruler by which spectra separations can be measured. This procedure eliminates the need for an exact calibration of the laser scan control which is quite non-linear. With the frequency markers it is necessary only to count FSR's; a linear interpolation between markers to determine fractional spacings is quite sufficient in most analyses. The etalon used in this work was carefully measured to have a FSR of 150.710(10) MHz using the method of exact fractions (Goldsmith et al., 1979).

An iodine saturated absorption system provides an absolute frequency reference (For a description of saturated absorption spectroscopy see Letokhov, 1976). The wave numbers of thousands of optical wavelength transitions in I_2 have been tabulated by Gerstenkorn and Luc (1978) who also provide details of how to determine the centroids of the resolved hfs components (1979). The I_2 transition energies are independent of any changes in the experimental apparatus since the I_2 is in an external cell. The I_2 thus provides unequivocal absolute dye laser frequency reference points. Since only one mass can be directed down the beam line at a time, the I_2 spectra act as a reference for data sets on different isotopes thus allowing accurate isotope shifts to be obtained.

Typically four spectra are recorded simultaneously as the laser frequency is increased: the photomultiplier tube (PMT) signal rate due to light collected by the fiber optics (Fig. 4), both the Doppler-broadened and Doppler-reduced I_2 signal rates, and the etalon signal rate (Fig. 5). A specially designed multiscale control produces a ramp signal which causes the ring laser to change frequency. As the ramp voltage increases, the spectra are recorded with channel-to-channel correspondence into a PDP 11/34 computer. Thus, for example, if four 1024 channel spectra are being taken, channels n, n + 1024, n + 2048, and n + 3072 accumulate counts at the same time, while all others are idle. The sweep time of the ramp can be varied manually, or set to scan quickly over peak-free regions of a spectrum. Typically the ramp sweep time is 30 seconds and many scans are added to form a data set.

Data sets for the same isotope can be added together by normalizing channels prior to adding by using the I_2 hfs peak positions.

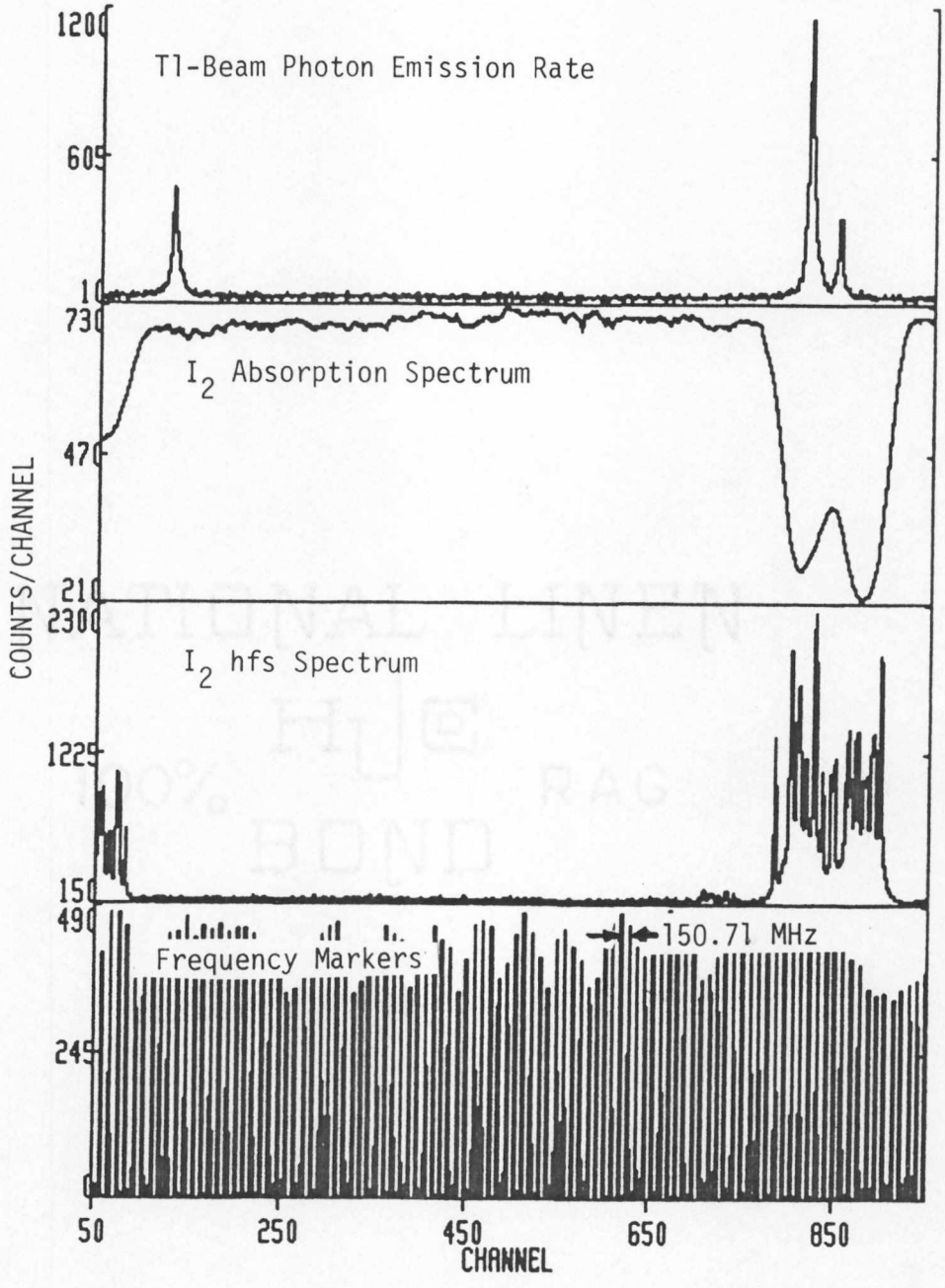


FIG. 5. Typical data set: ^{203}Tl. Higher channel numbers correspond to higher laser frequencies. The spectra are recorded simultaneously.

This is essential for on-line studies where production rates affect the signal-to-noise of the observed peaks. Stability of the laser system can be monitored by comparing data sets before adding. Laser drift, the change in the laser frequency scanning range with time, can be detected by noting the change in channel number of any particular I_2 hfs component. Any change in relative positions of atomic transitions of a single isotope with respect to the I_2 reflects separator accelerator voltage drifts. These drifts limit the number of data sets that can be added together without losing the resolution required for accurate measurements. Etalon marker drift, due to temperature or pressure changes, tends to broaden the frequency markers during long data set acquisitions, so short (two or three) scans are taken occassionally to provide well-resolved markers throughout the laser scan region.

Returning to the description of the components shown in Fig. 4, page 11, it is seen that the ion beam from the separator passes through a charge exchange cell. Normally, ionized atoms have their strongest transitions in the ultraviolet (UV). However, dye lasers are better suited for optical wavelength transitions. By neutralizing the ion beam in a charge exchange process wherein the ions pick up an electron from an alkali metal vapor in the cell, an atom beam is produced with which the visible dye laser beam may interact. Figure 6 shows neutralization curves, obtained for several elements of interest undergoing charge exchange with either Cs or Na, as a function of charge exchange cell temperature. It can be seen that Kr and Xe are most efficiently neutralized with Cs, while Tl is best neutralized with Na. In the case of Tl, the Na ionization potential is just 0.003 eV different from the energy

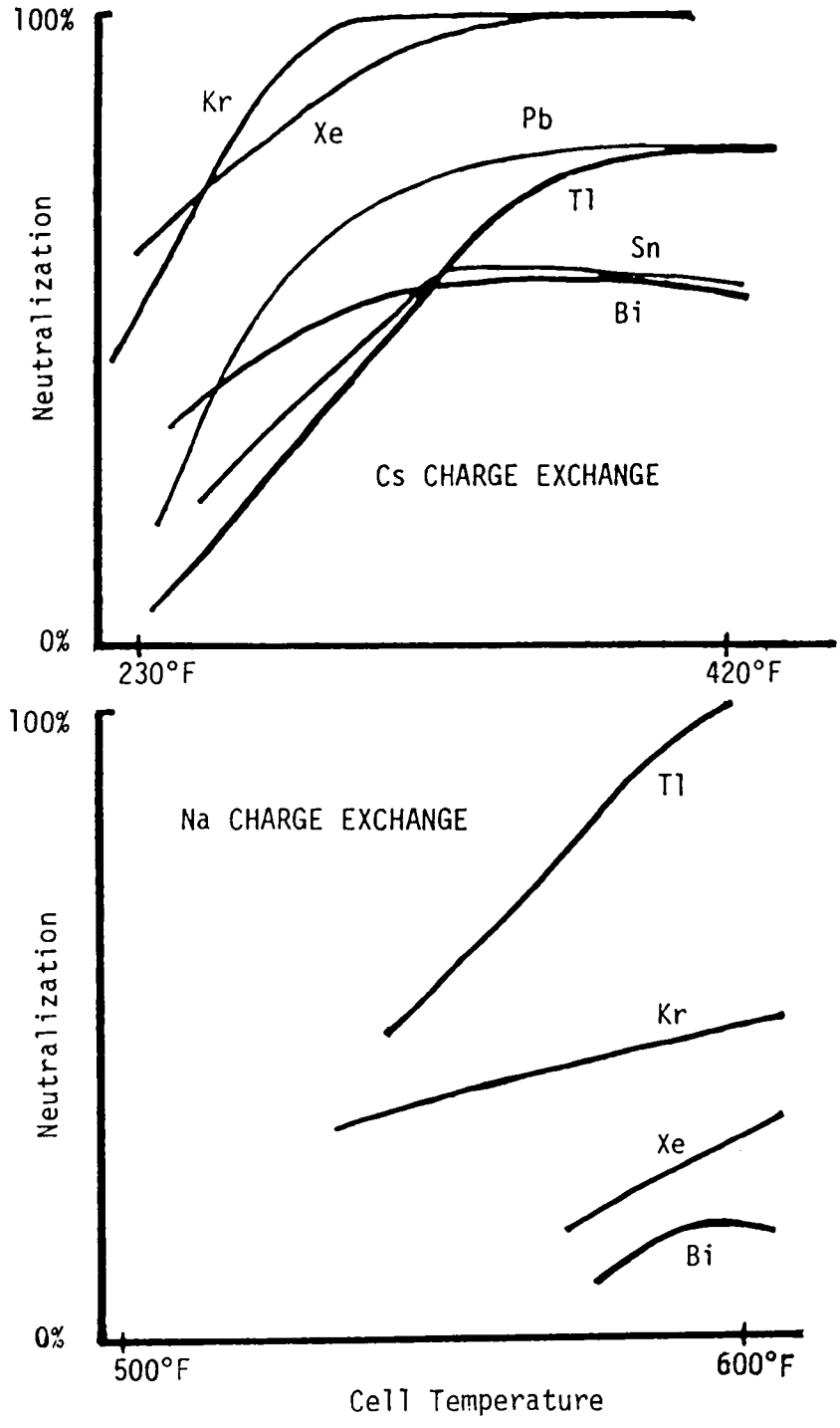


FIG. 6. Neutralization of fast ion beams.

required to ionize Tl from its $6s^2 6p\ ^2P_{3/2}$ metastable atomic state. This similarity plus the relatively wide spacing of atomic terms about Tl's metastable state cause virtually all of the Tl ions when neutralized to be left in this metastable state. This is precisely what is desired, for there exist dye laser accessible transitions at 535 nm from this level (Fig. 7). Furthermore, whereas once excited the Tl atom might decay back to the same metastable state, it is nearly equally possible to decay down to the ground state via a 377 nm transition: the transition rates are 0.705 and 0.625 x 10^8 s^{-1}, respectively (Reader et al., 1980). The proper choice of filters allows monitoring of the 377 nm wavelength range while blocking the 535 nm laser light, hence enormously reducing the PMT background counts due to stray or scattered laser light. The PMT, an EMI model 9635QB, was chosen for its particularly high quantum efficiency (~26%) at 377 nm and its very high gain.

To channel light from a cylindrical source, the atom beam, to the circular PMT face, fiber optics are used (Fig. 8). The fibers were chosen for high transmission at 377 nm (~72%). The length of the fibers parallel to the beam is a consequence of having the surface area of the fiber ends match the surface area of the face of the PMT tube. The specified numerical aperture of the fibers is 0.66, i.e., light entering the fibers at an angle up to $\sin^{-1}0.66$ from normal is transmitted. The fiber bundles themselves are complemented by an aluminized mirror which completes the encirclement of the atom beam. Calculations show that 44% of the light sphere emitted by an on-axis point source should be accepted by the fibers with the mirror in place. Coupled with the 72% UV transmission, the net fiber optic efficiency should be 32%. Whereas

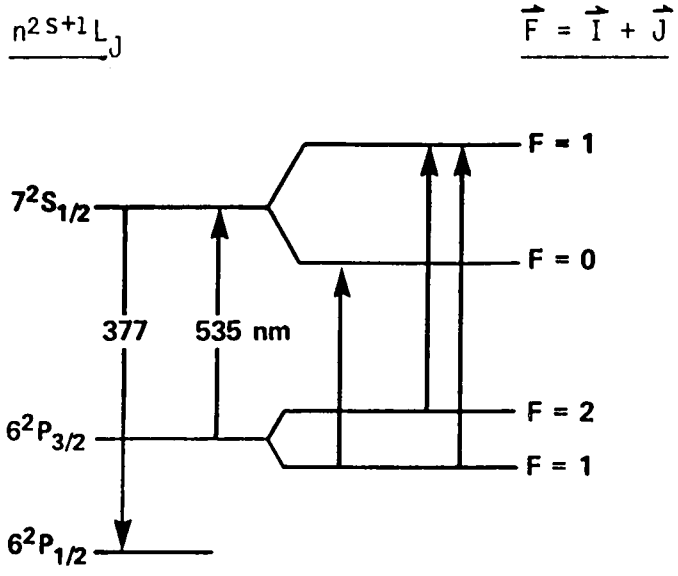


FIG. 7. Thallium atomic levels. The hfs splitting into different F values is not to scale. Laser excitation at 535 nm from the metastable $6^2P_{3/2}$ term results in the monitored decay to the ground state via the 377 nm transition.

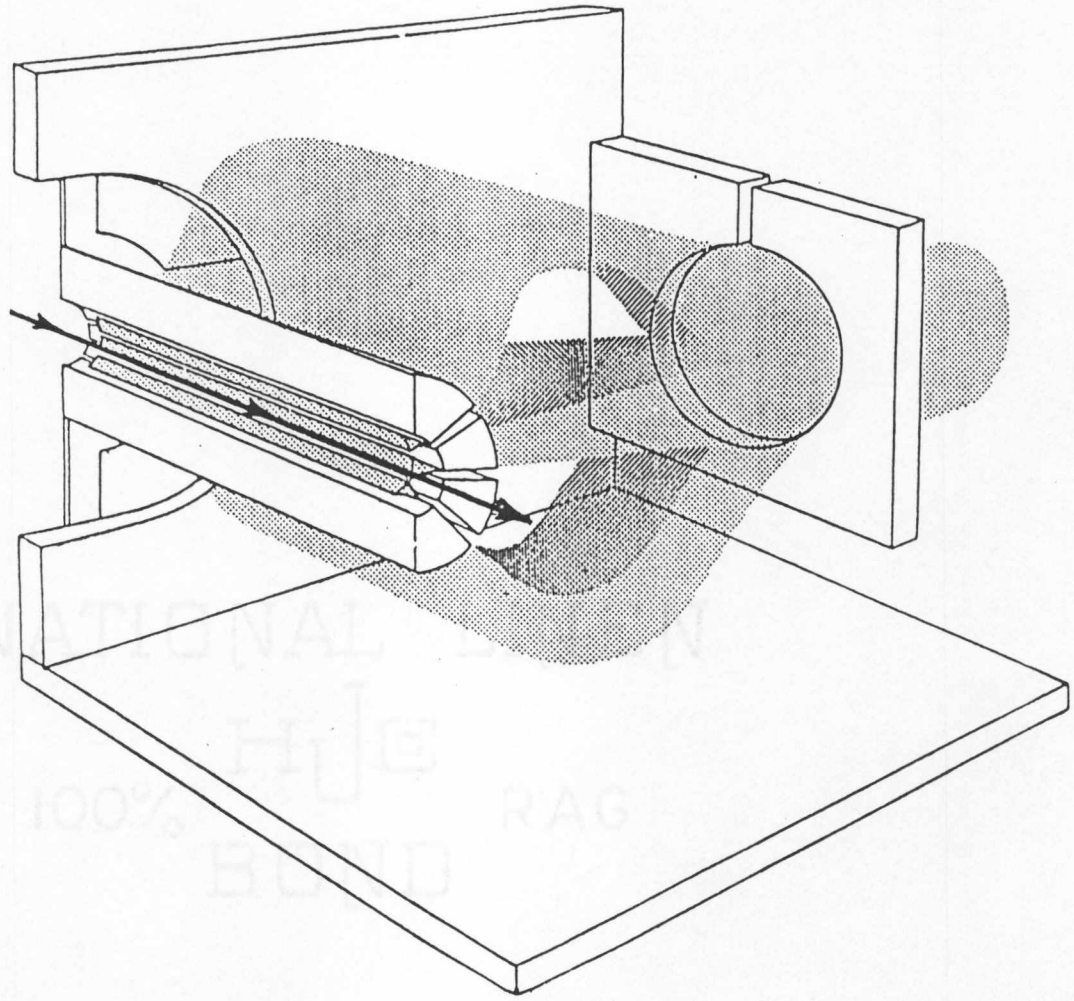


FIG. 8. The fiber optic light collector. The shaded portion represents the fibers. The overlapping laser and atom beams are indicated by the arrowed line. Not shown in the figure is a cylindrical mirror which completes the encirclement of the beams.

this efficiency is less than what could be expected by an ellipsoidal mirror, this fiber optic system is advantageous in that its efficiency is applicable to its length of 10.85 cm, which is considerably longer than the observation region of an ellipsoidal mirror or simple lenses. The aforementioned filter forms a vacuum chamber window against which the fibers are placed. A reflecting aluminized coupling tube helps prevent losses by spanning the space between the filter(s) and the photocathode of the PMT in its housing.

Proper placement of the fiber optics along the beam path is essential. In the case of Tl, the fibers are placed downstream of the cell to avoid having Na deposited on them. To prevent signals from occuring before the atoms arrive in the observation region, a solenoidal magnetic field is applied to Zeeman shift the Tl atomic levels out of resonance with the laser in the region prior to the observation zone. The magnetic field is sharply attenuated by μ-metal shielding and the magnets are slightly spaced from the fibers so that no Zeeman splitting is actually observed: at 50 keV, Tl atoms travel 21 cm/μs and with the excited state lifetime for decay to the ground state being 16 ns, most deexcitations occur within 1 cm. It has been found that for the final cell-to-fibers geometry chosen, the application of the magnetic field increases the signal rate threefold.

In order to get an unquestionable value for the detection efficiency of the system, the hfs of the commercially available radioactive isotope ^{201}Tl was measured. Previous tests using stable beams measured the efficiency as well, but counting the neutral beams at rates below a few times 10^6 atoms per second proved to be difficult. With ^{201}Tl,

accurate beam rates were measured by depositing the beam on a tape which was periodically moved so as to place the deposit spot in front of a GeLi detector where activity could be counted. This tape deposit-move-count system is referred to as the tape transport system and is also used in on-line work. The detector efficiency for this geometry was determined from calibrations using standard gamma-ray sources. Once the ^{201}Tl PMT signal was obtained, the beam rate was intentionally cut back to find a lower limit for practical observing and thus the sensitivity of the system. Figure 9 shows the composite spectra of ^{201}Tl taken at 8.5×10^4 atoms/s for 27 minutes in relation to the stable ^{203,205}Tl. The photon detection efficiency was found to be 1/1000, i.e., for the strongest peak, one in one thousand atoms is being detected. It was also estimated that with this efficiency the lowest beam rate for which it would be practical to accumulate data would be about 6×10^4 atoms/s. With this as the limit, many on-line produced Tl isotopes could be studied.

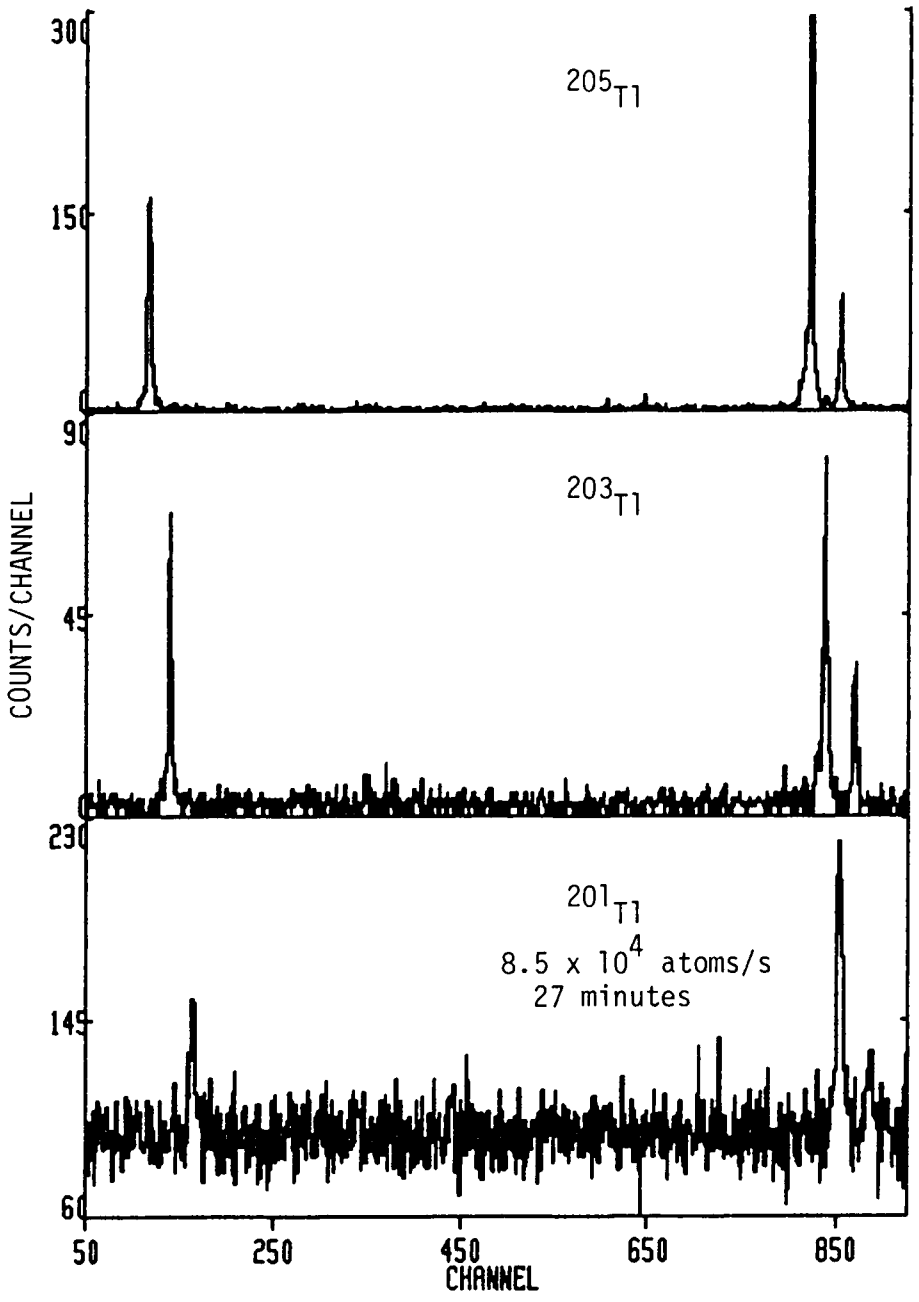


FIG. 9. ^{201,203,205}Tl hyperfine structure.

III. PROBLEMS ALONG THE WAY

The laser spectroscopy system described thus far did not come into being all at once. As with nearly all experiments, there were problems along the way that had to be solved. This section is for the experimentalist who may someday face similar tasks or for those who wonder why it took so long to perform these experiments. Important aspects not yet mentioned about the components are included, as are many of the encountered problems along with their solutions.

One of the developmental tasks has been the charge exchange cell. Several cells were tested. Problems associated with these were low neutralization efficiency, too rapid Na expiration, Na deposits in the wrong places and heater burnout. Of these, the first two were obvious manisfestations of density and temperature; they were corrected by using data such as in Fig. 6, page 17, to determine optimum operating temperatures for cells having enough Na volume. Sodium deposits have been as bad as to have coated insulators to deflection plates causing electrical breakdowns and to have blocked atom beam transmission through the cell. It was found that uneven heating was the major cause of these problems. Sodium melts at ~98°C and so all parts of the cell need to remain hotter than this. The thermocouples connected to the cell give accurate temperatures, but only of that to which they are connected; substantial gradients exist across the cell. The plug-in heater units themselves have a considerable gradient: a unit heated in vacuum was measured to have a temperature of 520°C at its middle, 245°C at one end, and 40°C on its wires 3.5 cm from the end. A modified charge exchange cell design with reduced mass and four heater units -- two for the cell

body and one for each end -- has proven to be the most efficient to date. The heaters have less mass to heat and so can operate at a lower power thus extending their lifetimes to several weeks. Sodium deposits have been nearly eliminated by collimation and by gradual temperature changes to and from those operating temperatures that have been found to be the best. A loaded cell now can run more than three days before losing all of its Na. This is generally sufficient for collecting data on one or two on-line isotopes.

The fiber optics system has undergone few structural changes. As mentioned earlier, the materials and design were chosen for maximum UV transmission and to match the face of the PMT. Prior testing with a sample of fibers showed that although pump-down time is increased with the outgassing of the large surface area of the fibers, the increase is not prohibitive. The design includes sites for two plug-in heaters whose purpose was to heat the fibers to drive off any Na deposits. Two cylindrical mirrors aluminized on either the near or back sides of the glass were tried and it was found that heating of the fibers caused degredation of the near-side coated mirror even resulting in aluminum flakes peeling off into the beam path. Since Na evaporation from the fibers was never as much as expected, the fiber optic system was displaced along the beam axis away from the charge exchange cell and more collimation was introduced. Careful alignment is required to prevent the laser or ion beams from striking the fibers; fortunately the laser beam itself makes an excellent alignment tool. In the new, unheated position the fibers have performed admirably, but it has become necessary to introduce the Zeeman magnets described below. Another

consideration has been the effect of radiation on the fibers themselves: it has been found that gamma radiation induces fluorescence but that most of it is blocked by the filter used (almost all of it can be blocked by a red Corning 2-58 filter), thus the effect is inconsequential. There have been some fibers broken in handling but the percentage is quite small. Finally, cleaning of the fiber ends using jeweler's grit has proven successful.

The further the fiber optic light collector is displaced from the charge exchange cell, the greater is the probability of transitions occuring before the atoms reach the observation region. To prevent laser excitations, one approach is to shift the level spacings of the atoms by applying a magnetic field. A very small magnetic field will cause the hfs F-levels to divide into component m_F levels separated by an amount dependent upon the applied field strength. For the lowest fields, the splitting increases linearly with applied field: this is the well-known Zeeman effect. Once the splittings become comparable in size to the original F-level splittings, F begins to be no longer a good quantum number. Increasing the field further decouples I and J completely to create a pure Paschen-Back effect. If the laser is tuned to the frequency at which a transition will occur between two zero-field F-levels, that transition will not take place if the atom is in a magnetic field which has changed the level spacing by more than the transition linewidth. For a Doppler-broadened Tl linewidth of 60 MHz, few observable atoms would be lost if the magnetic field changed the level separations by at least 60 MHz. The F = 2 to F = 1 energy difference for the $6^2P_{3/2}$ term in Tl is on the order of 520 MHz for spin 1/2 nuclei

(Heilig and Steudel, 1974). Thus the desired splitting is easily calculable assuming a Zeeman effect. As it turns out, not all of the 535 nm hfs transitions can be shifted. The three zero-field transitions become a total of 19 applied-field transitions, six of which are degenerate in energy with others. Five of the 19 transitions have the same energy as the zero-field transitions. The solenoidal geometry necessary for not deflecting the ions is perpendicular to the laser polarization and prevents application of the $\Delta m_F = 0, \pm 1$ selection rule. As a result, regardless of field strength some percentage of atoms is pumped away by the laser prior to their arrival in the observation region. The fractional loss is, however, tolerable. The situation is more complicated for isotopes with higher nuclear spins: for I = 9/2 there are six zero-field transitions and the lowest energy F - F' transition splits into 19 separate energy transitions, the next higher F - F' transition splits into 27 separate energies, etc. As with the spin 1/2, it was found that most of the transitions should be shifted the required amount for an applied field on the order of 250 gauss. Solenoidal magnets capable of supplying this field were designed by the author to surround the charge exchange cell and span the distance from the cell to the fibers.

The magnets themselves are of very simple design, being fine wire wound onto appropriate size spindles. Restricted by the working volume and the power supplies, several wire types were tested; the larger wires could carry more current but resulted in magnets with fewer turns. It is a simple derivation to show that the power required for a given magnetic field is constant for a given mass and volume of conductor. In practice using one-pound spools of shellac-coated wire, it was found

that the higher gauge (thinner) wires gave both more gauss per amp and more gauss per watt of joule heating than the thicker conductor wires. Twenty-eight gauge wire was chosen for its efficiency over lower gauge wires and its strength over higher gauge wires. As is often the case with small coiled magnets, almost all the dc current that could be supplied was used to obtain the desired fields. Joule heating was found to go as the square of the applied field as expected. Naturally, as the coils became hotter their resistances increased. To maintain the same field over a period of time meant applying a constant current for which an increasing voltage was needed. Higher voltages meant higher powers to dissipate from the magnets. This self-heating, along with heating from being close to the charge exchange cell, was responsible for insulation breakdowns and enormous outgassing in the early versions. The charge exchange cell was modified to its present form to accommodate a water-cooled version of the magnets. Both cell and magnets benefited from the changes. The cell body became flanked by two magnet windings through which its arms pass. A stand-alone, uncooled 8.5 cm long coil shielded in μ-metal spans the cell-to-fibers distance. Its long geometry allows higher fields inside with less power: the other coils' fields extend outside their width to encompass the cell. Coil performance was measured with a gaussmeter and shown to be satisfactory over the desired region. Continued good operation is monitored by measuring the coil resistances to make sure that no breakdowns have occured. For example, one of the cell coils measures resistances of 140 Ω at room temperature, 138 Ω when cooled, and 170 Ω when in use. The optimum magnetic fields and laser powers were determined experimentally.

In addition to design changes such as those already discussed, there were many other problems encountered. Occasional vacuum leaks or trivial (although perplexing) problems like bolts that disappear when dropped on the floor are normal in experimentation. For on-line work, target burnout is to be expected at high beam rates. Unexpected were the deaths of not one, but several, Ar^+ ion laser tubes requiring replacement and preventing laser use in the interim. Computer problems, both user and hardware but neither type anticipated, have had to be corrected. Tape transport problems in the form of the tape coming off of its take-up reel have happened. The transmission of ions through the laser experimental chamber has at times dropped off considerably. Several realignments and a thorough separator cleaning have increased transmission to over 90% only to see it fall off and reappear in an as yet not completely understood manner. Other delays as far as the spectroscopy of Tl is concerned have been some time spent on a defunct Li experiment and a successful relativity experiment using H (Juncar et al., 1985), although knowledge gained in these experiments was certainly beneficial for this research.

The dye laser uses Rhodamine 560 spiked with a small amount of ammonium hydroxide to produce several hundred milliwatts output of 535 nm laser radiation of which 10 to 20 mW is sent down the beam line during experiments. The spiked dye far outlasts its claimed lifetime, but nevertheless does require occasional changing. The laser beam diameter was measured to determine the best lens to use prior to the vacuum chamber in order to produce the desired beam waist in the observation region. Mode hops, where the laser scan range jumps in

frequency, are a daily occurrence but are minimized by careful cleaning and alignment of the ring laser. The laser table components require careful alignment but once set generally prove reliable over a long period. A striking exception to this is the frequency marker etalon's vacuum housing. Repeated breakdowns of the housing's epoxy window seals prompted a change to O-ring window seals. This made the housing air-tight, but the etalon still requires a considerable time to pump down apparently due to outgassing.

The PMT tube choice has already been explained. It is operated at +1300 V in the photon counting mode. Several PMT housings for the tube were tried with the final choice being a FACT 50 MK-III which was found to work very well. A specially designed coupler mates the housing to the vacuum chamber nearly eliminating light leak problems. The viewing port through which can be observed the end-of-the-beam-line Faraday cup, channeltron and tape spindle has been modified to be light-tight when not in use, thus also reducing the background. A Corning 7-51 filter is used which transmits 75% of 377 nm UV but a mere $10^{-6.5}$ of 535 nm light. However, as yet unexplained is that the addition of a second such filter has been observed to reduce the laser light background by only 3% more. Most filters and many other objects were found to fluoresce when exposed to (UV?) light; laser-induced fluorescences may be contributing to the background. Radiation-induced background in the PMT during on-line runs has been minimized with Pb shielding of collimators after tests found the PMT cathode to be sensitive to gamma radiation. Pulse height spectra of the PMT signals for light, gamma and X rays proved to be too similar to expect to be able to effectively

discriminate between them. Even with the shielding, the background rate is seen to jump from 30 - 50 counts/s up to 300 - 400 counts/s during on-line runs. When the separator beam is removed the background is observed to decay with the half-life of the isotope being studied showing that the counts are induced by radiation and not by light from the separator beams.

A channeltron, a cornucopia-shaped electron multiplier, is used to tune the beam through the laser chamber during on-line runs by detecting the spallation electrons from the neutral beam impacting on the tape. For very low beam rates, the separator beam can be tuned directly down the throat of the channeltron. Coincidence counting with the PMT was found to be impractical due to large beams of contaminants being present simultaneously with the desired atom beam and because the channeltron is sometimes sensitive to laser light.

Summarizing, as the system used for spectroscopy of Tl grew onto its final form, many problems were overcome. Component selection and development were done in a thoughtful manner to insure success. The PMT bias, discriminator settings, laser power, magnet currents, charge exchange cell temperatures and collimator sizes were all optimized for highest detection efficiency. A few problems were never solved and were simply tolerated. Some further improvements, such as a longer lasting charge exchange cell system with improved solenoidal windings or more Pb shielding for the PMT, could still be made but were not necessary for the data taken here. The key point is that good data were taken with the present apparatus as will be described in the next section.

IV. DATA ACQUISITION

Data on ^{203,205}Tl has been routinely available by placing some natural Tl in the ion source of the separator. Radioactive ^{201}Tl was investigated by obtaining it from a nuclear pharmacy and placing it, too, in the ion source. The short-lived Tl isotopes were not commercially available. To examine these, they had to be produced on-line using heavy ion collisions. It was found that the highest production rates utilizing the heavy ion beams available at HHIRF were obtained with W(^{16}O,xn)Tl and Ta(^{16}O,pxn)Tl reactions. Between these it was found in on-line developmental runs that stacked Ta target foils worked better. The maximum obtainable beam intensity of ^{16}O was used in order to produce the highest possible output of Tl for laser spectroscopy. Data on the light isotopes $^{189-193}$Tl were obtained in five on-line runs. Beams of 110 MeV $^{16}O^{6+}$, 125 MeV $^{16}O^{6+}$ and 155 MeV $^{16}O^{7+}$ were used to produce ^{192,193}Tl, ^{190,191}Tl and ^{189}Tl, respectively. Mass-separated beam rates of up to 4 x 10^5 atoms/s were produced, with lighter masses having lower rates. Isotopes with masses greater than 193 or less than 189 were not sufficiently produced to study; e.g., the ^{188}Tl beam rate was less than 2 x 10^4 atoms/s.

During the runs, most data were accumulated in five or ten minute sets, or, more accurately, in sets of ten or twenty scans since data collection was terminated only at the end of a preset number of scans. For each mass, wide scans were made to locate the peaks and to verify that no other nearby peaks were missed. Scans centered on the observed peaks represented the bulk of the data accumulated. Close-up spectra

focusing on a few of the peaks of the full spectrum were made to allow more precise measurements of the hfs splittings.

The first data, obtained on 23 September 1984, was on ^{192}Tl. It was chosen first because it was produced with one of the highest cross-sections and it was expected to have a relatively small magnetic moment. A small moment produces a narrow hfs splitting allowing smaller laser scan ranges and letting the total signal counts per channel increase faster. A portion of the data collected is shown in Fig. 10. The I_2 hfs spectrum peaks are the same as those in Fig. 5, page 15; it can be seen from their width or from counting the number of frequency markers that the scan range was much reduced compared to the spin 1/2 case. The ^{192}Tl data shown were a summation of data sets obtained with a separated beam rate of 1 x 10^5 atoms/s over a cummulative time of 45 minutes. The scan range was approximately 4 GHz. The effect of low signal rates is made very clear by the comparison of the signal shown in Fig. 10 with that shown in Fig. 11 which was obtained just ten days later in the second successful on-line run. The latter spectrum was made at a beam intensity three times greater than the former and is but a single data set of five minutes. The higher beam rate was the result of increased tandem output and a change in Ta target density from the 16.3 mg/cm^2 of the first run to the 24.5 mg/cm^2 of all subsequent runs. The later data are obviously "cleaner." Interpretation of the data is reserved for the next section.

Figure 12 shows summed data for ^{193}Tl covering some 20 GHz. Both ground state and isomer hfs can be seen in this summed data taken at an average rate of 3.5 x 10^5 atoms/s for a total of three hours and ten

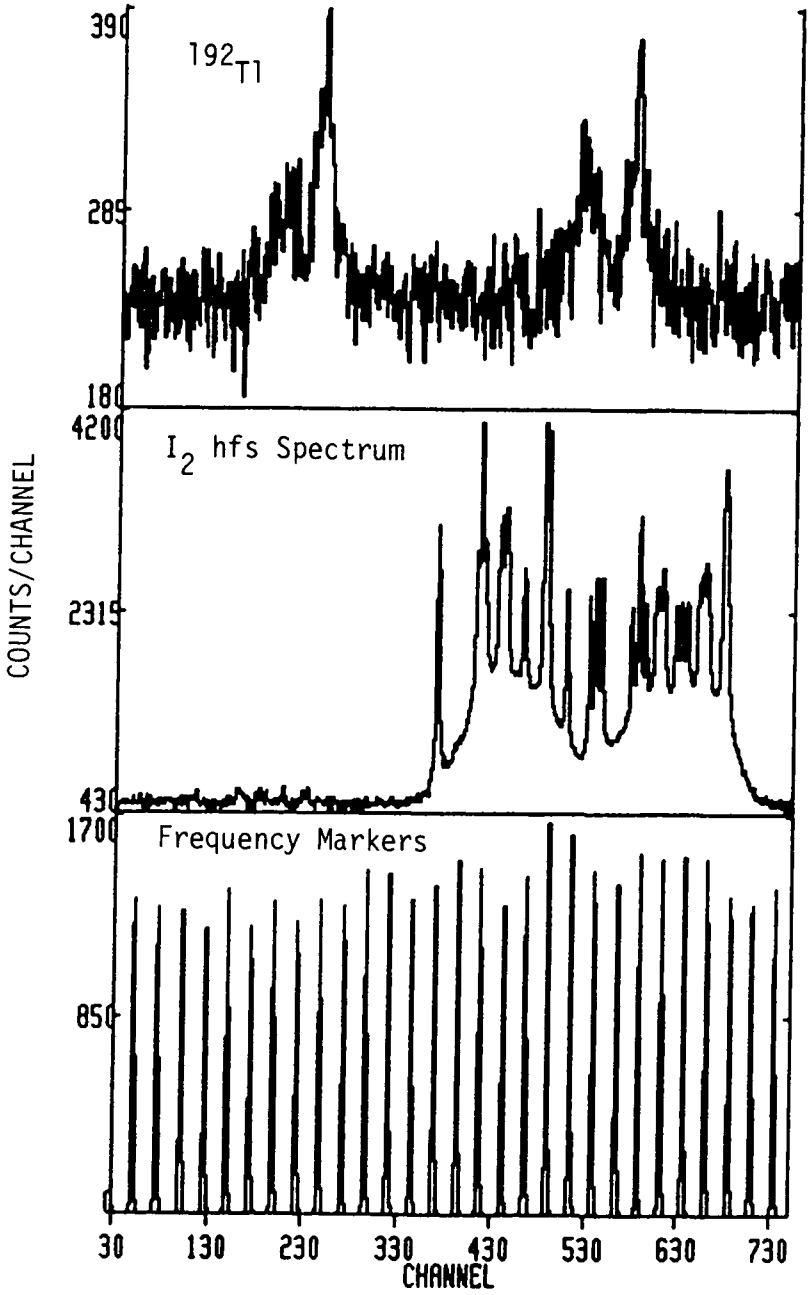


FIG. 10. First on-line data: ^{192}Tl. The Tl spectrum was recorded in 45 minutes with a separated beam rate of 1 x 10^5 atoms/s.

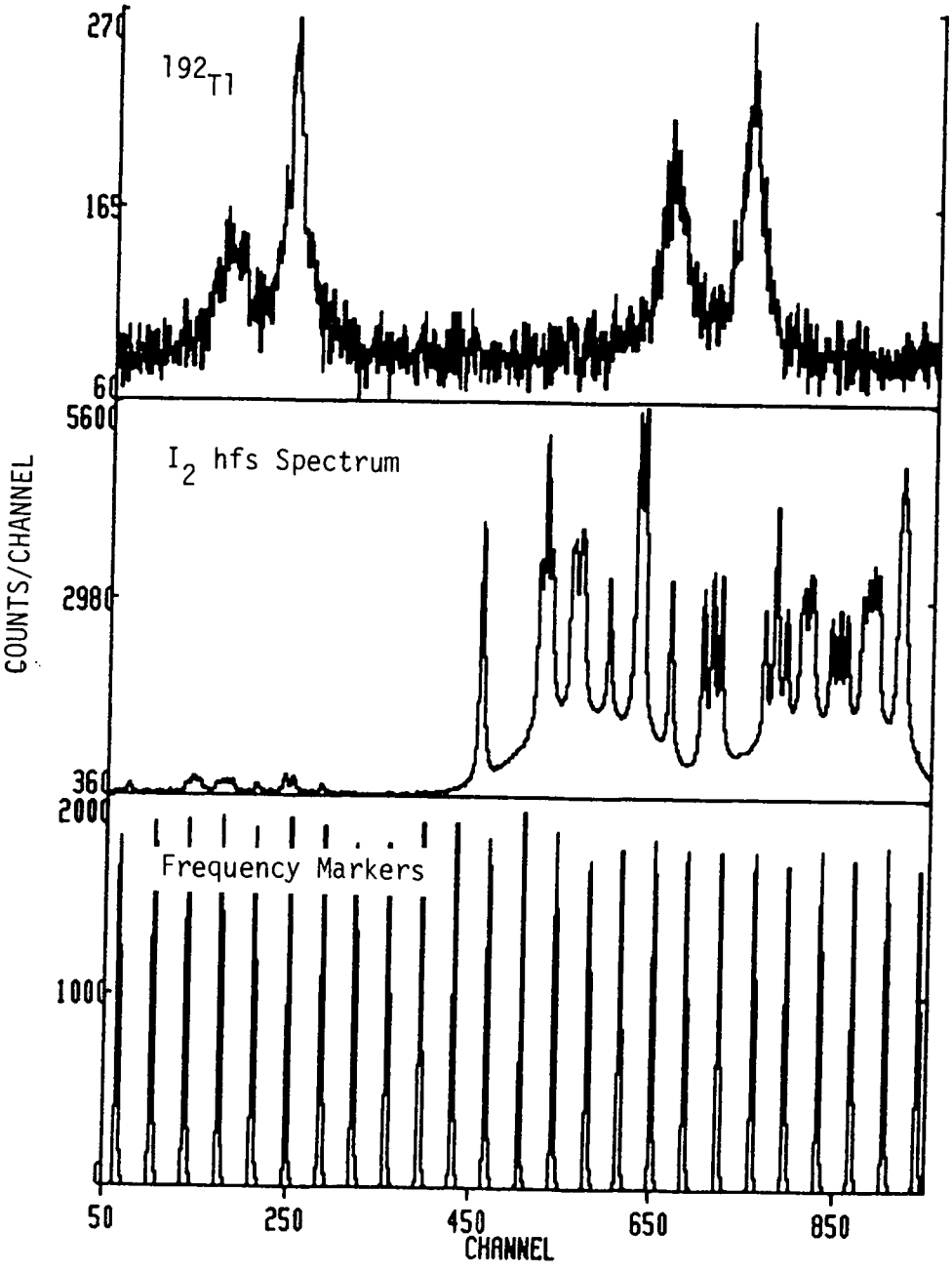


FIG. 11. Second set of on-line data (2 Oct 84). The Tl signal was recorded in five minutes with a separated beam rate of 3 x 10^5 atoms/s.

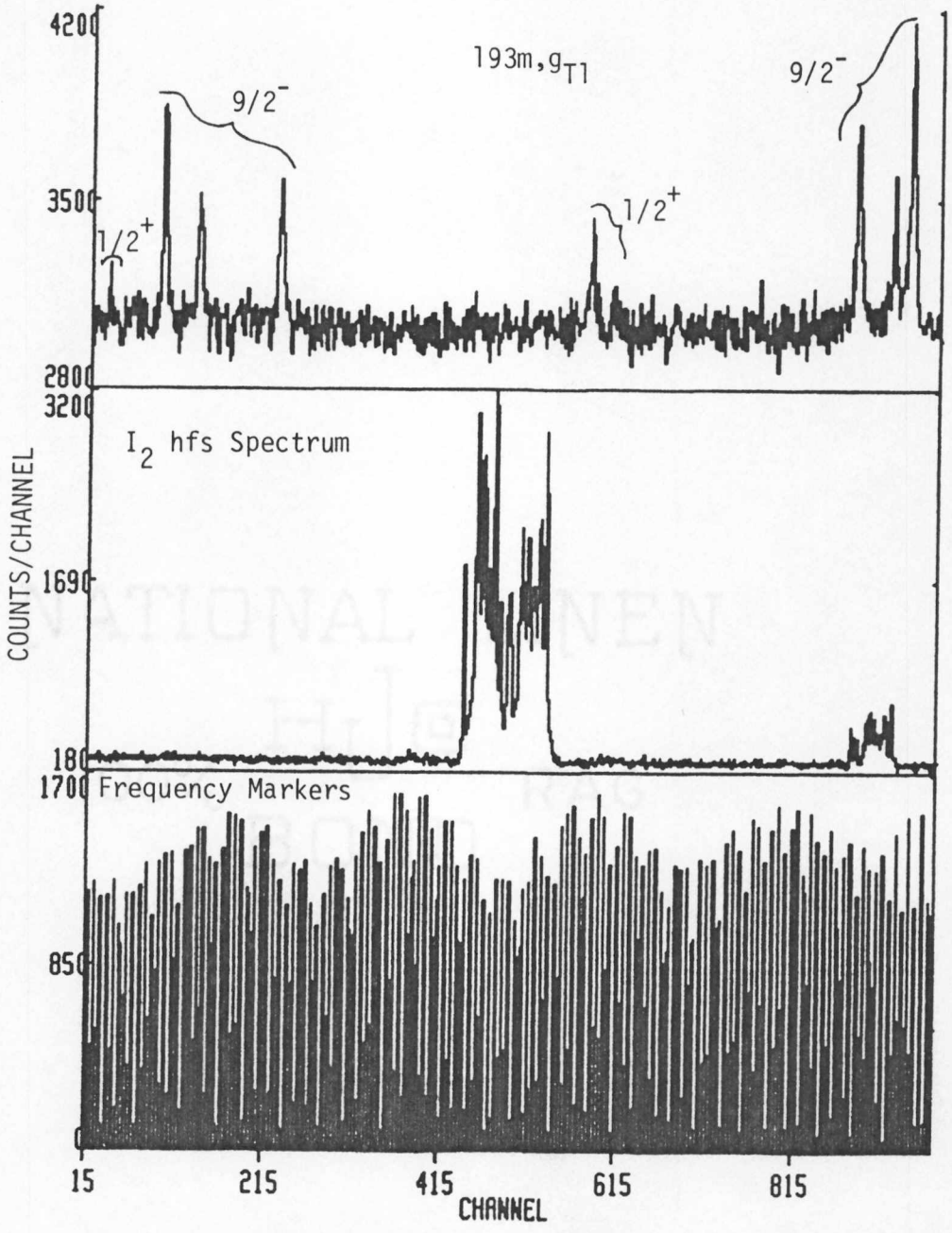


FIG. 12. Data set for ^{193}Tl. Both ground state and isomer appear in the Tl spectrum. Data were recorded with a beam rate of 3.5 x 10^5 atoms/s for a total of 3 hours, 10 minutes.

minutes. The weakest of the three spin 1/2 hfs transitions is nearly indistinguishable from the noise in the summed data but was clearly detected in the close-up scans of the region.

For demonstration purposes, the best summed spectra were compressed to the same scale and are shown in relation to each other, to ^{203,205}Tl, and to the reference I_2 spectrum in Fig. 13. The many data sets on close-up regions of an isotopes' spectrum did not lend themselves to being included in the full spectrum summation, thus the data shown does not represent all of the data taken. This is particularly reassuring in the case of ^{189}Tl where the statistics are the worst. The average beam rates and total times to obtain the spectra of Fig. 13 are given in Table I.

The total times to obtain the summed spectra do not reflect the time spent running on-line. Ten eight-hour shifts were used on ^{192,193}Tl, five on ^{190,191}Tl and three on ^{189}Tl for a total of 18 shifts. A very sizable fraction of each run was spent building the tandem beam intensity, changing targets or cover foils, tuning the separator beam and calibrating with ^{203,205}Tl. Some time was also lost when the separator beam was intentionally withheld on occasion to let the PMT

TABLE I. Summed spectra information for Fig. 13.

^{x}Tl	Average Beam Rate	Total Time
193	3.5×10^5 s^{-1}	3h10m
192	3.0×10^5	45m
191	1.8×10^5	50m
190	0.7×10^5	50m
189	0.9×10^5	51m

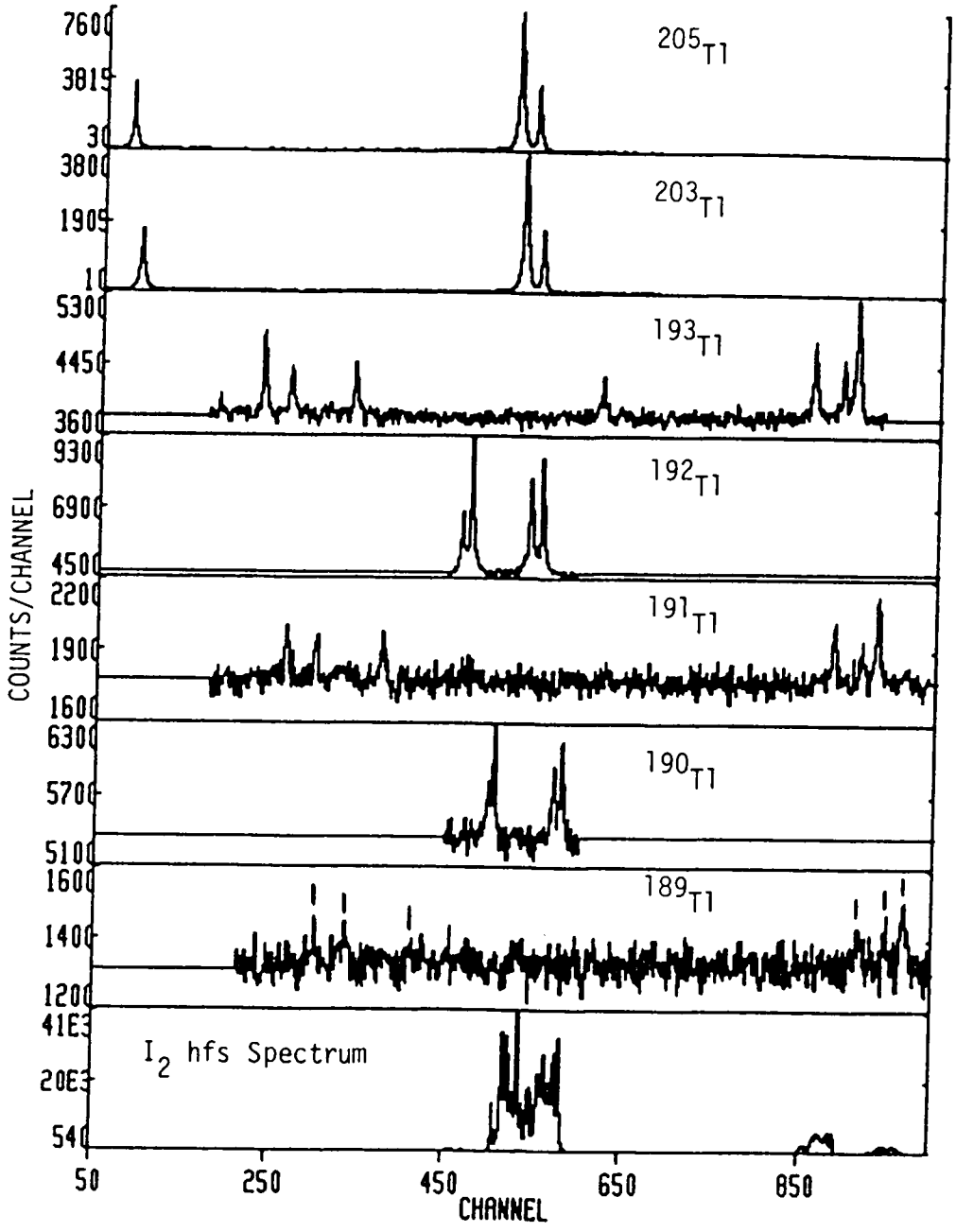


FIG. 13. Normalized data set for $^{189\text{-}193}Tl$. The separate Tl spectra are shown in relative positions to the I_2 hfs spectrum. The observed shifts in the centers of gravity of the Tl spectra are due to a combination of their isotope shifts and their different Doppler shifts.

radiation-induced background decay to improve the signal-to-noise of the data. Longer times were lost in the one-time on-line repairing of the tape transport, correcting of a computer bug and cleaning out of a clogged charge exchange cell. Much time was spent in the first runs on ^{192,193}Tl in searching for the peaks and trying to determine what was being seen. The method of operation was optimized and ^{192}Tl became a reference as to system performance from run to run (except for the ^{189}Tl run where ^{192}Tl was not produced well). In the last of the runs, transmission through the experiment beam line dropped to less than 30%, so although rates approaching 3×10^5 s^{-1} were available on the center beam line, the data were accumulated at nearly the lower practical observing limit. Nevertheless, several sets of data sufficient for the measurement of the hyperfine structures and isotope shifts were collected, so complete data from $^{189-193}$Tl were obtained.

V. DATA ANALYSIS

A. Theoretical Background

Having obtained data, there remained the analysis to extract the nuclear information. The details and descriptions of the causes of hfs and IS are treated in several of the articles in the list of references. For more than the cursory description which follows, the reader is referred to reviews on hfs by White (1934), Schwartz (1955 and 1957), Armstrong (1971) and Sobelmann (1977). Some reviews on IS are those of Breit (1958), Stacey (1966), Bauche and Champeau (1976), Stroke (1982) and King (1984). Both hfs and IS are treated in the books by Kopfermann (1958) and Kuhn (1969).

Examination of Fig. 13 shows that the Tl spectra obtained came in three general forms: those having three peaks, those having six peaks widely spaced and those having four peaks closely spaced. These appearances are a direct consequence of the nuclear interaction with the electrons. Figure 14 shows the possible hfs transitions from the Tl $6^2P_{3/2}$ to $7^2S_{1/2}$ levels for all possible spins of the nucleus. In general, the number of hfs components is determined by the spin of the nucleus and the electron configurations. The amount that the levels are separated, hence the separation of peaks in a spectrum, is related to the electromagnetic moments of the nucleus.

The nuclear and atomic angular momenta I and J couple to form the total angular momentum F of the electrons-plus-nucleus ensemble. The coupling is due to the orbital motion and spin of the electrons causing a magnetic field $\langle H_e(0) \rangle$ at the site of the nucleus where there is

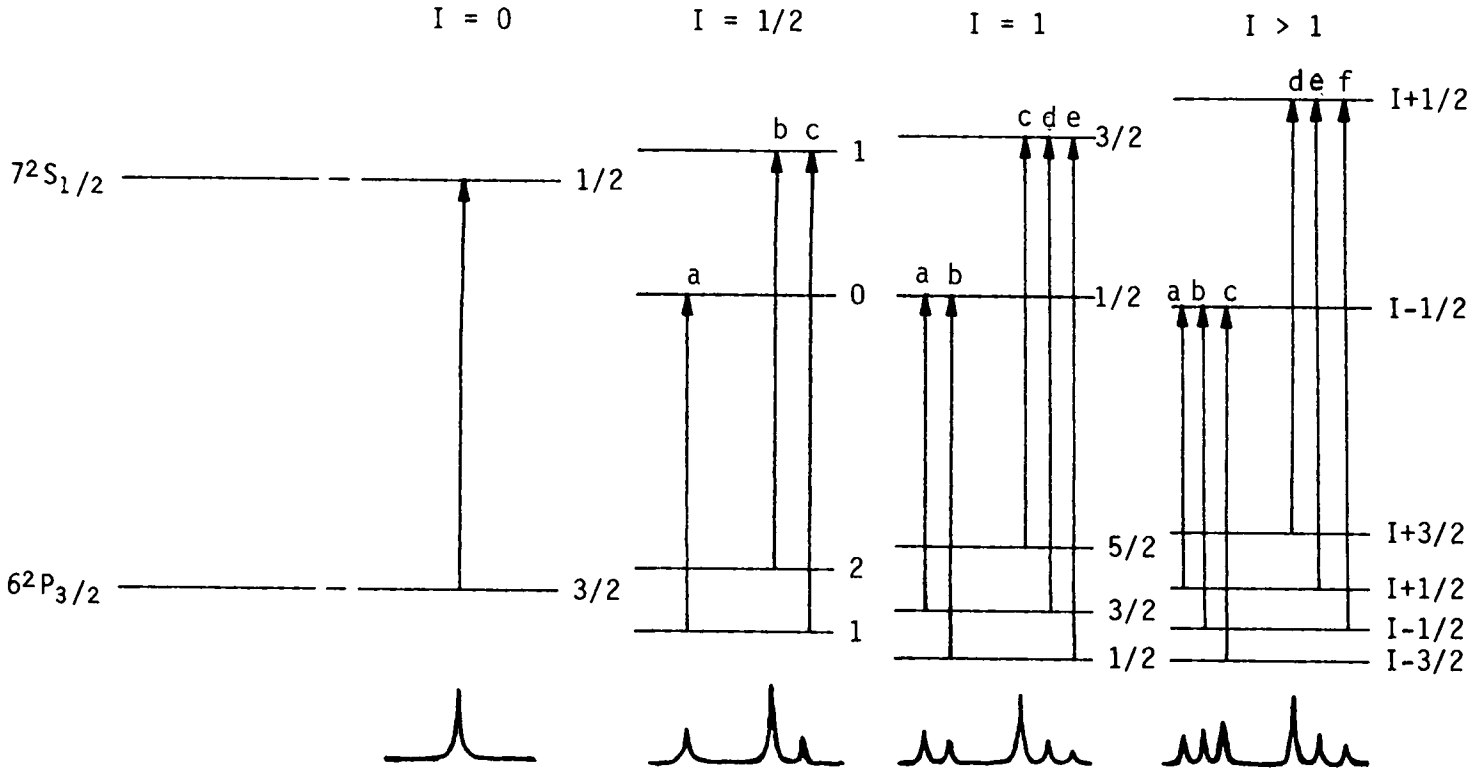


FIG. 14. Thallium hfs splitting for various nuclear spins. Atomic terms are given at left. Levels are numbered with their F-values for the four possible cases of nuclear spin listed along the top. Allowed transitions and their notations in the text are given. Expected spectral patterns are shown. The hfs separations are not to scale.

located a magnetic dipole of moment μ. The interaction energy is simply

$$W_F = - \langle \vec{H}_e(0) \rangle \cdot \vec{\mu} = A \, \vec{I} \cdot \vec{J}$$

$$= A \frac{F(F+1) - I(I+1) - J(J+1)}{2} \qquad (1)$$

where A is a constant for a given nucleus and atomic term. A term is split by this energy into levels with separate F values. For a chain of isotopes, the factor $\langle H_e(0) \rangle$ is very nearly a constant. Thus, to a very good approximation, by measuring A and knowing or calculating $\langle H_e(0) \rangle$ the dipole moment of the nucleus can be obtained. The situation is complicated by the screening of electrons and relativistic correction factors. Furthermore, in deriving Eq. 1, a point nucleus is assumed. One of the first corrections for this came from Rosenthal and Breit (1932), who developed a corrective factor to allow for the non-coulomb potential felt by the electrons when inside the nucleus. Since the change in this factor is very small between isotopes, the ratio $\mu/(IA)$ is essentially constant for a given element and atomic term, with the only correction normally necessary being that of Bohr and Weisskopf (1950), who considered the extended nuclear volume. The hyperfine anomaly, defined (Schwartz, 1957) as

$$^1\Delta^2 \equiv \frac{\mu_1 \, I_2 A_2}{I_1 A_1 \, \mu_2} - 1 \simeq \frac{1+\alpha_1/\mu_1}{1+\alpha_2/\mu_2} - 1 \qquad (2)$$

where atom 1 is heavier than atom 2, gives a measure of how much these effects of non-point nuclei change between isotopes. For Tl, α for the $7^2S_{1/2}$ term has been estimated to be $\pm$ 0.01 n.m. ($j_\nu = l \pm 1/2$ or $j_\pi = l \mp 1/2$) based on similar values for gold (Ekstrom et al., 1980).

Knowing μ, I and A for the stable Tl isotopes, and knowing I and measuring A for a radioactive isotope allows Eq. 2 to be used to determine the radioactive isotope's magnetic dipole moment.

The magnetic dipole is not the only moment which is measurable from hfs spectra. Deformed nuclei also have non-zero higher moments. A quadrupole deformation produces an electric quadrupole moment which interacts with the electrons' charge distribution. The energy of this interaction is related to the moment, Q, and V_{zz}, the second derivative of the potential due to the electrons evaluated at the nucleus, by

$$\Gamma_Q = B \frac{(3/4)(K)(K+1)-(IJ)(I+1)(J+1)}{(2IJ)(2I-1)(2J-1)} \qquad (3)$$

where $K \equiv (F)(F+1) - (I)(I+1) - (J)(J+1)$

and $B \propto Q\, V_{zz}$.

The extra energy Γ_Q adds to or subtracts from the hfs levels determined by Eq. 1. As with the dipole constant A, the quadrupole constant B can be found from experiment, but it is necessary that the hfs not be that of an S term, since these are spherically symmetric and thus have no quadrupole effect. If the nearly constant V_{zz} can be calculated or derived by knowing the moment Q for one isotope, the Q's for all of the other isotopes can be found by comparison.

The highest moment to be considered here is the magnetic octupole moment. It has been observed in both Ga (Daly and Holloway, 1954) and in In (Kusch and Eck, 1954). Its proportionally longer relation for energy change (Jaccarino et al., 1954) can be added to Eq. 1 and 3 to give the total shift of a hfs level from the term's center of gravity:

$$W_F = A\frac{K}{2} + B\frac{(3/4)(K)(K+1)-(IJ)(I+1)(J+1)}{(2IJ)(2I-1)(2J-1)} + \tag{4}$$

$$C\frac{5}{4}\frac{K^3+4K^2+(4K/5)[-3IJ(I+1)(J+1)+I(I+1)+J(J+1)+3]-4IJ(I+1)(J+1)}{IJ(I-1)(2I-1)(J-1)(2J-1)}.$$

C is the constant related to the magnetic octupole moment Ω. The hfs separations of a particular atomic term with I > 1 and J > 1 are found by taking the differences in Eq. 4 for various F values:

$$W_{F_2,F_1} = W_{F_2} - W_{F_1} \tag{5}$$

$$= \frac{A}{2}(K_2-K_1) + \frac{3B}{4}\frac{K_2(K_2+1) - K_1(K_1+1)}{(2IJ)(2I-1)(2J-1)}$$

$$+ \frac{5C}{4}\frac{(K_2^3-K_1^3)+4(K_2^2-K_1^2)+(4/5)(K_2-K_1)[-3IJ(I+1)(J+1)+I(I+1)+J(J+1)+3]}{IJ(I-1)(2I-1)(J-1)(2J-1)}.$$

An hfs separation W_{F_2,F_1} will appear directly in the optical spectra in the form of peak separations if F_2 and F_1 have transitions to a common level in the other atomic term.

To determine all three constants, it is first necessary to identify the observed transitions. As a pertinent example, consider the case of Tl, whose possible 535 nm hfs transitions are given in Fig. 14. There are four possible splittings arising from different nuclear spins. A spin I = 0 nucleus would have no hfs detail and appear as a single peak. For spin I > 0, the $7^2S_{1/2}$ term splits into a doublet. Only the magnetic dipole moment can be obtained from its splitting. On the other hand, the $6^2P_{3/2}$ splitting offers progressively more nuclear information as the spin I increases. An I = 1/2 nucleus has no observable quadrupole moment but splits the $6^2P_{3/2}$ allowing the dipole moment to be measured, albeit the $6^2P_{3/2}$ is less sensitive to the magnetic moment than is the $7^2S_{1/2}$ state. To its advantage, however, the $6^2P_{3/2}$ overlap

with the nucleus is vanishingly small and it thus has a hfs anomaly of zero. For $I > 1/2$, deviations from the Lande interval rule (Eq. 1) occur in the $6^2P_{3/2}$ levels due to quadrupole deformations. Octupole moments appear for $I > 1$ nuclei. No higher moments are detectable with higher I's since the $J = 3/2$ becomes the limiting factor. For small higher-than-dipole moments, the observed peaks would be ordered in increasing energy as they are drawn in Fig. 14. Two of the greatest aids in labeling peaks in Tl spectra are that (a) for $I > 1/2$, two pairs of transitions have the same energy spacing, and (b) the ratio of dipole constants $A(7^2S_{1/2})/A(6^2P_{3/2})$, which from Eq. 1 is just the ratio of $\langle H_e(0)\rangle_{S1/2}/\langle H_e(0)\rangle_{P3/2}$, is relatively unchanging between isotopes. For Tl this ratio is approximately 46.

The centers of gravity of hfs transitions are known to change from isotope to isotope. These isotope shifts of both atomic terms and, as a result, spectral lines are measurable quantities. Observed isotope shifts are composed of a field shift (FS) due to volume changes and a mass shift (MS) due, obviously, to a change in mass. The MS itself is composed of the normal mass shift (NMS) and the specific mass shift (SMS). The NMS is due to the kinetic energy of the nucleus and is given simply by

$$\mathrm{NMS} = \frac{\nu}{1836} \quad \frac{A' - A}{A\ A'}$$

where ν is the transition frequency and A is the atomic number. At low masses the NMS is the dominant effect, but for the Tl 535 nm line it amounts to only ~ 8 MHz per amu. The SMS is due to electron correlations and cannot be readily calculated. For Pb, Thompson et al. (1983)

assumed the relation SMS = (0 ± 10) NMS, whereas for Hg, Bonn et al. (1976) used SMS = (0 ± 0.5) NMS. The value (0 ± 1) NMS was chosen for Tl based on the arguments of Heilig and Steudel (1974).

The FS of a line has been discussed by a host of authors. It is most generally stated that the FS is proportional through a virtually constant electronic factor to λ, where λ is the sum of the change in the even radial moments between two nuclei:

$$\lambda = \sum \frac{C_i}{C_1} \delta\langle r^{2i}\rangle \quad . \tag{6}$$

The coefficients C_i are given by Seltzer (1969). In fact, various authors have claimed that optical transitions measure the following:

1. $\delta\langle r^{2\sigma}\rangle$, with $\sigma=(1-\alpha^2Z^2)^{-1/2}$ — Racah (1932) and Rosenthal and Breit (1932);
2. $\delta\langle r^2\rangle$ — Bodmer (1953);
3. $\sum a_n\delta\langle r^{2n}\rangle$ (same as Eq. 6) — Seltzer (1969);
4. $\delta\langle r^{2\sigma'}\rangle$, with $\sigma'=(1-0.177\alpha^2Z^2)$ — Wu and Wilets (1969);
5. $\delta\langle r^{1+\sigma}\rangle$ — Dunlap (1972);
6. $\delta\langle r^2\rangle$ — Heilig and Steudel (1974).

The series expansion is used in this work, since from it deformations can be derived.

To determine isotope shifts, the centers of gravity of hfs spectra are found by measuring transition energies and weighting them with their theoretical line strengths. The line strengths of many transitions are tabulated by Kopfermann (1958) or can be easily calculated by the formulas in Tolansky (1948). These have the results or the simplified specific-case forms of the expression for the line strengths,

which for a transition between levels F and F' is proportional to

$$(2F+1)(2F'+1)\begin{Bmatrix} I & F & J \\ 1 & J' & F' \end{Bmatrix}^2$$

where the term in brackets is a six-j symbol (see, for example, Shore and Menzel, 1967). The relative line strengths of interest for Tl are given in Fig. 15.

B. Experimental Analysis: Extraction of hfs and IS from Data

Each hfs spectrum obtained in an experiment was recorded simultaneously with the frequency markers from an etalon and the hfs spectrum of I_2 in a cell to permit accurate frequency determinations. Repeated accurate measurements of the I_2 hfs were made in order to simplify the data set comparisons. There are two I_2 hfs multiplets in the laser frequency interval of interest. If ideally resolved, these multiplets would have either 15 or 21 components. Regarding Fig. 13, page 38, the 12 closely spaced peaks in the center of the I_2 spectrum correspond to the unresolved peaks numbered 773 and 774 on sheet 50, part 3 of Gerstenkorn and Luc's 1978 atlas. For the sake of simplicity, the peaks hereafter are simply referred to as peaks 773 and 774. Peak 773 is a 15 component multiplet which on the scale of Fig. 13 is seen as the six peaks on the left of the center group, while peak 774 is a 21 component multiplet seen as as the six peaks on the right side of the center group. Individual hfs components are labeled "a" through "u" with "a" being the highest in frequency. The difference in the 15 and 21 component structures is that the triplet peaks abc, hij and stu in the 21 component spectra are single peaks named "b", "i" and "t" in the 15

$I = 1/2$, $J' = 1/2$, $J = \frac{3}{2}$

F \ F'	1	0
2	100	
1	20	40

$I = 2$, $J' = 1/2$, $J = \frac{3}{2}$

F \ F'	5/2	3/2
7/2	100	
5/2	40	35
3/2	10	40
1/2		25

$I = 9/2$, $J' = 1/2$, $J = \frac{3}{2}$

F \ F'	5	4
6	1300/13	
5	660/13	440/13
4	240/13	660/13
3		700/13

$I = 6$, $J' = 1/2$, $J = \frac{3}{2}$

F \ F'	13/2	11/2
15/2	2600/26	
13/2	1400/26	875/26
11/2	550/26	1400/26
9/2		1625/26

$I = 7$, $J' = 1/2$, $J = \frac{3}{2}$

F \ F'	15/2	13/2
17/2	8100/81	
15/2	4480/81	2720/81
13/2	1820/81	4480/81
11/2		5400/81

FIG. 15. Relative line strengths for Tl. Each hfs group is normalized so that its most intense line has a strength of 100.

component spectra thus giving the three quadruplet peaks the same labeling. The 12 peaks in the Fig. 13 I_2 spectrum are therefore bounded on the left by the 773 "t" peak and on the right by the 774 "b" peak, or actually, abc peak. Gerstenkorn and Luc (1979) provide the information that the center of gravity of an I_2 multiplet is located at very nearly 5/9 of the distance from its "t" to its "b" peak, and that this position corresponds to the wave number value listed in their 1978 atlas.

In order to simplify the data analysis here, the wave number of a single component was determined so that it alone would be sufficient for data set comparisons. For this purpose, the 774 "b" peak was chosen since it is narrow and has good statistics. Its triplet nature resolves only on extremely narrow scan ranges of about 500 MHz per 1024 channels, where it is seen that the "b" peak is nearly centered and is also the tallest of the three. The separation of the 774 "b" and "t" peaks was measured to be 858(4) MHz. The distance from the "b" peak to the center of gravity of the multiplet is thus just 4/9 of this value, or 381(3) MHz or 0.0127(1) cm^{-1}. The tabulated value of the centroid of this multiplet is 18698.4908 cm^{-1}. To this must be added Gerstenkorn and Luc's 1979 correction of - 0.0056 cm^{-1}. In addition, the I_2 saturated absorption spectroscopy system uses the first-order modulated wave from an acoustical optical modulator (AOM) which requires a correction of + 40 MHz or + 0.0013 cm^{-1}. Combining all of these values, it is found that in a plot of spectra with an I_2 reference the position of the "b" peak of the 774 multiplet corresponds to an absolute wave number of 18698.4992 cm^{-1}. Gerstenkorn and Luc state that their correction makes their wave numbers accurate to ± 0.001 cm^{-1} (± one standard deviation).

The centers of gravity of the Tl spectra were measured relative to this "b" peak in order to extract the isotope shifts. For example, labeling the Tl normal-ordered transitions alphabetically by increasing frequency (this is opposed to the I_2 scheme), it can be seen that for a spin 1/2 Tl 535 nm hfs, which has line strengths in the ratio 2:5:1, the center of gravity (c.g.) is given by

$$\text{c.g.} = \sigma_{I_2} + \frac{2\Delta\sigma_a + 5\Delta\sigma_b + \Delta\sigma_c}{8} \quad ,$$

where σ_{I_2} is the wave number of the I_2 reference, $\Delta\sigma$ is the difference in wave numbers of a Tl peak and the I_2 reference, and a,b,c are the peak labels. Similar formulas apply to the other spins.

Once the observed peaks are identified, the center of gravity can be found. In order to use this to determine isotope shifts, the Doppler shift must be considered. In collinear spectroscopy, a moving atom whose rest-frame transition has wave number σ_0 is excited by laser light at wave number σ_m. The relativistic Doppler effect relates these two wave numbers by the equation

$$\sigma_m = \sigma_0 \frac{(1 - \beta^2)^{1/2}}{1 - \beta\cos\theta} \qquad (7)$$

where $\beta = v/c$ = (the velocity of the atoms)/(the speed of light) and θ is the angle between the laser and the atom beam propagation directions. For light travelling in the same direction as the atom beam, known as the parallel geometry, $\theta = 0$, while for the antiparallel geometry $\theta = \pi$. The parallel (+) and antiparallel (-) geometries let Eq. 7 reduce to

$$\sigma_{\pm} = \sigma_0 \frac{(1 - \beta^2)^{1/2}}{1 \mp \beta} = \sigma_0 \left[\frac{1 \pm \beta}{1 \mp \beta}\right]^{1/2} \quad . \qquad (8)$$

By measuring σ_+ and σ_- for a given mass and acceleration voltage, the rest-frame wave number can be obtained by taking the square-root of the product of σ_+ and σ_-, i.e.,

$$\sigma_0 = \sqrt{\sigma_+ \sigma_-} \tag{9}$$

Equation 9 is relativistically correct to all orders of β and does not require the knowledge of β. The accuracy of collinear fast atom beam laser spectrocopy can thus be used to obtain a similarly accurate value of the rest-frame transition of an atom without doing an experiment using a cell. This approach has even been used to test the accuracy of the time dilation formula to a new precision in an experiment performed at UNISOR by Juncar et al. (1985).

For this research, the rest-frame wave number of the center of gravity of the 535 nm line of ^{203}Tl was measured to be 18684.7901(10) cm^{-1} using the parallel-antiparallel method just described. Due to time constraints and difficulty of alignment, the parallel-antiparallel method was not used on each isotope. Instead, the Doppler shifts of all of the isotopes were calculated by first obtaining the Doppler shift and velocity βc for ^{203}Tl and then using appropriate formulas to deduce the other isotopes' Doppler shifts. To do this, note that Eq. 8 can be solved for β to yield

$$\beta = \frac{(\sigma_+/\sigma_0)^2 - 1}{1 + (\sigma_+/\sigma_0)^2} \quad . \tag{10}$$

For some calculators where round-off errors would affect the accuracy of inserting numbers into this equation, two alternate forms are offered. Setting Eq. 8 equal to the rest-frame wave number σ_0 plus a Doppler shift S and then solving for β gives the exact formula

$$\beta = \frac{(S/\sigma_0) + (1/2)(S/\sigma_0)^2}{1 + (S/\sigma_0) + (1/2)(S/\sigma_0)^2}$$

or in power series form:

$$\beta = (S/\sigma_0) - \frac{1}{2}(S/\sigma_0)^2 + \frac{1}{4}(S/\sigma_0)^4 + (\text{higher order terms}).$$

Knowing $\sigma_0(203)$ and measuring $\sigma_+(203)$ for each on-line run gives $\beta_{203}c$, the velocity of ^{203}Tl in the observation region.

Since each isotope is accelerated by the same potential V_{acc}, their β's are related. However, the Tl ions after being accelerated are then slowed unequally by picking up an electron in the charge exchange process. Assuming that the ions pick up free electrons from rest in the charge exchange, from momentum conservation the observed velocity $\beta_1 c$ for an atom of mass m_1 is found to be related to the velocity of the ion of mass m_{1+} before the charge exchange by the exact formula

$$\beta_{1+}^2 = \frac{(m_1/m_{1+})^2 \beta_1^2}{1 + \beta_1^2[(m_1/m_{1+})^2 - 1]} \quad . \qquad (11)$$

Assuming that the initial energy given to each isotope is the same and by relating relativistic energies, it can be shown that a second isotope accelerated by the same potential would have a velocity $\beta_{2+}c$ related to β_{1+} by another exact formula

$$\beta_{2+}^2 = 1 - \left[\frac{m_{1+}}{m_{2+}}\left(\frac{1}{\sqrt{1 - \beta_{1+}^2}} - 1\right) + 1\right]^{-2} \quad . \qquad (12)$$

Once β_1 is determined by the measurement of σ combined with σ_0, then β_{1+} can be derived from Eq. 11. From β_{1+} can be obtained β_{2+}. Finally, β_2, the factor for the observed velocity of the second isotope, can be

obtained by using

$$\beta_2^2 = \frac{(m_{2+}/m_2)^2\ \beta_{2+}^2}{1 + \beta_{2+}^2[(m_{2+}/m_2)^2 - 1]} \quad . \tag{13}$$

Equations 11, 12 and 13 can be combined by straightforward, albeit cumbersome, algebra to relate the observed velocities of two different isotopes using the assumptions above to yield the exact equation

$$\beta_2^2 = \frac{X}{m_2^2(1-\beta_1^2) + X} \tag{14}$$

where $X = (2m_{1+})(m_{1+}-m_{2+})\{1-\beta_1^2 - \sqrt{(1-\beta_1^2)[1-\beta_1^2+\beta_1^2(m_1/m_{1+})^2]}\ \}+\beta_1^2 m_1^2$.

Equation 14 is accurate for any accelerated and then neutralized elements. Without charge exchange, Eq. 12 is all that is needed to compare β's. For the particular case of Tl, direct substitution into Eq. 14 using $m_+ = m_0 - m_e + IP$, where m_e is the mass of the electron and IP is the ionization potential, yields

$$\beta_2 = \sqrt{(m_1/m_2)}\ \beta_1 \tag{15}$$

to better than 13 parts in 10^8 for $m_2 = 189$ and $m_1 = 205$. Equation 15 was therefore used in the analysis of data whereas Eq. 14 is supplied for those using other velocities or lighter masses where Eq. 15 might not be sufficiently accurate.

To extract isotope shifts, the following procedure was used. A reference isotope (^{203}Tl) is chosen whose rest-frame wave number, σ_0, is known. Its Doppler-shifted center of gravity is measured. Subtracting its rest-frame value gives its Doppler shift. Another isotope, with a rest-frame transition $\sigma_{02} = \sigma_{01} + IS$ where IS is its isotope shift with

respect to the reference, is then measured to have a laboratory-frame wave number of σ_2. The second isotope has a Doppler shift

$$S_2 = \sigma_2 - \sigma_{02}$$
$$= \sigma_2 \left(1 - \sqrt{(1-\beta_2)/(1+\beta_2)} \right)$$

which can be found without knowing the rest-frame wave number by using Eq. 14 or 15 once β_1 is known from a calibration data set on the reference isotope. Notice that the observed difference in the centers of gravity is

$$(\sigma_2 - \sigma_1) = (\sigma_{02} + S_2) - (\sigma_{01} + S_1)$$
$$= (\sigma_{01} + IS + S_2) - (\sigma_{01} + S_1)$$
$$= (S_2 - S_1) + IS \quad . \tag{16}$$

The isotope shift is equal to the difference in the observed wave numbers minus the difference in Doppler shifts. This form is easier to handle than obtaining and manipulating the rest-frame wave numbers because the terms in Eq. 16 are all of the same size (GHz) whereas the isotope shifts are many orders of magnitude smaller than the wave numbers themselves.

Yet another way of expressing the observed shifts is

$$(\sigma_2 - \sigma_1) = \sigma_{01} \left[\sqrt{\frac{1+\beta_2}{1-\beta_2}} - \sqrt{\frac{1+\beta_1}{1-\beta_1}} \right] + IS \sqrt{\frac{1+\beta_2}{1-\beta_2}} \quad .$$

This form can be used with the expansion

$$\sqrt{\frac{1+\beta}{1-\beta}} = 1 + \beta + \frac{1}{2}\beta^2 + \frac{1}{2}\beta^3 + \frac{1}{2}\beta^4 + \frac{3}{8}\beta^5 + \ldots$$

in doing calculations in order to avoid several possible round-off errors.

Numerical analysis shows that the uncertainty of 0.001 cm^{-1} in $\sigma_0(203)$ leads to five significant digits in β_{203}, β_m, S_{203} and S_m, but, since it is a systematic error, the difference in the roughly equal S_{203} and S_m is also accurate to five significant digits. Even though $\sigma_0(203)$ is known to only within 30 MHz, the associated uncertainties in Doppler shifts are less than 1 MHz. Another uncertainty which affects the Doppler shift calculation is in the masses used in Eq. 14 or 15. However, an error of 0.001 amu (~ 1 MeV/c^2) in the mass of a Tl isotope would mean only as much as a 1 MHz error in S_m. The masses used for calculations here were determined from the mass excesses listed by Tuli (1985). Nearly all of the excesses listed for Tl were determined by systematics, but errors greater than 2 MeV/c^2 would be very doubtful. The most serious uncertainty by far is whether or not the accelerating voltage remains constant throughout an experiment. The change in observed wave number with voltage for Tl at 50 kV is about 4 MHz per volt. The voltage is not changed during experiments but is subject to drift. Several calibration data sets are interspersed with on-line data to monitor this voltage stability.

Not only is β needed to determine the IS, but the actual hfs spacing as well. Each hfs transition is observed to be shifted according to Eq. 8. The observed spacings are thus larger than the rest-frame spacings by the factor $[(1+\beta)/(1-\beta)]^{1/2}$, or about 1.00075 for Tl at 50 kV (the actual number changes slightly from mass to mass). The observed spacings are interpreted in terms of level spacings by studying the observed pattern and relating it to the hfs schemes as shown in Fig. 14, page 41, keeping in mind that higher-than-dipole moments can

rearrange the energy ordering of levels. The equal separation of two pairs of the peaks for $I > 1/2$ and the ratio of A factors being about 46 are instrumental in peak labeling. Once peaks are labeled properly, rest-frame level spacings are extracted; e.g., for $I > 1$, the equal separation of two pairs of peaks is just the $6^2P_{3/2}$, $F = I+1/2 \rightarrow F = I-1/2$, level spacing. The $7^2S_{1/2}$ level spacing is the Doppler-corrected difference in the "c" and "a" peaks for the $I = 1/2$ data, while for the $I > 1$ spins it is obtained by taking the average of the "f" - "b" and "e" - "a" spacings.

Using the Lande interval rule, the S splitting is just $(I+1/2)$ times the $A(7^2S_{1/2})$ hfs constant, since higher-than-dipole moments do not affect an S term. For $I = 1/2$, the $6^2P_{3/2}$ splitting is simply twice the $A(6^2P_{3/2})$ constant since $(I+3/2) = 2$. The $6^2P_{3/2}$ splitting for $I > 1/2$ was fit in two ways. The displacement energy of a level and the hfs constants A, B and C are related by Eq. 4. Level spacings are given by Eq. 5. Solving simultaneous equations of the form of Eq. 5 will give the hfs constants in terms of the level spacings (a general solution for the constants in terms of the $P_{3/2}$ level spacings is given in Schwartz' 1955 article). The constants for Tl were determined first by solving such equations and secondly by doing a least-squares fit to the data using the latter relations and assuming that the constant C was zero. The justification for this assumption was based on the In and I octupole moments. These moments were detected using very precise ABMR data to obtain C's of 2.45(37) kHz for ^{127}I (Jaccarino et al., 1954) and 0.497(33) kHz for ^{115}In (Kusch and Eck, 1954), while the A's and B's are on the order of many MHz. The octupole moments observed are among the

largest known, but their effects on the hfs spectra required measurements of the separation of hyperfine components several orders of magnitude more precise than the laser data supplies. Since the A and B constants agreed well within their experimental errors using both the three-equation/three-unknowns and the least-squares fit, and since any C term would be expected to be on the kHz scale well within the MHz uncertainty of the level separations, the least-squares fit was chosen as being more reasonable.

Level ordering found for the odd-mass isomers is given in Fig. 16. The quadrupole moment, through the B coefficient, is sufficient to invert the levels as shown. When interpreting the even-mass Tl data, a special problem was encountered. The nuclear spins have not been measured (Tuli, 1985). The observed hfs had four peaks, but no nuclear spin will result in only four transitions. From systematics, an I = 2 ground state and an I = 7 isomer are assumed; both should have six hfs transitions. Gamma-ray data acquired simultaneously with the laser data were used to show what proportion of ground state and isomeric state nuclei were being produced at mass 192. This determination was made by comparing the ratio of the observed intensities of gamma-ray lines in the ^{192}Tl decay. Originating from the 4^+ level in ^{192}Hg, the 635 keV line of ^{192}Tl decay had been calculated by Sousa et al. (1981) to be only 11% as strong as the 423 keV line for the low-spin ground state but 91% as strong for the high-spin isomer. The ratio in the laser experiments was over 90% suggesting the beam consisted of virtually all high-spin isomers.

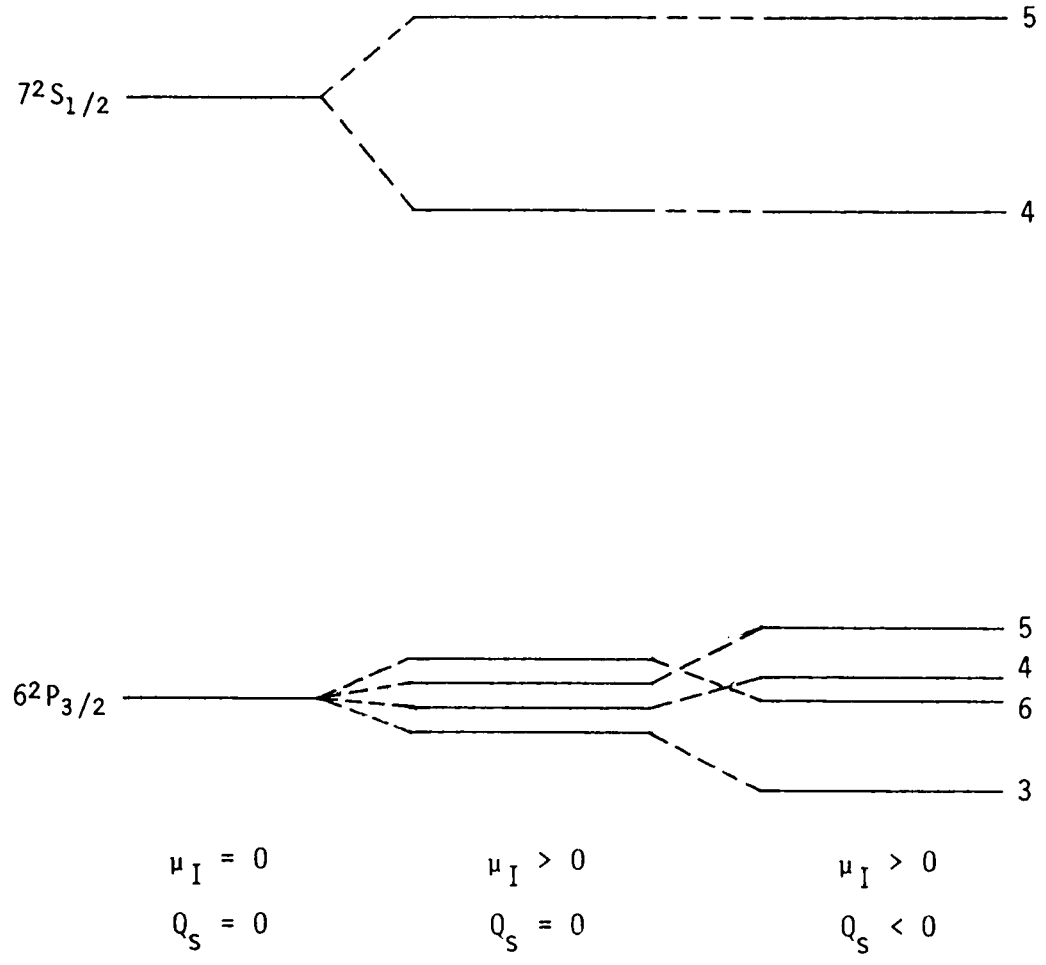


FIG. 16. Effect of nuclear moments on Tl atomic levels for I = 9/2. The hfs spectra of the light odd-mass Tl isotopes taken in this work reveal a level ordering corresponding to $\mu_I > 0$ and $Q_s < 0$.

To correctly assign the hfs peaks in the ^{192}Tl data, on-line time was spent recording the relative peak heights for varied laser powers in hopes of using the optical pumping model (see appendix) to decipher the data. It was found that the first of the peaks increased in relative height while the third and fourth became roughly equal and as large as the second peak for decreasing laser powers. The accuracy of the data and of the model were not, however, sufficient to uniquely determine peak assignments. Since six peaks are to be expected for $I > 3/2$ and the isomer is assumed to be have $I = 7$ (although $I = 6$ is not unreasonable), it was clear that for these Tl isotopes there is seen either a triplet and three single peaks or two doublets and two single peaks. Since two pairs of the peaks necessarily have the same separation and the peaks observed are not equally separated, it follows that none is a triplet and that the equally spaced pairs are in fact unresolved, appearing as single peaks. It is found that of the possible permutations of the assignments of the two doublets and two single peaks, in only <u>one</u> case is the resultant ratio $A(7^2S_{1/2})/A(6^2P_{3/2}) \simeq +46$ as it should be. This occurs for the ordering of peaks "c ab d ef." The level ordering required for this is shown in Fig. 17. Having derived the peak locations through the physics argument, the optical pumping model predictions were reexamined for agreement. It was found that the deduced ordering should indeed result in the peak behavior noted at lower laser powers. Furthermore, by taking the peak widths and shapes from the well resolved ^{193}Tl data and fitting the ^{192}Tl data using the derived ordering, the six relative peak areas of the fit were found to agree extremely well with the model. Agreement with both spin $I = 7$ and

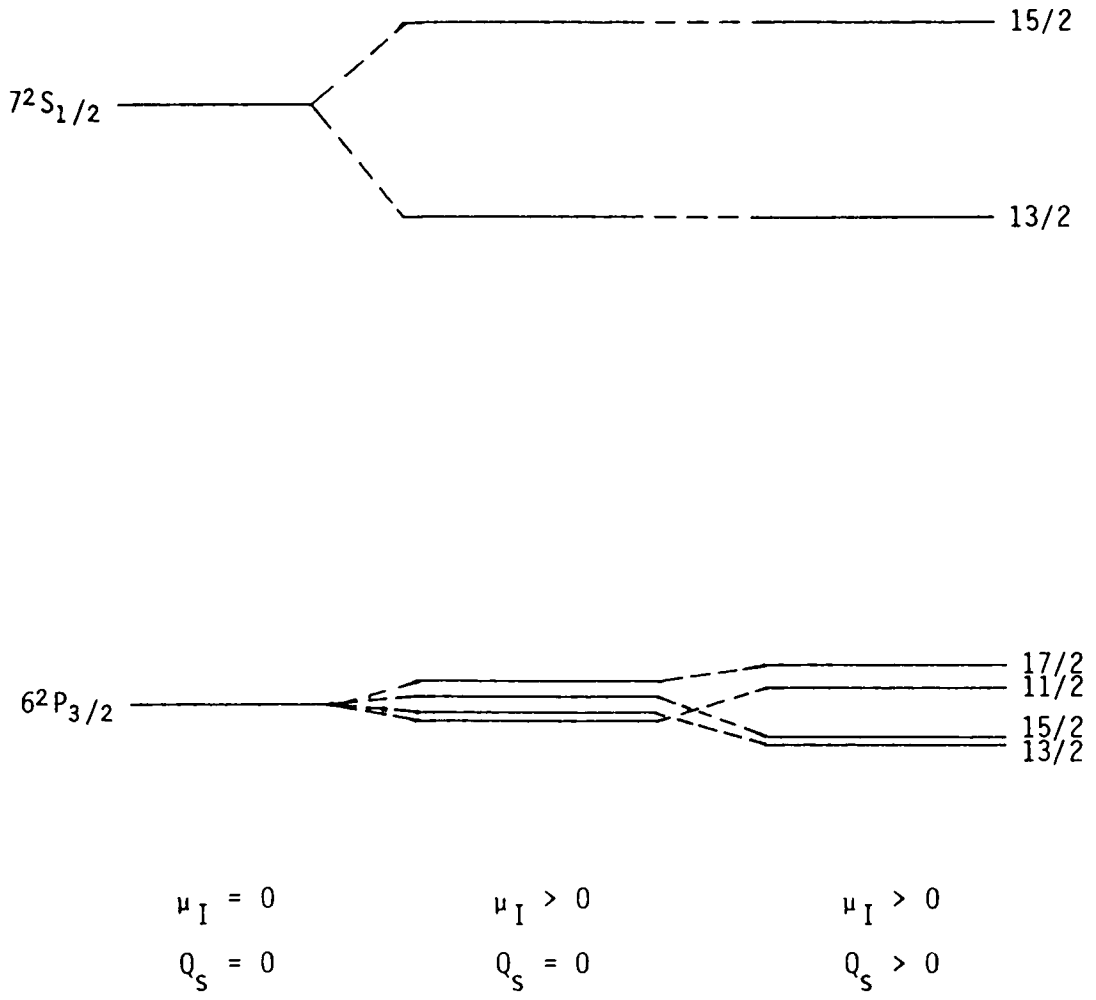


FIG. 17. Effect of nuclear moments on Tl atomic levels for I = 7. The hfs spectra of the light even-mass Tl isotopes taken in this work reveal a level ordering corresponding to $\mu_I > 0$ and $Q_s > 0$. The 15/2 to 13/2 level spacing in the $6^2P_{3/2}$ multiplet is much less than the 60 MHz experimental linewidth of the 535 nm transitions.

I = 6 assignments were good since these two nuclear spins cause virtually identical relative intensities. The data was thus analyzed for both spin assumptions pending an actual measurement of the isomeric spin. The A and B hfs constants for all Tl isotopes measured at UNISOR are given in Table II. Previously measured constants of ^{201,203,205}Tl by other groups are included in the table for comparison. The values from this work are consistent with the previous measurements. The precision obtained here is much less than that of the ABMR meaurements of Petersen, Palmer and Shirley (1968) but greater than that of the optical measurements of Hull and Stroke (1961).

Even though $A(6^2P_{3/2})$ is free of the hyperfine anomaly, $A(7^2S_{1/2})$ gives a more accurate magnetic dipole moment since its value is more precisely measured. An unknown moment is found by relating to a known moment of an isotope and using a rewritten form of Eq. 2 :

$$\mu_X = I_X A_X \frac{\mu_0}{I_0 A_0} \frac{(1+\alpha_X/\mu_X)}{(1+\alpha_0/\mu_0)} \quad . \qquad (17)$$

The reference isotope was chosen to be ^{205}Tl which has I = 1/2, an $A(7^2S_{1/2})$ of 12292.4(8.3) MHz and a dipole moment of 1.6382136(1) n.m. (Ekstrom, Wannberg and Shishodia, 1976). The values of α are as given on page 42 using the nuclear shell model: for ^{189,191,193}Tl, which are $\pi h_{9/2}$ nuclei, α is + 10^{-2} n.m.; for ^{193g,201,203,205}Tl $(\pi s_{1/2})$ α = - 10^{-2} n.m.; and for ^{190,192}Tl $(\pi s_{1/2}\nu i_{13/2})$ $\alpha = \alpha_\pi + \alpha_\nu = 0$. Owing to the accuracy and the magnitude of α, it is sufficient to use on the right side of Eq. 17 the magnetic dipole moment found assuming no anomaly, i.e.,

$$\mu_X = (0.00026654(18)\text{n.m./MHz})\ I_X A_X \qquad (18)$$

TABLE II. Tl hyperfine constants measured at UNISOR (in MHz). The best previous measurements are included where possible.

^{x}Tl	A($7^2S_{1/2}$)	A($6^2P_{3/2}$)	B($6^2P_{3/2}$)	
205	12292.4(8.3)	264.65(80)	-	
	12291. (15.)[a]	265.038273(2)[b]		
203	12179.7(5.6)	262.3(1.0)	-	
	12184. (15.)[a]	262.029972(2)[b]		
201	12045.3(9.4)	255.0(5.0)	-	
	12052.(120.)[c]	510.(120.)[c]		
193g	11942. (14.)	259.9(7.0)	-	
193m	3263.0(2.4)	66.7(2.3)	-2476.(20.)	
192m	275.9(1.9)	5.8(1.0)	526.(18.)	If I = 7
	318.3(2.1)	7.2(1.3)	507.(17.)	If I = 6
191m	3225.9(3.4)	66.5(3.4)	-2562.(31.)	
190m	263.9(2.3)	5.4(1.6)	296.(24.)	If I = 7
	304.5(2.6)	6.6(1.8)	286.(23.)	If I = 6
189m	3204.5(4.8)	65.3(4.8)	-2578.(44.)	

[a] Odinstov, 1960.
[b] Petersen, Palmer and Shirley, 1968.
[c] Hull and Stroke, 1961.

where in Eq. 18 the ^{205}Tl numerical values have been used. The moments obtained from Eq. 17 are listed in Table III along with all other known Tl dipole moments as well as all of the known 535 nm isotope shifts. The associated one standard deviation uncertainties listed with each of the dipole moments derived in this work do not include the uncertainties in the values of α used. This uncertainty should amount to less than 0.01 n.m. (Ekstrom et al., 1980. Equation 18 may be used with the values of $A(7^2S_{1/2})$ listed in Table II to determine the magnetic dipole moments in Tl neglecting the correction for the hfs anomaly). The absolute magnitude of the Tl magnetic dipole moments are plotted in Fig. 18. The isotope shifts of the 535 nm line are plotted in Fig. 19.

It can be seen from Table III that the values from this work are consistent with previous values of the moment and isotope shift, and represent an improvement in accuracy in the case of ^{201}Tl. With the exceptions of ^{203,205,207}Tl, the isotope shifts measured here are more precise than previous optical measurements by a factor of from two to six. This improvement is attributable to the linewidths in these collinear laser experiments (~ 60 - 150 MHz) as compared to the previous optical experiments which used lamps as the light sources and which had corresponding Doppler widths of ~ 0.9 - 1.5 GHz (Hull and Stroke, 1961; Goorvitch, Davis and Kleiman, 1969).

TABLE III. Tl magnetic moments and 535 nm isotope shifts.

^{x}Tl	μ (n.m.)	IS (GHz)	^{x}Tl	μ (n.m.)	IS (GHz)
207g	1.8676(2)[a]	1.783(3)[a]	198g	±0.00(1)[b]	-6.87(12)[c]
205m	0.41(5)[d]	-	197g	1.58(2)[c]	-7.02(12)[c]
205g	1.6382136(1)[e]	0.0[f]	196m	-	-8.64(12)[g]
204m	1.187(6)[h]	-	196g	±0.07(1)[b]	-
204g	±0.09(1)[b]	-1.08(12)[i]	195g	1.58(4)[g]	-8.22(12)[g]
203m	0.16(5)[j]	-	194m	-	-10.37(12)[g]
203g	1.6222569(1)[e]	-1.766(21)[k]	194g	±0.14(1)[b]	-
	1.6231(13)[l]	-1.758(18)[l]	193m	3.9482(39)[l]	-7.033(17)[l]
202m	0.896(42)[m]	-	193g	1.5912(22)[l]	-9.743(19)[l]
202g	±0.06(1)[b]	-3.12(12)[i]	192m	0.5180(36)[l]	-10.892(30)[l] I=7
201g	1.61(2)[i]	-3.72(12)[i]		0.5121(34)[l]	-10.877(30)[l] I=6
	1.6051(17)[l]	-3.537(15)[l]	191m	3.9034(48)[l]	-8.265(65)[l]
200g	±0.04(1)[b]	-5.07(12)[i]	190m	0.4953(36)[l]	-12.286(65)[l] I=7
199g	1.60(2)[b]	-5.31(12)[i]		0.4900(42)[l]	-12.275(65)[l] I=6
198m	±0.64(7)[b]	-6.48(12)[n]	189m	3.8776(63)[l]	-9.484(70)[l]

[a] Neugart, 1984. μ(207) does not include a hfs anomaly correction.
[b] Ekstrom, Wannberg and Shishodia, 1976.
[c] Davis et al., 1966.
[d] Chen et al., 1972.
[e] Ekstrom, Wannberg and Shishodia (1976) who utilized the value from Baker and Burd (1963) with some corrections.
[f] All isotope shifts here are given relative to 205.
[g] Goorvitch, Davis and Kleiman, 1969.
[h] Maier, 1972.
[i] Hull and Stroke, 1961.
[j] Karlsson et al., 1965.
[k] Odinstov, 1960.
[l] Present work. μ includes the hfs anomaly but no errors due to same. Values for both spin assignments in ^{190m,192m}Tl are given.
[m] Hashimoto et al., 1974.
[n] Goorvitch, Kleiman and Davis, 1967.

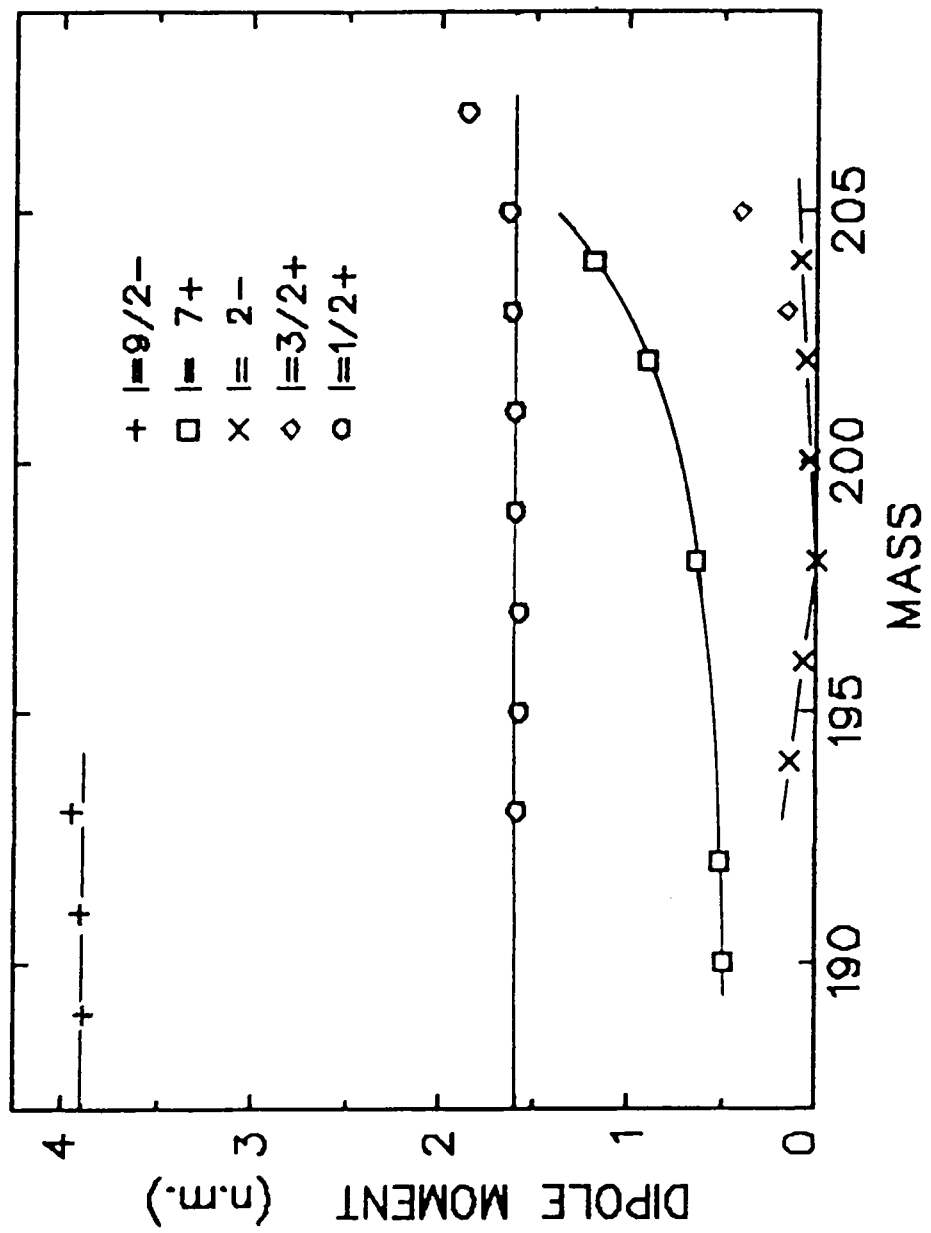


FIG. 18. Tl magnetic dipole moments. See Table III for data origins.

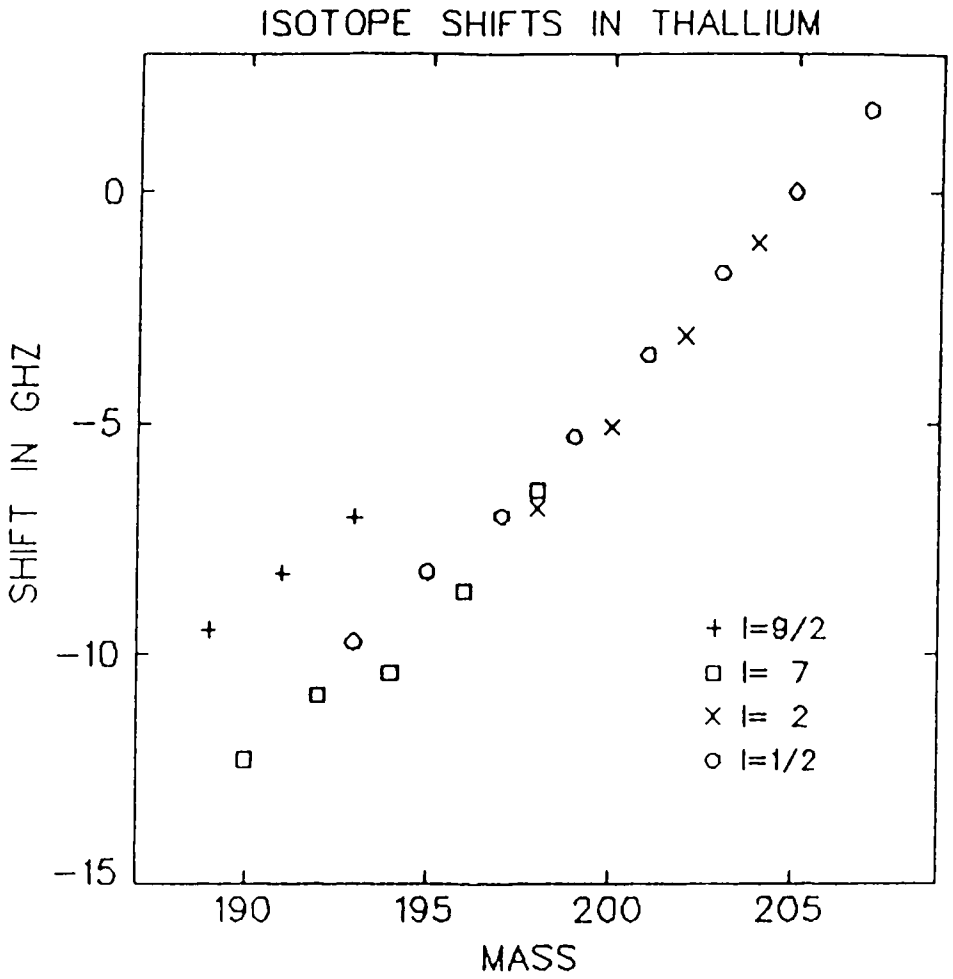


FIG. 19. Tl 535 nm isotope shifts. ^{205}Tl is the reference. isotope. See Table III for the data origins.

VI. INTERPRETATION OF RESULTS

It can be seen from the plot of the Tl magnetic moments, Fig. 18, that all of the spin $1/2^+$ nuclei have moments of about 1.6 n.m. The spin 2^- nuclei, none of which were measured by this laser system, have moments less than 0.2 n.m. and possibly are showing a nearly linear behavior with mass number, passing through $\mu = 0$ at mass 198. The admixtures in the spin 7^+ isomers evidently contribute less with lower mass resulting in a leveling-off of moments for lower masses. A very good discussion of the moments of ^{194}Tl and higher is given by Ekstrom, Wannberg and Shishodia (1976) so one will not be made here. Finally, the $9/2^-$ moments are all nearly 3.9 n.m., comparable to the 9/2 moments of 4.1 n.m. in Bi (Schmorak, 1980).

The isotope shifts of the 535 nm line are plotted in Fig. 19. The most noticable details are that the data points lie generally along a line, with the exception of the $9/2^-$ data which lie somewhat above the others. There is also considerable odd-even staggering in the data. The odd-even staggering effect has been discussed by many authors (Tomlinson and Stroke, 1962; Sorensen, 1966; Uher and Sorensen, 1966; Reehal and Sorensen, 1971; Stroke, Proetel and Kluge, 1979; Barrett and Jackson, 1977). Generally, isotope shifts (hence $\delta\langle r^2\rangle$) between nuclei with even numbers of neutrons are nearly equal. However, the addition of one neutron often produces less than 1/2 of the IS of two neutrons. Hence, when plotting shifts, the odd-neutron data point lies closer to the lighter neutron-pair point than to the heavier one. This is "odd-even staggering." It is a field shift effect. It is most often

seen in heavy elements, but has been observed in masses as low as Ca (however, not noticably in Na). Tomlinson and Stroke have theorized that neutron pairs favor higher angular momentum states due to their pairing energy versus the single particle energy. Odd neutrons have no pairing and so favor lower angular momentum states. In Hg, isomer states with odd neutrons lie halfway between even-neutron levels, i.e., there is no staggering, implying that paired and unpaired $i_{13/2}$ neutrons cause equal changes in $\langle r^2 \rangle$. In 1979, Stroke, Proetel and Kluge amended this by saying that the lighter isomers experience a large Coriolis force that decouples the neutron from the core causing the neutron's angular momentum to align with the axis of rotation of the nucleus rather than the nucleus' axis of symmetry. The staggering parameter

$$\gamma \equiv \frac{\langle r^2 \rangle_{N+1} - \langle r^2 \rangle_N}{(1/2)\{\langle r^2 \rangle_{N+2} - \langle r^2 \rangle_N\}}$$

is used as a measure of the polarization of the nucleus by one neutron relative to the polarization by two. For no staggering, $\gamma = 1$; for most staggering $\gamma < 1$; and it is possible to have $\gamma < 0$. Neutrons with the higher-j component of a nuclear fine structure doublet, having greater spin-orbit energy and so being more likely found in the core, are better for increasing deformations. However, "in the collective region, where the deformations and particle orbits may change radically upon the addition of one or two neutrons, one must consider in detail the effects of such variations" (Tomlinson and Stroke, 1962). In an attempt to explain staggering, Sorensen showed that near-spherical odd-mass nuclei are expected to have smaller $\langle \beta^2 \rangle$, where β is the nuclear deformation parameter, than adjoining even-mass nuclei. Barrett and Jackson point out

that "the situation is complicated by the density dependence of effective forces and the 'blocking' of a pair of states by the odd neutron." They add that the smaller $\langle\beta^2\rangle$ is due to this blocking. Whatever the origins are of staggering, the Tl isotope shifts track well the shifts observed in the Hg, Pb and Fr isotones as shown in Stroke's review article (1982). The relative isotope shifts of Hg, Pb and Tl, including data from this work, are shown in Fig. 20. The similarity of the long isotope chains in Hg and Tl is particularly striking.

The trends in the Tl IS data for the individual spins seem to be rather smooth with the exception of a kink in the spin 7^+ data between masses 192 and 194. Assuming that the optical data obtained on ^{192}Tl was solely that of the isomer state, which is what the gamma-ray intensities indicate, then the discontinuity in the I = 7 data may indicate (a) a change of spin in ^{190,192}Tl, (b) a sizable deformation setting in without a spin change, or (c) there is some misanalyzed data. Items (a) and (b) can only be proven by a measurement of the nuclear spins in these isotopes. As for misanalyzed data, the leading candidate seems to be that of the previous data for the reasons that follow: Examining the paper of Goorvitch, Davis and Kleiman (1969) which presented the ^{194,195,196}Tl data, it can be seen that their data was not completely resolved because the different masses had overlapping spectra. They deduced peak positions from repeated careful measurements of interferograms with a densitometer but, and this is the key point, they assumed that the magnetic moments for even-mass Tl isotopes are all less than 0.089 n.m. At the time, this was a valid assumption based on the paper by Brink et al. (1957). However, the data in this work and

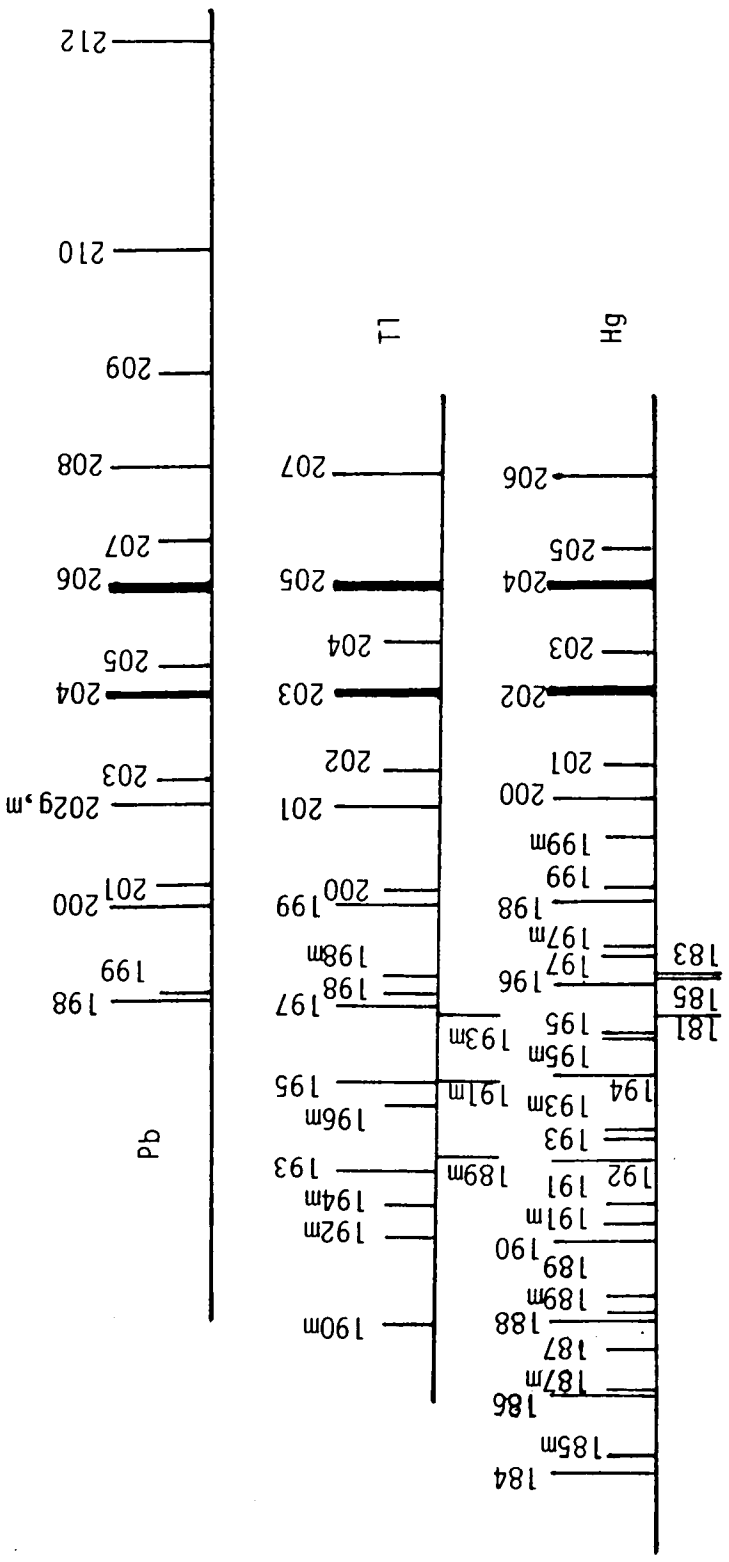


FIG. 20. Relative isotope shifts of Hg, Tl and Pb. The N = 122,124 isotope shifts are set equal and aligned. Data are taken from compilations by Bonn et al. (1976), Thompson et al. (1983) and this work.

that of Ekstrom, Wannberg and Shishodia (1976) give moments of 0.495, 0.518 and 0.641 n.m. for the ^{190,192,198}Tl isomers; it is only in the ground state that such low moments seem to occur. With their assumption of small μ, they assumed that the even-mass Tl hfs was unresolved within their linewidth of about 1.5 GHz. Their deduced ^{194,196}Tl separation was 58 mK = 1.74 GHz. This compares to the present work's $7^2S_{1/2}$ separation between peaks of 2.07 GHz for ^{192}Tl and 1.98 GHz for ^{190}Tl. If indeed they had misinterpreted these peaks and they were in fact both from ^{194}Tl, the IS would be nearly the average of their ^{194}Tl and ^{196}Tl values which would place the ^{194}Tl IS in line with ^{190,192,198}Tl. The ^{196}Tl could then also be assumed to be closer to the 195 "b+c" peak end of their data, which would in turn also raise the ^{196}Tl IS data point into the now ^{190,192,194,198}Tl line. This could also conceivably lower the ^{195}Tl point with respect to the other spin $1/2^+$ data, even though the ^{195}Tl magnetic moment seems appropriate. With these changes, the shifts in Tl would also better resemble those in Hg down to neutron number 108. The argument presented here is not offered as conclusive evidence but as a possibility that remains to be proven. On the basis of this argument, the laser studies of light Tl isotopes are to be extended after the completion of this dissertation to the isotopes ^{194,195}Tl. Due to cross-sections and available beams, it is not believed that an experiment on ^{196}Tl will be possible at UNISOR. It is hoped that both the isomer and ground state of ^{195}Tl will be observed. The data should either confirm or refute the interpretation of the 1969 data given above, and with its better resolution should also produce more accurate moments and even give quadrupole moments.

The isotope shift can be interpreted in terms of nuclear information by correcting for the mass shift (as described on page 45) and then factoring out the electronic term from the resulting field shift to leave the nuclear parameter λ (Eq. 6). By assuming a deformed radius given by $r_d = r_b (1 + \beta Y_{20})$ where β is the deformation parameter and r_b normalizes the mass to that of a sphere of radius $r_0 A^{1/3}$, the nonrelativistic radial moments can be calculated for each isotope from straightforward integrals. Using Seltzer's values (1969) for Tl,

$$\lambda = \delta\langle r^2\rangle - 0.0111\ \delta\langle r^4\rangle + 2.936\times10^{-6}\ \delta\langle r^6\rangle + \ldots \quad .$$

Factoring the $\delta\langle r^2\rangle$ out of the right side of the equation and with some manipulation using calculations of the radial moments, it can be shown that for Tl

$$\lambda \simeq 0.93\ \delta\langle r^2\rangle_A + 0.89\ \delta\langle r^2\rangle_\beta \qquad (19)$$

where A and β refer to mass-only and deformation-only changes in mean-square radii. This agrees with formulas for λ used by Thompson et al. (1983) for Pb and by Bonn et al. (1976) for Hg. As with most other electronic constants in Tl, the proportionality factor between the field shift and λ is not accurately calculable due to screening electrons. In principle, other isotope shift methods including muonic X rays and electron scattering could be used for calibration, but these give moments $\langle r^k e^{-\alpha r}\rangle$, not differences in radial moments, and thus comparisons with optical data are always model dependent. The muonic data on Tl in fact measures the rather obtuse value $\langle r^{2.419} e^{-0.15158}\rangle$ (Engfer et al., 1974). Engfer et al. also interpret the data of Backe et al.

(1972) (with whom they were co-authors) using a Fermi distribution with $\delta t = 0$ to obtain a thus model-dependent $^{203,205}Tl$ IS of - 0.115(3) fm^2. Euteneuer, Friedrich and Voegler (1978) combined their elastic electron scattering data with the muonic X-ray data of Backe et al. to derive rms radii of 5.4634(46) fm for ^{203}Tl and 5.4699(46) fm for ^{205}Tl. Combining these, one finds $\delta\langle r^2\rangle = 0.071(71)$ fm^2, a number whose uncertainty is as great as the number itself.

Faced with no certain calibrations, various normalizations were tried. The field shifts were extracted from the IS using the method described earlier. With the above-mentioned muonic atom data of 0.115(3) fm^2 for the $^{203,205}Tl$ IS and assuming higher moments are negligible, an electronic factor of 15.16(43) GHz/fm^2 was deduced. This agrees with factors derived by using the droplet model (Myers and Swiatecki, 1966, 1969 and 1974; Myers, 1969, 1970, 1977 and 1982; Myers and Schmidt, 1981 and 1983; Pearson, 1982). The latest version of the droplet model as described by Myers and Schmidt (1983) is quoted as having an accuracy of 0.01 fm^2. It gives the $^{203,205}Tl$ shift to be 0.106 fm^2 and thus indicates an electronic factor of 16.4(1.6) GHz/fm^2. If the muonic atom data is used for calibration, a plot of $\delta\langle r^2\rangle$ for the Tl isotopes would have data points which, with the exception of the $9/2^-$ data, fall about one-fourth of the way between the predictions of the droplet model and the values of $\delta\langle r^2\rangle$ obtained from calculations for a spherical nucleus having radius $r_0A^{1/3}$. Such a plot for Pb is given by Thompson et al. (1983). In order to deduce deformations in Tl, the method chosen was to normalize the droplet model values to the measured field shifts.

One normalization attempted was to assume that the stable ^{203,205}Tl have virtually no change in deformation. A line drawn through these points, representing the droplet model predictions, results in points falling on both sides of the line. However, both the droplet model and the expression given by Neugart (1981) for Eq. 19 show that deformations would result in points only on one side of the $\beta = 0$ line. In particular, Neugart relates the field shift to a volume and a deformation effect, the deformation effect being proportional to $\delta\langle\beta^2\rangle$. This $\delta\langle\beta^2\rangle$ term cannot possibly take both positive and negative values in going away from $\beta = 0$ since from there $\delta\langle\beta^2\rangle$ is necessarily positive for non-imaginary deformations. The data was thus fit by normalizing the droplet model so that no points would lie below the $\beta = 0$ line. Being one nucleon away from from a doubly-closed shell, ^{207}Tl was taken to have a deformation of zero. The isotope with the greatest shift per change in mass number relative to ^{207}Tl is ^{200}Tl. The droplet model was fit to these two points by also assuming zero deformation in ^{200}Tl. Figure 21 shows the results of this normalization. Lines obtained for non-zero deformations are included in the plot. Since the assumption of zero deformation in ^{200}Tl is somewhat unfounded, it can be assumed that the lines in Fig. 21 represent the minimum slopes and that deformations obtained for isotopes by reading the plot are minimum values. Regardless of the actual values, the plot shows that in going away from the closed-shell of ^{207}Tl, deformations are increasing. The deformations for each nuclear spin are in general smoothly changing with the exception of the ^{192,194}Tl discontinuity discussed earlier. Finally, the isomer shift in ^{193}Tl is seen to be the result of a large change

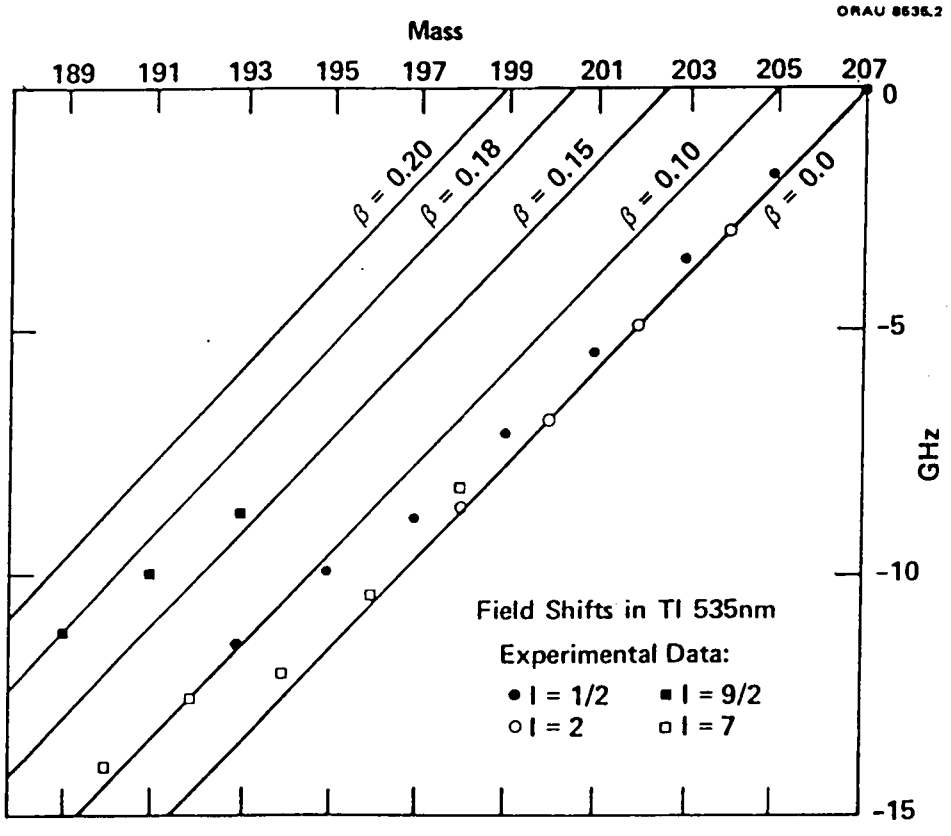


FIG. 21. Tl 535 nm field shifts and droplet model deformations. The field shifts are derived from the isotope shifts listed in Table III, page 64. Predictions of the deformed droplet model, normalized to masses 200 and 207, are given as lines in the figure.

in deformations between the ground and excited states: a change of as much as 60% if the normalization is correct.

Fortunately, the IS data are not the only source of information available on the deformations of the light isotopes. There is remaining information which comes from the hfs quadrupole constants B. No previously measured quadrupole moments are known in Tl, so no calibration exists. Also, the screening electrons and relativistic correction factors prevent an accurate simple calculation of the electronic factor relating B and Q. A complex calculation using a relativistic Hartree-Fock approach has, however, been done by Lindgren and Rosen (1975). Using their value for $\langle r^{-3} \rangle_{02}$, the relation obtained between the spectroscopic quadrupole moment and B is

$$Q_s = B/(1128 \text{ MHz/b}) \quad .$$

The Q_s values obtained in this manner may be either too large or too small but are proportionally correct.

The moments in the even-mass Tl result from the coupling of an odd proton and an odd neutron, and do not lend themselves to simple relations with the intrinsic quadrupole moments Q_0. Assuming the moments are proportional to the B's, then from the constants listed in Table II, page 62, there is roughly a 60% change in the quadrupole moments going from ^{190}Tl to ^{192}Tl. This change shows up in the narrowed spacings of the peaks in the ^{190}Tl data relative to those of ^{192}Tl. The actual values of these moments are not estimated here.

For the $9/2^-$ nuclei, there is the well-known relation for axially symmetric deformation and strong coupling of the odd proton (see, e.g.,

TABLE IV. Tl quadrupole moments and deformations.

Tl	Q_s	Q_0	β_2	$\langle\beta_2^2\rangle^{1/2}$
	(eb)		from Q_0	from IS
193g	-	-	-	0.099(1)
193m	-2.20(2)	-4.02(3)	-0.144(1)	0.158(1)
191m	-2.27(3)	-4.16(5)	-0.150(2)	0.170(2)
189m	-2.29(4)	-4.19(7)	-0.153(3)	0.181(2)

Bohr and Mottelson, 1975):

$$Q_s = Q_0 \frac{3K^2 - I(I+1)}{(I+1)(2I+3)} \quad .$$

The strong-coupled character of the $h_{9/2}$ band suggests predominantly oblate deformation (Newton et al., 1970). Negative values of Q_0 are obtained for I = 9/2 and K = 9/2 and are listed in Table IV, as are the deformations β_2 obtained by the relation for a rotational quadrupoloid:

$$Q_0 = \frac{3}{\sqrt{5\pi}} ZA^{2/3} r_0^2 \beta_2 (1 + 0.36\beta_2) \quad .$$

The relation between this expression of the quadrupole moment and its deformation β_2 compared to other quadrupole deformation parameters is given in the enlightening review by Lobner, Vetteg and Honig (1970). It suffices to say that β, β_2 and the soon-to-be-encountered ε_2 are equal to within a few percent for the deformation magnitudes here. The β's from the droplet model fit of the field shifts were converted to β_2's for the table.

The deformations obtained from the quadrupole moments are somewhat smaller in a nonproportional fashion than those obtained from the IS. The errors shown in Table IV represent measurement uncertainties but not uncertainties in the proportionality constants used. Thus the moments are proportionally correct (and the derived β_2's nearly so) but may be too large or too small. The disagreement in derived deformations from the IS and Q_S is not unreasonable as the same type of discrepancy has been previously observed in the neutron-deficient Hg isotopes where Q_0 is underestimated from Q_S due to violations of strong coupling and axial symmetry (Bonn et al., 1976). Also, to first order the IS measures $\langle\beta^2\rangle^{1/2}$ while the quadrupole moment measures $\langle\beta\rangle$, the two of which are not necessarily equal. The differences in Tl are larger for the lighter isotopes and may be in part due to mixing with a coexisting state of opposite and larger deformation, which could simultaneously reduce the quadrupole moment and increase the effective radius.

A theoretical calculation was carried out by Georg Leander of UNISOR to see if all the observed features of the Tl isotopes would emerge from the deformed shell model. It is an a priori microscopic calculation in the sense that the parameter values are standard. First the equilibrium shape of the intrinsic mean field was determined in the Strutinsky approximation to Hartree-Fock theory for both the $1/2^+$ and $9/2^-$ configurations of $^{185-199}$Tl. Details of the calculation are as described by Nilsson et al. (1969). The only difference in the present calculation compared to the older ones of Dionisio et al. (1976) and Wieclawik et al. (1976) is the use of updated spin-orbit and orbit-orbit strengths in the single-particle potential (Bengtsson and Ragnarsson,

1983, with the change κ_n,μ_n = 0.095,0.18 for N = 3 and 0.080,0.22 for N = 4). The new strengths are a universal set proposed by the Lund group for use in all regions of nuclei with several improvements over the older sets. The main difference in the present results compared to older ones of Dionisio et al. and Wieclawik et al. is that the $9/2^-$ excitation energy now has a minimum around A = 189 - 187 as is observed in experiment (see Fig. 22, part a). The quadrupole deformation coordinate ε_2 is shown by the dashed line in Fig. 22, part c for the $9/2^-$ configuration (for the $1/2^+$ configuration, $\varepsilon_2 \simeq -0.07$). Both the value and the rate of change of the deformation in ^{189,191,193}Tl are seen to be compatible with the experimental results. Clearly the rate of change of the deformation is more than enough to account for the mass dependence in the $9/2^-$ excitation energy, through the deformation dependence of the lowest Nilsson orbit from the $h_{9/2}$ shell. The mechanism for the upturn in the lightest Tl isotopes is more subtle, namely a difference in the rate at which the Strutinsky shell correction changes as a function of mass at the respective deformations of the $1/2^+$ and $9/2^-$ configurations.

The main reason for doubting the role of deformation in the past was based on the notion that a simple correspondence exists between the deformation and the rotational moment of inertia. The observation in $^{185-199}$Tl of almost identical strong-coupled bands based on the $9/2^-$ level would then be incompatible with changing deformation. In order to derive moments of inertia at the calculated $9/2^-$ equilibrium deformations, the formalism of Andersson et al. (1981) and of Arve, Chen and Leander (1983) was used. The change in the Hamiltonian from a rotation

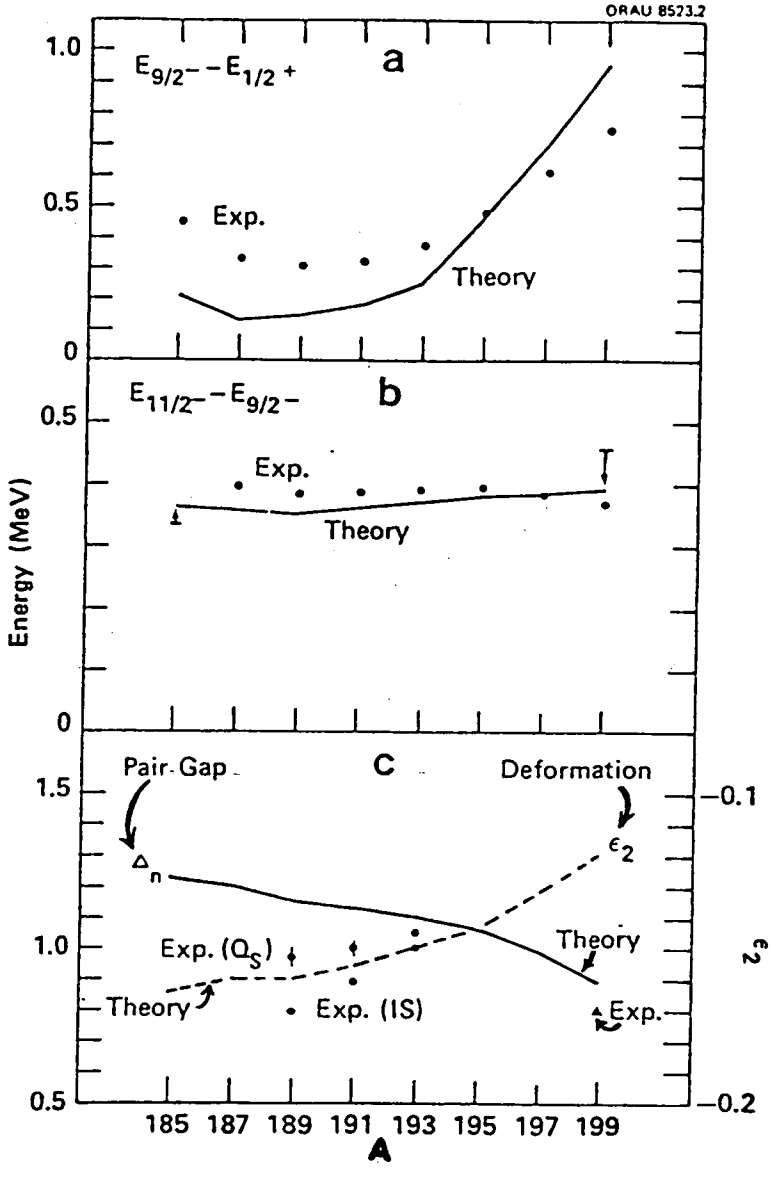


FIG. 22. Comparison of theory and experiment in Tl. Part a shows the level spacing of the $9/2^-$ isomer relative to the ground state. Part b shows the $11/2^-$ to $9/2^-$ spacing in these same odd-A isotopes. Part c shows both the neutron pairing gap energy, plotted on the left, and the deformation, whose scale is on the right side of the figure. In all three parts, the experimental values are given as points and the theory by lines.

of the intrinsic mean field, $F = -[H_{int},J_+]/\kappa$, is treated in the random phase approximation (RPA). The effective coupling constant κ is fixed by the physical requirement of M-degeneracy, i.e. a zero-energy root to the RPA equation. The lowest positive-energy root is collective and represents the $11/2^-$ first excited band member.

The results are plotted and compared to experiment in Fig. 22, part b. The agreement in overall magnitude between theory and experiment is somewhat arbitrary since the scaling of the theoretical results is sensitive to the prescription for the strength of the pairing interaction (for the RPA calculations it was determined by the average gap method with $\tilde{\Delta} = 14/\sqrt{A}$ MeV). The significant result is that the rotational excitation energy stays almost as constant for $^{185-199}$Tl in theory as in experiment, despite the changing deformation. The microscopic mechanism for this lies in changing neutron pairing correlations, as can be verified by varying $\varepsilon, \Delta_p, \Delta_n$ and N one at a time, holding the others fixed. The self-consistent neutron gap parameter, Δ_n, is plotted in Fig. 22, part c and is seen to increase with decreasing mass. Thus, when the number of valence neutron holes increases, both the deformation and the neutron pairing correlations increase with opposite and compensating effects on the moment of inertia. The latter point is illustrated quantitatively by the arrows on the endpoints of the theoretical curve in Fig. 22, part b. These arrows show the shift that comes from the use of the self-consistent and N-dependent values of Δ_n, rather than a single intermediate value. In summary, the calculation demonstrates an interesting aspect of the competition between quadrupole and pairing correlations, at least in these near-singly-closed-shell nuclei.

In conclusion, a brief restatement is in order. The $6^2P_{3/2}$ and $7^2S_{1/2}$ hyperfine structures and the 535 nm line isotope shifts of $^{189m,190m,191m,192m,193g,m,201,203,205}Tl$ have been measured using the collinear fast atom beam laser spectroscopy system at UNISOR. The magnetic dipole moments obtained from the hfs are consistent with other data. The isotope shifts indicate that deformation is increasing with decreasing mass, and that there is a large deformation change between $^{193g,m}Tl$. A deformed shell model calculation indicates that quadrupole and pairing correlations are balancing to maintain the constant level spacing of bands built on the $9/2^-$ isomeric level while the level varies in energy with respect to the $1/2^+$ ground state.

At the time of this writing, future UNISOR experiments are planned to measure $^{194,195}Tl$ and to extend measurements below ^{189}Tl. If a satisfactory method to produce them is found, the low-spin isotopes over the entire region $^{X-195}Tl$ will also be examined. These future experiments might settle the discrepancy of the $^{192,194}Tl$ isotope shift discontinuity and provide valuable information on the yet lighter mass $9/2^-$ isomers whose level energies are known to rise again relative to the ground state after a minimum at mass 189.

LIST OF REFERENCES

LIST OF REFERENCES

Andersson, C.G., et al., Nucl. Phys. A361, 147 (1981).

Armstrong, L., Jr., Theory of the Hyperfine Structure of Free Atoms (Wiley, New York, 1971).

Arve, P., Y.S. Chen and G.A Leander, Phys. Scr. T5, 157 (1983).

Back, E., and J. Wulff, Z. Phys. 66, 31 (1930).

Backe, H., et al., Nucl. Phys. A189, 472 (1972).

Baig, M.A., and J.P. Connerade, J. Phys. B 18, 1101 (1985).

Baker, E.B., and L.W. Burd, Rev. Sci. Instrum. 34, 238 (1963).

Barrett, R.C., and D.F. Jackson, Nuclear Sizes and Structure (Clarendon, Oxford, 1977).

Bauche, J., and R.-J. Champeau, Adv. At. Mol. Phys. 12, 39 (1976).

Bengtsson, T., and I. Ragnarsson, Phys. Scr. T5, 165 (1983).

Bodmer, A.R., Proc. Phys. Soc. London 66, 1041 (1953).

Bohr, A., and B.R. Mottelson, Nuclear Structure, Vol. 2 (W.A. Benjamin, London, 1975).

Bohr, A., and V.F. Weisskopf, Phys. Rev. 77, 94 (1950).

Bonn, J., et al., Z. Phys. A 276, 203 (1976).

Breit, G., Rev. Mod. Phys. 30, 507 (1958).

Brink, G.O., et al., Phys. Rev. 107, 189 (1957).

Carter, H.K., et al., Nucl. Instrum. Methods 202, 361 (1982).

Chen, M.Y., et al., Nucl. Phys. A181, 25 (1972).

Coenen, E., et al., in Proceedings of the Seventh International Conference on Atomic Masses and Fundamental Constants, Darmstadt, 1984, edited by O. Klepper (Technishe Hochschule, Darmstadt, 1984).

Crawford, M.F., and A.L. Schawlow, Phys. Rev. 76, 1310 (1949).

Daly, R.T., Jr., and J.H. Holloway, Phys. Rev. 96, 539 (1954).

Davis, S.P., H. Kleiman and T. Aung, J. Opt. Soc. Am. 54, 566 (1964).

Davis, S.P., et al., J. Opt. Soc. Am. 56, 1604 (1966).

Demtroder, W., Laser Spectroscopy (Springer-Verlag, Berlin, 1981).

Diamond, R.M., and F.S. Stephens, Nucl. Phys. 45, 632 (1963).

Dionisio, J.S., et al., J. Phys. G 2, L183 (1976).

Dunlap, B.D., Phys. Rev. A 6, 2057 (1972).

Ekstrom, C., et al., Nucl. Phys. A348, 25 (1980).

Ekstrom, C., G. Wannberg and Y.S. Shishodia, Hyp. Inter. 1, 437 (1976).

Engfer, R., et al., At. Data Nucl. Data Tables 14, 509 (1974).

Euteneuer, H., J. Friedrich and N. Voegler, Nucl. Phys. A298, 452 (1978).

Fairbank, W.M., Jr. (private communications regarding his OPTPUM program).

Flusberg, A., T. Mossberg and S.R. Hartman, Phys. Rev. A 14, 2146 (1976).

Gerstenkorn, S., and P. Luc, Atlas du Spectre D'Absorption de la Molecule D'Iode (C.N.R.S, Paris, 1978).

Gerstenkorn, S., and P. Luc, Rev. Phys. Appl. 14, 791 (1979).

Goldsmith, J.E.M., et al., Appl. Opt. 18, 1983 (1979).

Goodman, A.L., Nucl. Phys. A287, 1 (1977).

Goorvitch, D., H. Kleiman and S.P. Davis, J. Opt. Soc. Am. 56, 1416 (1966).

Goorvitch, D., H. Kleiman and S.P. Davis, Nucl. Phys. A99, 1 (1967).

Goorvitch, D., S.P. Davis and H. Kleiman, Phys. Rev. 188, 1897 (1969).

Goudsmit, S., Phys. Rev. 43, 636 (1933).

Hashimoto, O., et al., Nucl. Phys. A218, 180 (1974).

Heilig, K., and A. Steudel, At. Data Nucl. Data Tables 14, 613 (1974).

Heyde, K., et al., Phys. Rep. 102, 291 (1983).

Hull, R.J., and H.H. Stroke, Phys. Rev. 122, 1574 (1961).

Jaccarino, V., et al., Phys. Rev. 94, 1798 (1954).

Juncar, P., et al., Phys. Rev. Lett. 54, 11 (1985).

Kahler, A.H., Ph.D. thesis, University of Tennessee, 1978.

Karlsson, E., et al., Nucl. Phys. 61, 582 (1965).

Kaufman, S.L., Opt. Commun. 17, 309 (1976).

King, W.H., Isotope Shifts in Atomic Spectra (Plenum, New York, 1984).

Kopfermann, H., Nuclear Moments, translated by E.E. Schneider (Academic, New York, 1958).

Kuhn, H.G., Atomic Spectra (Academic, New York, 1969).

Kusch, P, and T.G. Eck, Phys. Rev. 94, 1799 (1954).

Letokhov, V.S., in High Resolution Laser Spectroscopy, edited by K. Shimoda (Springer-Verlag, New York, 1976).

Lindgren, I., and A. Rosen, Case Studies At. Coll. Phys. 4, 93 (1975).

Lobner, K.E.G., M. Vetteg and V. Honig, Nucl. Data Tables A7, 495 (1970).

Maier, K.H., Nucl. Phys. A195, 577 (1972).

McLennen, J.C., A.B. McLay and M.F. Crawford, Proc. Roy. Soc. London A 125, 570 (1929).

McLennen, J.C., A.B. McLay and M.F. Crawford, Proc. Roy. Soc. London A 133, 652 (1931).

Myers, W.D., Phys. Lett. 30B, 451 (1969).

Myers, W.D., Nucl. Phys. A145, 387 (1970).

Myers, W.D., Droplet Model of the Nucleus (IFI/Plenum, New York, 1977).

Myers, W.D., in Proceedings of the 1982 Conference on Lasers in Nuclear Physics, Oak Ridge, 1982, edited by C.E. Bemis, Jr., and H.K. Carter (Harwood, New York, 1982).

Myers, W.D., and K.-H. Schmidt, in Proceedings of the Fourth International Conference on Nuclei Far from Stability, Helsinger, 1981, edited by P.G. Hansen and O.B. Nielsen (CERN, Geneva, 1981).

Myers, W.D., and K.-H. Schmidt, Nucl. Phys. A410, 61 (1983).

Myers, W.D., and W.J. Swiatecki, Ark. Fys. 36, 343 (1966).

Myers, W.D., and W.J. Swiatecki, Ann. Phys. 55, 395 (1969).

Myers, W.D., and W.J. Swiatecki, Ann. Phys. 84, 186 (1974).

Neugart, R., Nucl. Instrum. Methods 186, 165 (1981).

Neugart, R., private communication (1984).

Newton, J.O., et al., Nucl. Phys. A148, 593 (1970).

Nilsson, S.G., et al., Nucl. Phys. A131, 1 (1969).

Odinstov, A.I., Opt. Spectros. (USSR) 9, 75 (1960).

Pearson, J.M., Nucl. Phys. A376, 501 (1982).

Petersen, F.R., H.G. Palmer and J.H. Shirley, Bull. Am. Phys. Soc. 51, 1203 (1968).

Racah, G., Z. Phys. 71, 431 (1931).

Racah, G., Nature 129, 723 (1932).

Reader, J., et al., Wavelength and Transistion Probabilities for Atoms and Atomic Ions (U.S. Government Printing Office, Washington D.C., 1980).

Reehel, B.S., and R.A. Sorensen, Nucl. Phys. A161, 385 (1971).

Rosenthal, J.E., and G. Breit, Phys. Rev. 41, 459 (1932).

Schmidt, A.G., et al., Phys. Lett. 66B, 133 (1977).

Schmorak, M.R., Nucl. Data Sheets 31, 283 (1980).

Schuler, H., and J.E. Keyston, Z. Phys. 70, 1 (1931).

Schuler, C.J., et al., J. Opt. Soc. Am. 52, 501 (1962).

Schwartz, C., Phys. Rev. 97, 380 (1955).

Schwartz, C., Phys. Rev. 105, 173 (1957).

Seltzer, E.C., Phys. Rev. 188, 1916 (1969).

Shore, B.W., and D.H. Menzel, Principles of Atomic Physics (Wiley, New York, 1967).

Sobelman, I.I., Atomic Spectra and Radiative Transitions, (Springer-Verlag, New York, 1977).

Sorensen, R.A., Phys. Lett. 21, 333 (1966).

Sousa, D.C., et al., Phys. Rev. C 24, 2245 (1981).

Spejewski, E.H., R.L. Mlekodaj and H.K. Carter, Nucl. Instrum. Methods 186, 71 (1981).

Stacey, D.N., Rep. Prog. Phys. 29, 171 (1966).

Stroke, H.H., Atomic Physics 8, 509 (1982).

Stroke, H.H., D. Proetel and H.-J. Kluge, Phys. Lett. 82B, 204 (1979).

Thompson, R.C., et al., J. Phys. G 9, 443 (1983).

Tolansky, S., Hyperfine Structure in Line Spectra and Nuclear Spin (Methuen, London, 1948).

Tomlinson, W.J., III, and H.H. Stroke, Phys. Rev. Lett. 8, 436 (1962).

Tuli, J.K., Nuclear Wallet Cards (National Nuclear Data Center, New York, 1985).

Uher, R.A., and R.A. Sorensen, Nucl. Phys. 86, 1 (1966).

Weast, R.E., editor of the Chemical Rubber Company Handbook of Chemistry and Physics, Ed. 53 (CRC Press, West Palm Beach, 1972).

White, H.E., Introduction to Atomic Spectra (McGraw-Hill, New York, 1934).

Wieclawiik, W., et al., in Proceedings of the Third International Conference on Nuclei Far from Stability, Cargese, 1976, edited by R. Klapisch (CERN, Geneva, 1976).

Wu, C.S., and L. Wilets, Ann. Rev. Nucl. Sci. 19, 527 (1969).

APPENDIX

THE OPTICAL PUMPING MODEL

The optical pumping model described below was first developed for this project by W.M. Fairbank, Jr., to determine what percentage of Tl atoms would emit light over a finite observation region after having been excited by laser light following a charge exchange process. His original computer program OPTPUM has inputs of observation length, distance from the charge exchange location to the center of the observation region, Doppler width of the transition and three somewhat nondescript constants obtained by combinations of statistical weights and transition rates describing each hyperfine transition. The output, such as is given in Fig. A1, consists of the percentage of atoms which emit light in the observation region tabulated for various laser powers and laser frequency offsets from the central frequency of the transition width. This provides both the relative amplitudes and shapes of the lines to be expected in the collinear experiments. Fairbank's model has been adopted by this author and applied to a wide range of geometries and to all nuclear spins of interest.

The program OPTPUM considers one hfs transition at a time. About a center frequency, u = 0, is "drawn" a Doppler curve which is then subdivided into 120 pieces. For each piece, the amplitude and position u_0 of the Gaussian is used to make a Lorentzian lineshape whose width corresponds to the natural linewidth of the Tl transition. These 120 small Lorentzians are each depleted a different amount by a laser at a third frequency u. Using the results from rate equations, these depletions are calculated and the 120 values are summed for a given laser frequency and geometry to determine what percentage of atoms are excited

X,Y,Z= 2621.0000 94.1000 0.5260
DOBS= 10.85 D= 8.50
DOPPLER WIDTH= 60.00MHZ

FREQ.	0.05	0.10	0.20	0.50	1.00	2.00	5.00	10.00	30.00	100.00
0.00	1.14	2.21	4.14	8.63	13.24	17.34	19.12	17.44	11.71	5.63
15.00	1.01	1.96	3.67	7.70	11.94	15.94	18.41	17.69	13.05	6.70
30.00	0.71	1.37	2.59	5.54	8.86	12.50	16.33	17.75	16.11	9.65
45.00	0.40	0.79	1.51	3.34	5.60	8.58	13.19	16.57	18.88	13.66
60.00	0.21	0.41	0.79	1.81	3.23	5.42	9.79	14.08	19.87	17.68
75.00	0.11	0.21	0.41	0.98	1.85	3.36	6.92	11.10	18.91	20.73
90.00	0.06	0.12	0.24	0.58	1.13	2.16	4.85	8.43	16.74	22.36
105.00	0.04	0.08	0.16	0.39	0.76	1.49	3.50	6.39	14.22	22.58
120.00	0.03	0.06	0.11	0.28	0.55	1.09	2.62	4.92	11.86	21.75
135.00	0.02	0.04	0.08	0.21	0.42	0.83	2.03	3.88	9.88	20.29
150.00	0.02	0.03	0.07	0.17	0.33	0.66	1.62	3.14	8.27	18.57
165.00	0.01	0.03	0.05	0.14	0.27	0.54	1.33	2.58	6.99	16.80
180.00	0.01	0.02	0.05	0.11	0.23	0.45	1.11	2.17	5.97	15.12
195.00	0.01	0.02	0.04	0.10	0.19	0.38	0.94	1.84	5.15	13.58
210.00	0.01	0.02	0.03	0.08	0.16	0.32	0.80	1.58	4.48	12.21
225.00	0.01	0.01	0.03	0.07	0.14	0.28	0.70	1.38	3.92	10.99
240.00	0.01	0.01	0.02	0.06	0.12	0.25	0.61	1.21	3.47	9.93
255.00	0.01	0.01	0.02	0.05	0.11	0.22	0.54	1.07	3.09	8.99
270.00	0.00	0.01	0.02	0.05	0.10	0.19	0.48	0.95	2.76	8.17
285.00	0.00	0.01	0.02	0.04	0.09	0.17	0.43	0.86	2.49	7.45
300.00	0.00	0.01	0.02	0.04	0.08	0.16	0.39	0.77	2.25	6.81

FIG. A1. Output generated by OPTPUM. The first three lines are input parameters: (x,y,z) here are those for the I = 1/2 "b " peak. The fourth line has laser power (mW) columnar headings. The first column is the laser offset frequency. Remaining columns are calculated percentages of atoms which will emit (377 nm) light in the observation region for the given laser frequency and power.

and decay to the ground state while in the observation region. This sum is repeated for two slightly different charge exchange positions and the three sums are averaged to take into account that the charge exchange within the cell occurs along the beam and not at a distinct point. This average is a single tabulated entry in the output. Repeating for the same laser frequency but with different laser powers produces one row of the table. Repeating all of the above for each different laser-from-center-frequency offset (15 MHz steps from 0 to 300 MHz) produces all of the rows in the table.

To understand and adapt OPTPUM, whose FORTRAN version is given in Fig. A2, it is necessary to understand the notation it uses. Figure A3 shows the assignment of subscripts used for the various levels: 1 refers to the laser-depleted level, 2 is the excited state, 3 is the levels other than the ground state to which the excited state might decay, and 0 is the ground state. Directions of transitions are indicated by their Einstein coefficients and order of subscripts. Hence stimulated absorption and emission are indicated by B_{12} and B_{21} respectively, while spontaneous emission has the form A_{2X}. Since a narrowband laser is used, the only stimulated transitions are B_{12} and B_{21}; all other subscripted possibilities are vanishingly small due to the energy differences involved. This assumes that the splitting of the states is greater than the linewidth. Using the statistical weight $g_i = 2F + 1$, the relation between the Einstein coefficients and the line strengths S_{ik} for a narrowband laser are given by Demtroder (1981, page 59) to be

$$A_{ik} = \frac{16\pi^3\nu^3}{3\varepsilon_0 hc^3 g_i} S_{ik}$$

```
      DIMENSION S(10)
      DIMENSION P(10)
      DATA P/.05,.1,.2,.5,1.,2.,5.,10.,30.,100./
      DATA SAT1/108.4/
      DATA AM1/15.14/
      DATA V/21.7/
      DATA DNUN/21.17/
      WRITE(5,200)
  200 FORMAT(' X,Y,Z')
      READ(5,1000)X
      READ(5,1000)Y
      READ(5,1000)Z
      WRITE(5,250)X,Y,Z
      WRITE(6,250)X,Y,Z
  250 FORMAT(' X,Y,Z=',3F10.4)
      WRITE(5,44)
   44 FORMAT(' OBSERVATION DISTANCE IN CM')
      READ(5,1000)DOBS
      WRITE(5,45)
   45 FORMAT(' CELL DISTANCE IN CM')
      READ(5,1000)D
      WRITE(5,50)DOBS,D
      WRITE(6,50)DOBS,D
   50 FORMAT(' DOBS=',F8.2,' D=',F8.2)
      WRITE(5,75)
   75 FORMAT(' DOPPLER WIDTH IN MHZ')
      READ(5,1000)DNUD
      WRITE(5,80)DNUD
      WRITE(6,80)DNUD
   80 FORMAT(' DOPPLER WIDTH=',F10.2,'MHZ')
      DNUD1=DNUD/(2.*SQRT(ALOG(2.)))
      DB=.05
      SLP=SQRT(3.1415926)
      CC=DB/(3.1415926*SLP*DNUN/2.)
      WRITE(5,115)(P(I),I=1,10)
      WRITE(6,115)(P(I),I=1,10)
  115 FORMAT('       ',10F7.2)
      WRITE(6,116)
  116 FORMAT('  FREQ.')
      WRITE(5,117)
  117 FORMAT('  FREQUENCY LIMITS,STEP:I1,I2,I3')
      READ(5,1001)K1
      READ(5,1001)K2
      READ(5,1001)K3
      K1=K1+1
      K2=K2+1
      DO 500 K=K1,K2,K3
      DO 420 I=1,10
      S(I)=0
      RK=K
      U=RK-1
      RI0=P(I)*AM1/SAT1
      DO 410 L=1,3
      RL=L-2
      D=D+RL*0.635
      SUM=0.
      DO 400 J=1,120
```

FIG. A2. The OPTPUM program.

```
      RJ=J
      B=DB*(RJ-60.5)
      EB=EXP(-B*B)
      U0=B*DNUD1
      RNU=2.*(U-U0)/DNUN
      RI=RI0*CC*EB/(1.+RNU*RNU)
      RK=(133.+Y*RI)/2.
      Z1=X*RI
      Z3=RK*RK-Z1
      IF (Z3.GT.0.) GO TO 110
      Z2=1.E-6
      GO TO 130
  110 Z2=SQRT(Z3)
  130 A1=Z2-RK
      IF (A1.EQ.0.) GO TO 400
      A2=-Z2-RK
      T1=(D-DOBS/2.)/V
      T2=(D+DOBS/2.)/V
      XXT=A1*T1
      IF(XXT.LT.-160.) XXT=-160.
      F1=EXP(XXT)
      XXU=A1*T2
      IF(XXU.LT.-160.) XXU=-160.
      F2=EXP(XXU)
      XXV=A2*T1
      IF(XXV.LT.-160.) XXV=-160.
      F3=EXP(XXV)
      XXX=A2*T2
      IF(XXX.LT.-160.) XXX=-160
      F4=EXP(XXX)
      C1=Z1/(2.*Z2*A1)
      C2=Z1/(2.*Z2*A2)
      SIG=(C1*(F2-F1)-C2*(F4-F3))*Z*100.
      SUM=SUM+SIG
  400 CONTINUE
      S(I)=S(I)+SUM
  410 CONTINUE
      S(I)=S(I)/3
C     WRITE(5,411)U,P(I),S(I)
C 411 FORMAT(3F12.4)
  420 CONTINUE
      WRITE(5,550)U,(S(I),I=1,10)
      WRITE(6,550)U,(S(I),I=1,10)
  500 CONTINUE
  550 FORMAT(11F7.2)
 1000 FORMAT(F10.0)
 1001 FORMAT(13)
      END
```

FIG. A2. (continued).

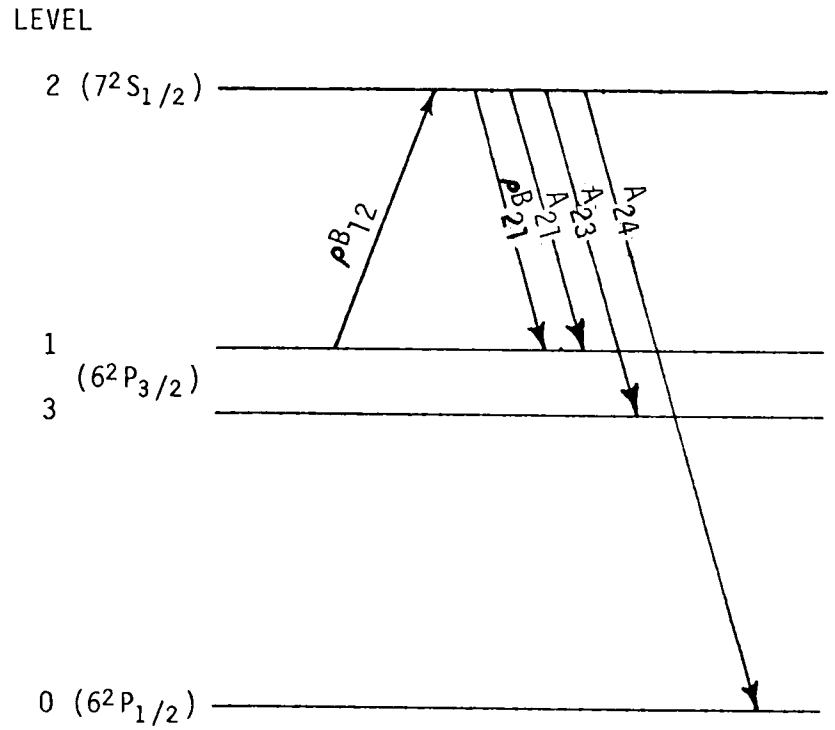


FIG. A3. Transitions and their notation for the optical pumping model. Corresponding Tl terms are given in parentheses.

$$\text{and} \qquad B_{ik} = \frac{2\pi^2 e^2}{3 g_i \epsilon_0 h^2} S_{ik} \quad .$$

These can be combined to show

$$\rho B_{12} = \rho \frac{\lambda_0^2}{h\nu^2 2\sum A_{2i}} A_{21} \frac{g_2}{g_1}$$

$$= \frac{\rho}{\rho_0} A_{21} \frac{g_2}{g_1}$$

where ρ_0 is a characteristic intensity. For the Tl 535 nm line, ρ_0 is 108 mW/cm^2 (SATI in OPTPUM). The quantity ρ is the laser intensity. OPTPUM defines RIO to be the ratio ρ/ρ_0 = P(I)*AM1/SATI where AM1 is a constant factor converting the power P in mW to an intensity in mW/cm^2. The OPTPUM version shown in Fig. A2 has the power listed in a data array at the first of the program. The input coefficients x, y and z are defined as

$$x = (A_{23} + A_{20}) \frac{g_F}{g_{F'}} a_{FF'}$$

$$y = \left(1 + \frac{g_F}{g_{F'}} \right) a_{FF'}$$

$$\text{and} \qquad z = \frac{g_F}{g_{F'}} \frac{A_{20}}{A_{23} + A_{20}} \quad ,$$

$$\text{where} \quad a_{FF'} = \frac{\sum g_F}{g_F} \frac{S_{FF'}}{\sum\sum S_{FF'}} A(S_{1/2} \rightarrow P_{3/2})$$

and where F refers to the J = 1/2 hfs terms and F' to the J = 3/2 hfs terms.

The problem of solving the associated rate equations lends itself to a matrix solution. Let N_i denote the population of each state, where i = 0, 1, 2 or 3. Define the vector

$$\vec{N} = \begin{bmatrix} N_2 \\ N_1 \\ N_3 \\ N_0 \end{bmatrix} \quad \text{,then } \vec{N}' = \begin{bmatrix} -(\rho B_{21}+A_{21}+A_{20}+A_{23}) & +\rho B_{12} & 0 & 0 \\ +(\rho B_{21}+A_{21}) & -\rho B_{12} & 0 & 0 \\ A_{23} & 0 & 0 & 0 \\ A_{20} & 0 & 0 & 0 \end{bmatrix} \begin{bmatrix} N_2 \\ N_1 \\ N_3 \\ N_0 \end{bmatrix} = \vec{\vec{M}}\,\vec{N}$$

which is the matrix form of the time-differential equations involved. The boundary conditions are

$$\vec{N}(0) = \begin{bmatrix} 0 \\ \frac{g_1}{\sum g_i} N \\ N - N_1(0) \\ 0 \end{bmatrix} = \begin{bmatrix} 0 \\ N_{10} \\ N - N_{10} \\ 0 \end{bmatrix}$$

where N is the total number of atoms originally in the metastable state. This thus assumes that the charge exchange process populates the states in a statistical fashion. The number N is set equal to 1 to give fractional values of N_i.

The equation $\vec{N}' = \vec{\vec{M}}\,\vec{N}$ can be solved by the normal matrix methods of setting the determinant $|\vec{\vec{M}} - \lambda\vec{\vec{I}}| = 0$ and solving for the eigenvalues λ. The four eigenvalue solutions are $\lambda = 0, 0,$ and

$$-\frac{1}{2}(\rho B_{21}+A_{21}+A_{20}+A_{23}+\rho B_{12}) \pm \left[\frac{1}{4}(\rho B_{21}+A_{21}+A_{20}+A_{23}+\rho B_{12})^2 - \rho B_{12}(A_{20}+A_{23})\right]^{1/2}$$

Using $\lambda_{\pm}$ to denote the non-zero eigenvalues and substituting these back into the matrix equations, the solutions for the given boundary conditions are found to be

$$N_2(t) = \frac{N_{10}\,\rho B_{12}}{\lambda_+ - \lambda_-}\,(e^{\lambda_+ t} - e^{\lambda_- t})$$

$$N_1(t) = N_{10}\left[\frac{\rho B_{12}}{\lambda_+ - \lambda_-}(-e^{\lambda_+ t}+e^{\lambda_- t}) - \frac{\rho B_{12}(A_{20}+A_{23})}{\lambda_+ - \lambda_-}\left(\frac{e^{\lambda_+ t}}{\lambda_+} - \frac{e^{\lambda_- t}}{\lambda_-}\right)\right]$$

$$N_3(t) = N - N_{10}\left\{\frac{A_{21}}{A_{20}+A_{23}} - \frac{\rho B_{12}A_{23}}{\lambda_+ - \lambda_-}\left(\frac{e^{\lambda_+ t}}{\lambda_+} - \frac{e^{\lambda_- t}}{\lambda_-}\right)\right\}$$

$$N_0(t) = \frac{N_{10}\,A_{21}}{A_{20}+A_{23}}\left\{1 + \frac{\lambda_+\lambda_-}{\lambda_+ - \lambda_-}\left(\frac{e^{\lambda_+ t}}{\lambda_+} - \frac{e^{\lambda_- t}}{\lambda_-}\right)\right\}$$

These populations apply to any case for which the aforementioned assumptions are valid. The time $t = 0$ is the time of charge exchange (after which the laser can first interact with the neutralized atom). As $t \to \infty$, all of the exponentials go to zero leaving the population distribution as should be expected with atoms only in states 3 and 0. $N_0(\infty)$ is the maximum possible fraction of atoms which could be detected since it is populated only by the monitored decay from the excited state.

The rate of decay to the ground state is simply $A_{20}N_2(t)$. The fraction of atoms observable for a particular laser frequency and power is determined by using the appropriate laser intensity ratio found from the numerical convolution of the Doppler and the Lorentzian profiles and then integrating $A_{20}N_2(t)$ over the time during which the atom is in the observation region or, equally, by taking the difference in N_0 between the entry and exit times of the atom in the observation region. The integration limits, being times, thus depend on the physical positioning and length of the light collector combined with the velocity of the atoms. For Tl at 50 keV, this velocity is about 21.7 cm/μs.

Varying of the input distance parameters of the OPTPUM program shows that the maximum number of detectable atoms occurs for an infinitely long observation region starting infinitessimally close to the charge cell, regardless of laser power. This is obvious. For a given non-zero distance to the observation region, however, the fraction observable is a strong function of laser power and observation length. A finite observation length close to the charge cell has the higher signal rates for higher laser powers but when backed away from the cell has peak rates at lower and lower laser powers. The further the displacement, the lower is the maximum signal rate. One consequence of the geometry which is not intuitively obvious is that at high laser powers the maximum signal rate occurs not at the center of the peak but at some offset frequency, as can be seen by the output in Fig. A1, page 89. This can be traced to the more efficient depletion of observable atoms before the observation region by the laser at or near the center frequency. This has been observed in experiment as well. Even prior to the formation of this central dip for increasing laser powers, it can be seen that peaks broaden with higher powers. Thus the optimum resolution occurs for the lowest laser powers while the power for the maximum signal rate depends on the geometry.

A very instructive modification of the OPTPUM program has been examining the emission rate as a function of distance and laser power using a single creation point. For the range 1 to 100 mW, it was found that the peak 377 nm emission rate occurs less than 1 cm after creation and even within 4 mm for more than 10 mW. The maximum emission rate is greater for the higher powers (3x and 18x for 100 mW compared to 10 mW

and 1 mW, respectively), but as a consequence of conservation of atoms the higher powers produce lower rates downstream: the 100 mW rate drops below the 20 mW rate after only 1.6 cm. Powers of 5 mW and less have nearly constant emission rates for several cm. For a given offset frequency the maximum emission rate is lower and is shifted slightly downstream.

Since OPTPUM provides its information on individual hfs components, comparisons between components both of the same and of different nuclear spins can be made. The approach used in this research was to use the known observation length and vary its displacement in the program so that the experimentally observed relative intensities were matched. This was done for each experimental geometry and with and without the magnetic fields in the cases of ^{203,205}Tl which have three well separated peaks. For a given geometry, the maximum signal rate for each hfs component comes at a slightly different laser power. Relative line strengths match their theoretical ratios (as given in Fig. 15, page 48) only at the lowest laser powers. Curves of efficiency-versus-laser-power as measured experimentally and using the power measured as the beam exits the laser table consistently have peak efficiencies at 2-3 times the power predicted by OPTPUM but with the same relative peak efficiencies. Normalizing experimental and computer-listed laser powers, best fits were within 10% and were considered quite sufficient for these purposes, although it is strongly believed that given enough time to change even more of the program's parameters, fits to within a few percent both in height and width should be possible. For the final geometry, the maximum percentage of total atoms observable varies from

19% for an I = 1/2 "b" peak down to about 4% for an I = 7 "f" peak (where peaks are labeled as in Fig. 14, page 41). Figure A4 shows the percentage of observable atoms expected as a result of optical pumping for each of the I = 7 hfs components as a function of laser power. It is seen that above 5 mW each curve branches. The lower branch corresponds to the center-frequency peak height while the upper branch corresponds to the maximum peak height. The largest peak ("d") reaches 7% before branching while all others lie between 4 and 5½%. These intensities can be conveniently normalized relative to the largest peak. Figure A5 shows such a normalization where the I = 7 "d" peak was set equal to 100% for all laser powers. The maximum peak heights were used. These curves proved helpful in analyzing the I = 7 data as described in the text.

With only small changes, the OPTPUM program could be adapted to accept transition rates and the atomic level quantum numbers so that it could calculate the parameters x, y and z itself for all appropriate levels. More sophisticated revisions would include levels which are not resolved and, even better, levels in a magnetic field observed with various laser polarizations. A Breit-Rabi type calculation would be required for the latter. Ultimately a nearly exact mathematical model of the system might prove accurate enough to determine spins if the statistics of the data are sufficient to obtain precise relative intensities and widths. The variation of parameters to fit known data exactly would then be a time-consuming but rewarding effort.

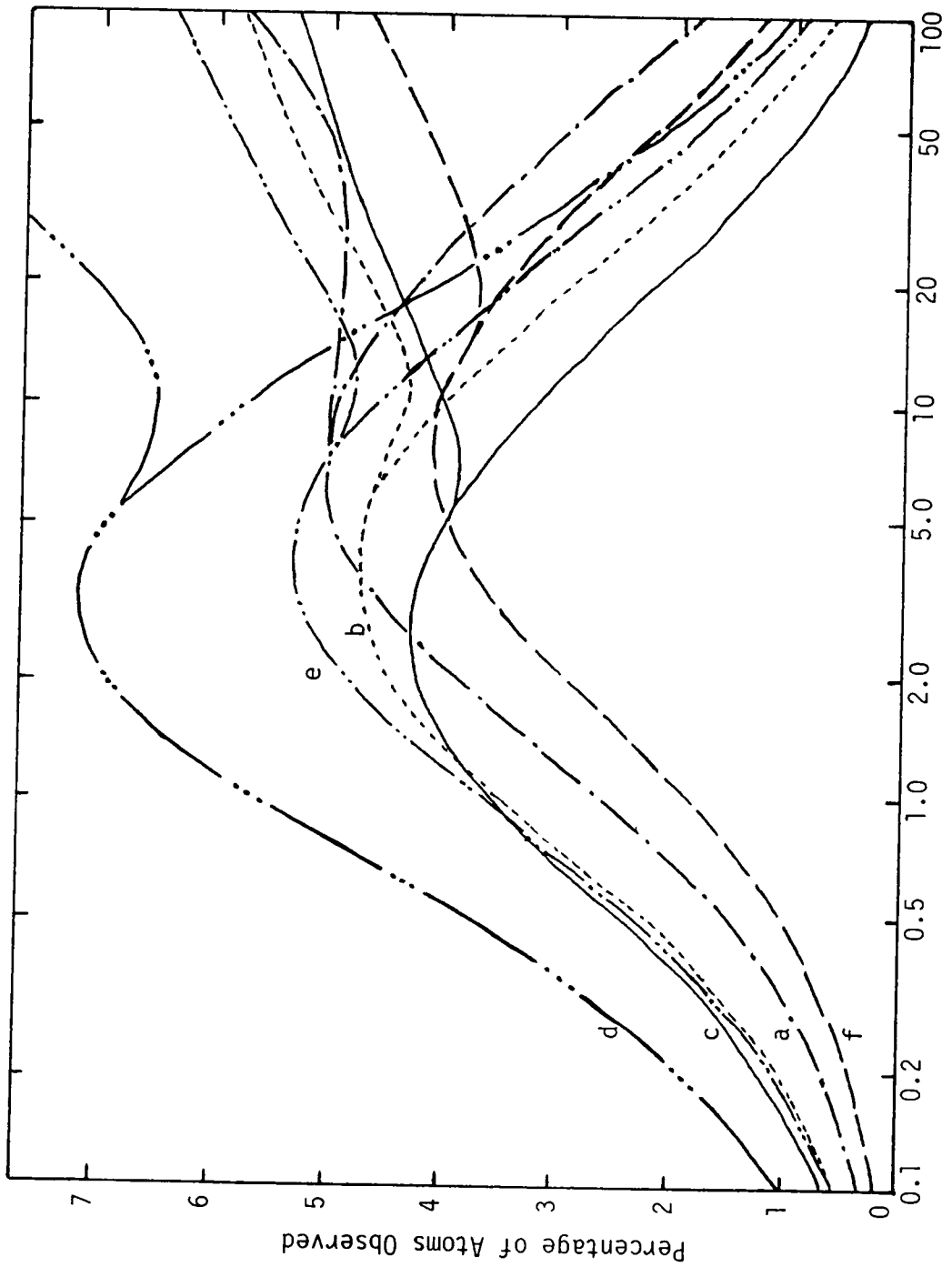


FIG. A4. Optical pumping of the 535 nm transitions in Tl for I = 7.

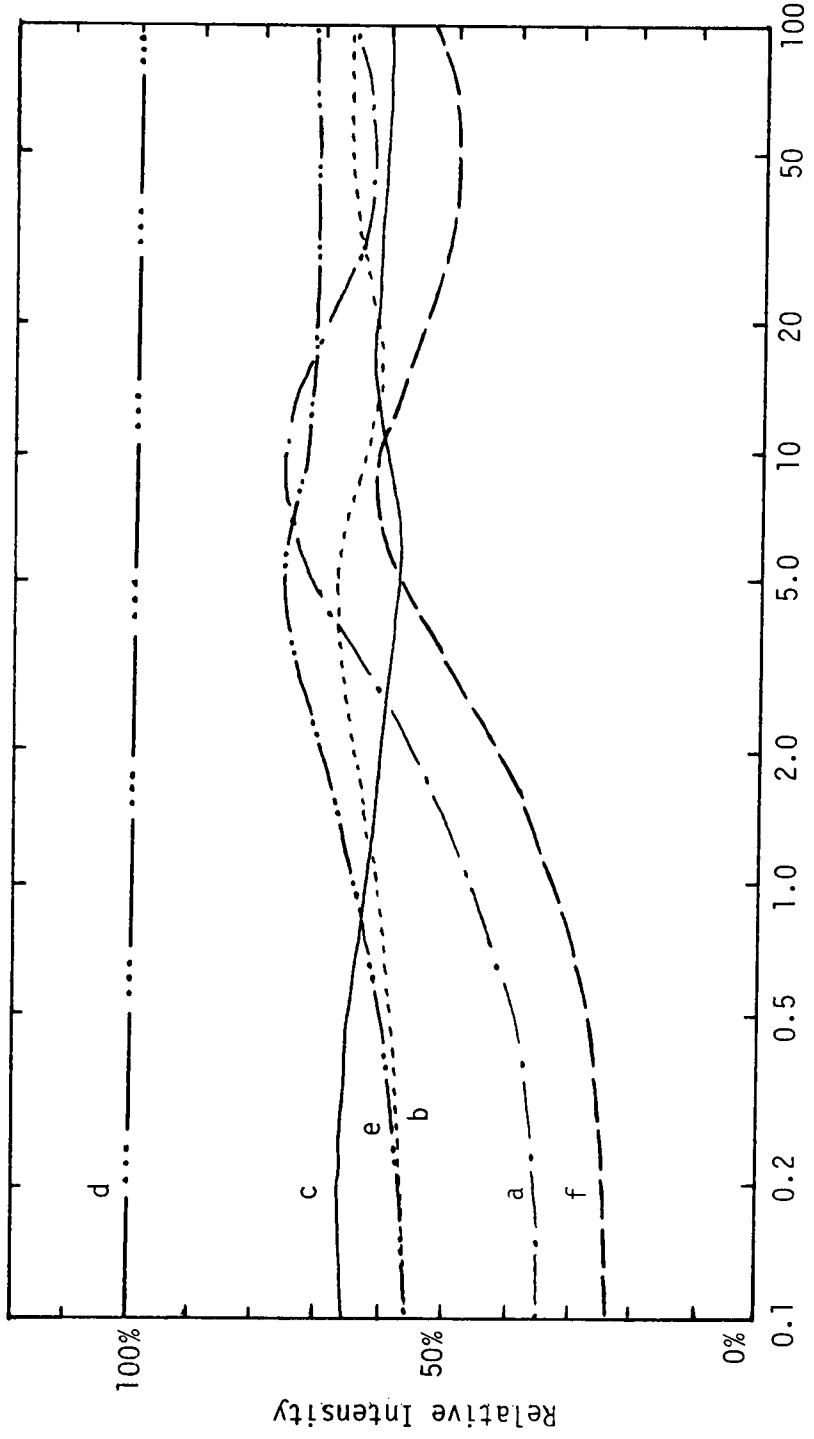


FIG. A5. Relative intensities of the hfs components in Tl for I = 7. The "d" peak of the 535 nm transitions is the reference.

VITA

John Alan Bounds was born in Knoxville, Tennessee on January 23, 1959. He attended schools in that city and was graduated as valedictorian from Holston High School in June 1976. The following September he entered the University of Tennessee, Knoxville. As an undergraduate he became a member of the honor societies Phi Eta Sigma, Gamma Beta Phi, Tau Beta Pi, Sigma Pi Sigma, Phi Kappa Phi, and Golden Key, prior to receiving in June 1980 a Bachelor of Science degree in Engineering Physics. He entered Graduate School in September 1980 to pursue a Ph.D. with a major in nuclear physics. Graduate research work at UNISOR was sponsored by the U.S. Department of Energy through the Laboratory Graduate Participation Program administered by Oak Ridge Associated Universities. After graduation he will take a temporary postdoctoral position with UNISOR to further the laser studies of nuclei far from stability, particularly those of thallium and lead. After UNISOR he will take a postdoctoral position at Los Alamos National Laboratory to work on isomer separation with lasers, changing nuclear properties with lasers, and developments towards gamma-ray lasers. When not doing physics, his favorite pastimes are bicycling and astronomy, being an avid amateur participant in both.